
Electrospray-Ionization Mass Spectrometry for the Analysis and Quantification of Carbanions

Dissertation

for the award of the degree

“Doctor rerum naturalium” (Dr. rer. nat.)

within the doctoral program Chemistry

of the Georg-August University School of Science (GAUSS)

submitted by

Niklas Frederik Eisele

from Usingen

Göttingen, 2023

Thesis Committee

Prof. Dr. Konrad Koszinowski, Institute of Organic and Biomolecular Chemistry

Prof. Dr. Philipp Vana, Institute of Physical Chemistry

Prof. Dr. Dietmar Stalke, Institute of Inorganic Chemistry

Members of the Examination Board

Reviewer: Prof. Dr. Konrad Koszinowski, Institute of Organic and Biomolecular Chemistry

Second Reviewer: Prof. Dr. Philipp Vana, Institute of Physical Chemistry

Other Members of the Examination Board

Prof. Dr. Dietmar Stalke, Institute of Inorganic Chemistry

Prof. Dr. Franc Meyer, Institute of Inorganic Chemistry

Jun.-Prof. Dr. Johannes Walker, Institute of Organic and Biomolecular Chemistry

Dr. Holm Frauendorf, Central Analytics

Date of the disputation: 25.01.2023

Declaration

Hereby I declare that I have written the present thesis under the supervision of Prof. Dr. Konrad Koszinowski independently and without illicit assistance from third parties. I confirm that I used none other than the mentioned source materials and aids. No part of this thesis has been submitted for the award of any other degree or diploma prior to this date.

Göttingen, 20.03.2023

Niklas Eisele

Danksagung

Ich danke...

... Konrad Koszinowski für die Möglichkeit, diese Arbeit unter seiner Anleitung anzufertigen. Deine Betreuung und Unterstützung machen diese Arbeit zu der, die sie geworden ist.

... Philipp Vana für fachliche Unterstützung und die Übernahme der Zweitkorrektur dieser Arbeit.

... allen Mitgliedern meiner Prüfungskommission für Ihre Zeit und Interesse, und dass Sie sich für die Prüfung zur Verfügung gestellt haben.

... Holm Frauendorf für die Unterstützung bei der Durchführung von HPLC Messungen.

... Lucas Riemann und Matthias Peters, die ich während ihrer Bachelorarbeiten betreut habe und die im Gegenzug mich unterstützt haben.

... dem gesamten Arbeitskreis Koszinowski, einschließlich der ehemaligen Mitglieder die ich in meiner Zeit dort kennen lernen durfte. Es hat Spaß gemacht, mit euch zu arbeiten und ich hoffe, dass wir in Zukunft in Kontakt bleiben.

... meiner Familie. Ihr habt mich auf meinem Weg hierher begleitet und unterstützt und ich weiß, dass ich mich auch in Zukunft auf euch verlassen kann.

Parts of the results presented in this thesis have been published in:

Direct Detection of Free and Counterion-Bound Carbanions by Electrospray-Ionization Mass Spectrometry,

N. F. Eisele, K. Koszinowski*, *J. Org. Chem.* **2021**, *86*, 3750-3757.

In-Situ Analysis of Anionic Coordination Polymerizations by Electrospray-Ionization Mass Spectrometry,

F. Kreyenschmidt⁺, N. F. Eisele⁺, V. Hevelke, R. Rahrt, A.-K. Kreyenschmidt, K. Koszinowski*, *Angew. Chem. Int. Ed.* **2022**, *61*, e202210211.

In-Situ-Analyse Anionischer Koordinationspolymerisationen durch Elektrosprayionisations-Massenspektrometrie,

F. Kreyenschmidt⁺, N. F. Eisele⁺, V. Hevelke, R. Rahrt, A.-K. Kreyenschmidt, K. Koszinowski*, *Angew. Chem.* **2022**, *134*, e202210211.

Live Monitoring of Anionic Living Polymerizations by Electrospray-Ionization Mass Spectrometry,

N. F. Eisele*, M. Peters, K. Koszinowski*, *Chem. Eur. J.* **2023**, e202203762.

Contents

1	Introduction and Theoretical Background.....	1
1.1	Motivation	1
1.2	Mass Spectrometry	2
1.2.1	Ion Sources.....	2
1.2.2	Transfer Optics.....	5
1.2.3	Mass Analyzers & Detectors	6
1.2.4	Fragmentation Experiments	8
1.2.5	Kinetic Method	9
1.3	Reactive Anionic Species.....	12
1.4	Anionic Polymerizations	15
1.5	Mass Spectrometry of Reactive Anionic Species	21
2	Objective	24
3	Results and Discussion.....	25
3.1	ESI-MS for the In-Situ Detection of Carbanions	25
3.1.1	Influence of Structure and Acidity.....	28
3.1.2	Influence of Concentration and Water	31
3.1.3	Influence from Changing the Solvent	34
3.1.4	Influence of Base and Counterion.....	37
3.2	ESI-MS for the in-situ Detection of Radical anions	40
3.2.1	Influence of Structure and Redox Properties	41
3.2.2	Influence of Concentration	44
3.2.3	Influence of Water Content in the Solvent	47
3.2.4	Influence from Changing the Solvent	48
3.2.5	Influence of the Reducing Agent	50
3.2.6	Reactivity of Radical Anions in Solution	51
3.3	Reaction Monitoring and Kinetic Observations.....	55

3.3.1	Michael-Addition of Dimedone to Butenone	55
3.3.2	Anionic Polymerization of 1,1-Substituted Cyclopropane	58
3.3.3	Anionic Coordination Polymerization of Isoprene on Cobalt(I)	70
3.4	Thermodynamic Parameter Determination	79
3.4.1	Alkali Metal Cation Affinity Determination for Carbanions.....	81
3.5	Comparison with Other Analytical Methods	88
4	Conclusion	91
5	Outlook.....	94
6	Experimental Section.....	96
6.1	Materials.....	96
6.2	Instruments	96
6.3	Experimental Procedures.....	98
7	References.....	101

1 Introduction and Theoretical Background

1.1 Motivation

An exact understanding of reactions, both mechanistic and kinetic, is required to design the most selective and efficient processes for the synthesis of chemicals. Improvements are enabled by the continuous development of precise analytical techniques, which each have their own advantages and limitations. Among the most powerful aspects for the in-depth investigation of reactions is the ability to perform in-situ measurements. Monitoring the reaction of interest directly and on-line is faster and can reveal additional information, which may be lost when preparing samples for ex-situ analytical methods.¹

Mass spectrometry is considered the most precise analytical technique for the characterization of ions. The separation is based on the mass of ions and can be used for identification and quantification of species, or to provide mass-selected gas-phase ions for further analysis using compatible analytical methods. This also includes fragmentation experiments and ion-molecule reactions, which can be used to uncover mechanistic details. The combination of a multitude of ionization methods and mass analyzers leads to high flexibility and adaptability. Of especially high importance are ionization methods capable of handling liquid sample solutions at atmospheric pressure, which is the requirement for performing in-situ experiments. First among those is the electrospray-ionization mass spectrometry.² This soft ionization method transfers ions from solution into the gas phase with minimal fragmentation and has for example already been utilized to investigate charged intermediates in reactions catalyzed by metal complexes, on whose basis a catalytic cycle was hypothesized.³

Whether ESI-MS is suitable to monitor the species occurring during a reaction usually has to be decided on a case by case basis and depends on the reactants, the experimental conditions, and the used instrument. However, by systematically changing the species and conditions, general trends may be discovered, which may simplify future decisions regarding the optimal strategy when planning an analytical approach. Carbanions in particular seem suitable for this systematic approach, due to their wide range of reactivities and their significance in synthetic chemistry.

1.2 Mass Spectrometry

The most direct definition of mass spectrometry (MS) is the “study of matter through the formation of gas-phase ions that are characterized [...] by their mass, charge, structure, and/or physic-chemical properties”.⁴ In this function, MS is highly precise and sensitive. Able to detect the smallest of concentrations and often providing quantitatively accurate results, MS is widely used in a multitude of different applications. The versatility is increased by the availability of various techniques and concepts on which the instrument can be based. This holds true for both the ion generation and the m/z separation. In general, however, all mass spectrometers follow the same combination of components: An ion source provides the gas-phase ions, whose trajectories are stabilized and focused by the transfer optics, which then deliver the ions to the mass analyzer. When necessary, a pressure gradient is also applied in this region of the instrument, allowing for very low pressures inside the mass analyzer. There, in combination with a suitable detector, signal intensities are assigned to the individual m/z depending on the number of corresponding ions. The mass spectrum is then generated by interfacing the detector with a computer.

1.2.1 Ion Sources

The selection of the ideal ion source has to be made depending on the intended application, as they differ greatly in various attributes.⁵ The first aspect is the “softness” of the ionization method. A soft method generates, for the most part, gas-phase ions corresponding to the whole analyte molecule, ionized by the attachment or removal of small ions. Only a low amount of in-source fragmentation occurs. A hard method on the other hand leads to significant fragmentation.⁶ The fragment ion ratios can be used to identify the sample using common fragmentation reactions and databases. Hard ionization methods are generally only suitable for pure samples. Electron ionization (EI), the primarily used hard ionization method, is most often encountered as an EI-MS detector in gas chromatography.⁷ As in-situ analytical methods are primarily used to monitor changes in solutions due to reactions, a soft ionization method is preferred instead.

Another condition to be fulfilled by the ionization method to be suitable for in-situ analysis is a large dynamic range when attempting to detect intermediates, no ion suppression effects, and a linear signal intensity-to-concentration correlation. These factors depend on the ionization method, but also on the experimental conditions,

especially the concentration. The linear response should be investigated first when performing quantitative mass spectrometry.⁸

The final defining attribute of the ionization method is the state of the sample that can be processed. This also includes whether the ionization takes place at atmospheric pressure or in a region of reduced pressure.⁹ For in-situ measurements, an ionization method utilizing sample solutions directly and at atmospheric pressure is required. Most of the commonly used techniques are therefore unsuitable. Aside from being a hard ionization method, EI also requires gaseous analytes in a vacuum,⁷ similar to the soft method field ionization (FI).¹⁰ Field desorption (FD) ionizes a solid analyte while it is being desorbed from an emitter.¹¹ Matrix assisted laser desorption/ionization (MALDI) requires the analyte to be mixed into a solid matrix before being ionized by laser irradiation.¹² It is therefore not conducive to in-situ measurements, similarly to fast atom bombardment (FAB)¹³ and secondary ion formation (SI),¹⁴ in which a solid sample is ionized using an atom or ion beam, respectively.

Potentially suitable methods are liquid injection field desorption ionization (LIFDI),¹⁵ atmospheric pressure chemical ionization (APCI),¹⁶ and electrospray ionization (ESI),² along with variants like desorption ESI (DESI)¹⁷ or acoustic mist ionization (AMI).¹⁸ LIFDI is capable of transferring a sample solution directly to a FD emitter under inert conditions, where the solvent is evaporated and FD takes place.¹⁵ In APCI, the sample solution is nebulized before the solvent evaporates and the ionization takes place in the gas phase through ion-molecule reactions.¹⁶ Alternatively, UV irradiation is used instead in atmospheric pressure photoionization (APPI).¹⁹ LIFDI, APCI, and APPI may be used to generate mass spectra depicting the solution composition, but neither method transfers ions already present in the solution into the gas phase directly. For that reason, AMI, ESI, and DESI are favored in the context of in-situ mass spectrometry of carbanions directly from solution. Among those three, ESI is the most common method and the experimental setup is more amenable to inert conditions for potentially sensitive species.

In an ESI source, the analyte, dissolved in a polar solvent, is fed through the inlet line and into a conductive capillary called needle (**Figure 1**). A high voltage is held between the capillary and an aperture on a distant side of the ion source, which often takes the form of a metal-coated glass capillary. The voltage causes a charge separation. In the negative-ion mode, cations are collected on the metal walls of the needle, while anions are forced to

the surface of the solvent, forming a Taylor cone. Supported by a constant flow of a nebulizer gas, usually nitrogen, droplets carrying a charge excess are formed. These droplets may contain anionic analytes directly, or the neutral analyte accompanied by small anions that were added to the ESI solvent for the purpose of forming aggregates with the neutral analyte. An opposing flow of a heating gas, usually nitrogen as well, causes solvent evaporation and the formation of free ions, and prevents neutral particles from reaching the sensitive inside of the mass spectrometer. Part of the anions reaching the positively charged coating are oxidized while the cations on the walls of the needle are reduced, but the remaining anions continue onward to the transfer optics, directed by an electrical field gradient inside the glass capillary.²⁰ For DESI and AMI, the general principles are similar. In DESI, charged microdroplets generated by conventional ESI are aimed at the sample, generating secondary droplets containing the analyte.¹⁷ AMI utilizes sound instead of a nebulizer gas to form charged droplets in a high-field area.¹⁸

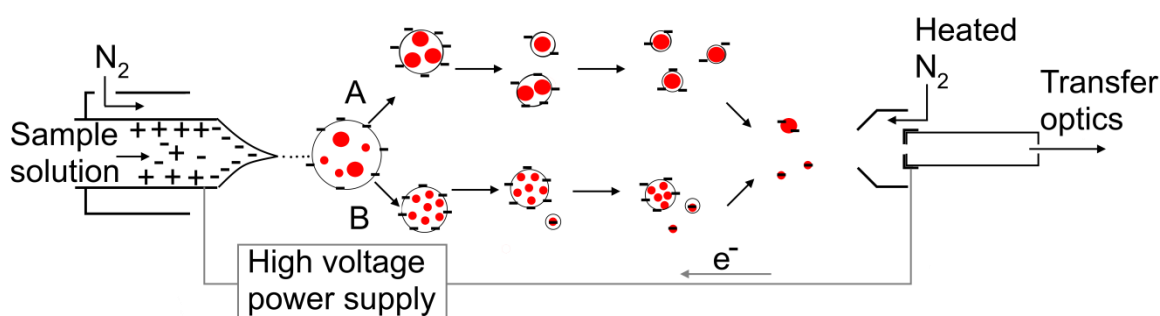


Figure 1: Schematic design of an electrospray-ionization source setup, including the charged residue model (A) and the ion evaporation model (B) for the generation of single gas-phase ions from neutral analytes (red). Anionic analytes may constitute part of the excess charge of the microdroplets instead.

The discussion regarding the exact processes leading from charged droplets to free ions in the gas phase led to two major models that are widely accepted. According to the charged residue model, the droplet size decreases until the Coulomb repulsion overcomes the surface tension of the droplet. The maximum charge for droplets of a defined size is also called the Rayleigh instability limit. Once this point is reached, smaller, highly charged droplets are released. This process repeats itself until the droplets carry at most a single analyte molecule, which is then released into the gas phase by evaporation of the remaining solvent.^{21,22} This model is preferred for the ionization of large analytes.²³ The formation of smaller droplets is usually indicated as coulombic fission, through the mechanism may include the formation of another Taylor cone at the location of the largest curvature.^{24,25}

In the ion evaporation model, the initially formed droplets reduce in size due to solvent evaporation as well, but for sufficiently small droplets, the Coulomb repulsion enables single solvated ions to leave the droplet before the Rayleigh limit is reached again. In contrast to the charged residue model, the rate for this to occur is strongly dependent on the physicochemical properties of the analyte ion through an exponential dependence on its solvation free enthalpy. Therefore, ion evaporation is the preferred model for low molecular weight analytes,²⁶ though only upon reaching very small droplet diameters of below 20 nm.²⁵ The offspring droplets are formed mostly by the outer layer of the parent droplet, so from the usual polar ESI solvents, hydrophobic analytes are transferred into the gas phase more efficiently than hydrophilic ones.²⁷ This tendency to be located closer to the surface of the droplet corresponds to the surface activity of the analyte.^{20,28}

1.2.2 Transfer Optics

Once the gas-phase ions enter the interior of the mass spectrometer, various components that together make up the transfer optics are responsible for handling the ions to ensure they reach the mass analyzer with minimal losses. This includes directing the ions onto an optimized pathway, controlling their velocity and reducing their spread in other directions, but also the removal of remaining neutral components that managed to pass the opposing flow of the heating gas during the ESI process. These processes serve to increase both transmission and sensitivity. The ion optics also facilitate the stepwise reduction in pressure necessary when working with ambient pressure ionization techniques like ESI.²⁹ Finally, the required ion handling may also include bundling a continuous ion flow into packages to enable pulsed operations of the mass analyzer when necessary.³⁰

Ions can be directed by applying either an electric or a magnetic field. Depending on their geometry, they serve different purposes.³¹ Electrostatic lenses can collimate an ion beam and influence the ions' velocity.³² In addition to this, skimmers and ion funnels in particular have a small aperture that enables differential pumping.³³ Multipoles, both electric and magnetic, consist of an even number of rods placed in a symmetric layout and serve as ion guides.³⁴ Depending on the application, other components may be used, such as a Wien filter, which uses both electric and magnetic fields to filter incoming ions depending on their velocity.³⁵

1.2.3 Mass Analyzers & Detectors

The mass analyzer is the central component of a mass spectrometer, as it is responsible for the separation based on the ions' m/z ratio. For this, different physical principles can be made use of, each having their own distinct advantages and disadvantages. These concern the available mass range, mass bias, accuracy, resolution, scanning speed and the potential to perform tandem MS.³⁶ MS/MS, synonym for tandem MS, provides mass spectra of mass-selected ions, usually after undergoing fragmentation or ion-molecule reactions.⁴ The type of detector needs to be compatible to the mass analyzer as well, which is why both will be covered in this section.

Two types of mass analyzer were used during this study. The first instrument was equipped with a three-dimensional quadrupole ion trap.²⁹ This design is based on the work of Wolfgang Paul, for which he was awarded a shared physics Nobel Prize in 1989.³⁷ The ion trap consists of a ring electrode and two end cap electrodes, arranged in a hyperbolic design (**Figure 2**). The end caps each contain an aperture through which ions can enter and exit the ion trap when necessary. The scanning process occurs in a pulsed fashion, though the trap itself is capable of collecting ions prior to analysis, so no such function is required from the transfer optics. During the accumulation, a radio frequency voltage in the ring electrode causes an electrical field in the storage space of the trap while the end caps are held at neutral. The resulting field effectively equals a potential well. Ions pass through the first end cap and enter the trapping potential, increasing the internal energy. Collisions with a bath gas inside the cell removes this energy, leaving the ions trapped inside the potential well. Usually helium of high purity is used for this purpose. By closing a gate lens once sufficient ions were accumulated, new ions are prevented from entering the ion trap during the later steps of the mass analysis.

The trapping potential depends on both the m/z of the ion and the radio frequency of the voltage, as described by the three-dimensional Mathieu equation. For similar reasons, the trapping potential has a lower mass cut-off. Once trapped, however, ions can be stored for up to multiple seconds. During scanning, the stability of ions inside the trap is then further influenced by an auxiliary field imposed by the end caps. By reaching resonance conditions for defined m/z , the ions are excited sequentially, leading to their ejection from the ion trap through the second end cap and their quantification by a Daly detector.^{29,38}

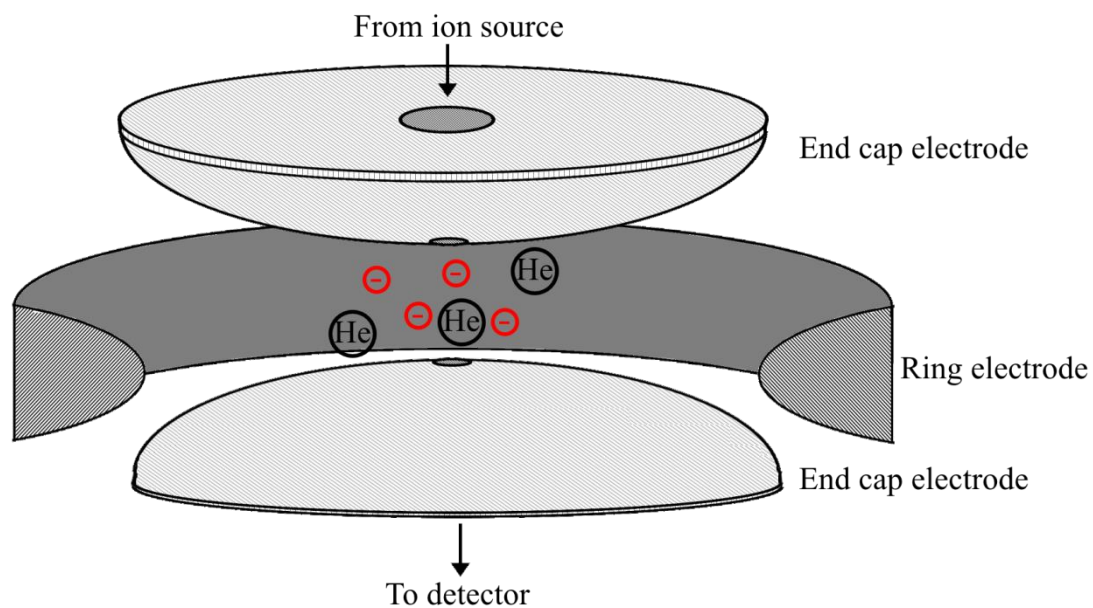


Figure 2: Schematic structure of a quadrupole ion trap.

The second mass spectrometer used in this study was equipped with a reflectron time-of-flight (TOF) mass analyzer. Instead of ejecting accumulated ions sequentially, a package of ions is injected into an extraction chamber, where an orthogonal voltage accelerates the ions to a defined kinetic energy. This results in a velocity depending on their m/z ratio. A detector located in a defined distance of a field-free drift tube then registers the impacts depending on the time after the acceleration, with the lighter ions arriving earlier due to their higher velocity. By including an ion mirror between the acceleration area and the detector, the flight time is increased and differences due to the ions' initial kinetic energy and position within the acceleration area are mitigated, allowing for better mass accuracy (Figure 3).³⁹

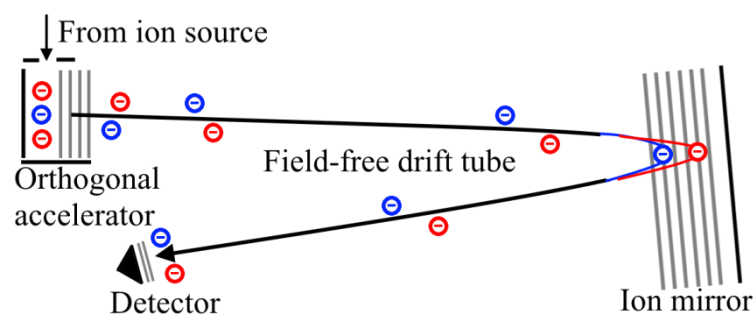


Figure 3: Schematic design of a reflectron TOF mass analyzer. The ion mirror allows ions with the same m/z , but higher (red) or lower (blue) initial velocity in direction of the acceleration to reach the detector at the same time.

1.2.4 Fragmentation Experiments

Fragmentation can occur during the ionization process and is either intentional when using a hard ionization method or unintended when using a soft technique.⁴⁰ The energy that is taken up by the ions can be estimated by analyzing a series of similar ions that contain a predetermined breaking point of varying stability and comparing the ratios of precursor and fragment ions.⁴¹ Generally though, fragmentation experiments are performed during tandem MS with isolated, mass-selected ions instead, in a step separate from the ionization process. Usually they are performed to increase the amount of structural information that can be gained from the gas-phase ions, though they may also help to prevent isobaric interference when quantifying ions with known fragmentation patterns.⁴² Not every mass analyzer is capable of inducing fragmentation, so in those cases, two analyzers may be connected for a tandem mass spectrometer.⁴³ The first one mass-selects the ions of interest and transfers them to a collision cell, where they are accelerated before colliding with a neutral gas. The fragments are then analyzed by the second, more accurate mass analyzer.³⁰

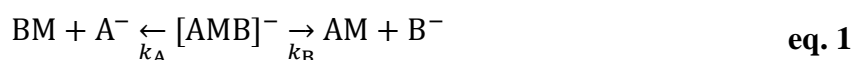
Three-dimensional quadrupole ion traps are capable of direct fragmentation experiments, which is one of their largest advantages over other instruments.⁴⁴ A target ion is mass-selected by ejecting most ions as usual while scanning, though skipping the resonance frequency that would eject the target mass. Afterwards, the ion is excited using the same resonance frequency at lower amplitude than is used for ejection. Through collisions with the helium contained within the ion trap, the internal energy of the target is gradually increased until it has accumulated enough to result in fragmentation. This process is known as collision-induced dissociation (CID). The fragments, usually containing relatively low internal energy, are then trapped by the potential well. Efficient resonance of the target ion requires a suitable potential on the ring electrode depending on the m/z of the target. This leads to an increased lower mass cut-off according to the Mathieu equation, with the optimal settings resulting in the cut-off being 27% of the precursor ion m/z .²⁹

The captured fragment ions can be ejected from the ion trap, performing the regular scan that results in a full mass spectrum, or they may be mass-selected and subjected to another round of CID. Experiments containing one fragmentation cycle is an MS/MS or

MS² experiment, while multiple cycles result in an MSⁿ experiment. This option is often not available to tandem mass spectrometers.

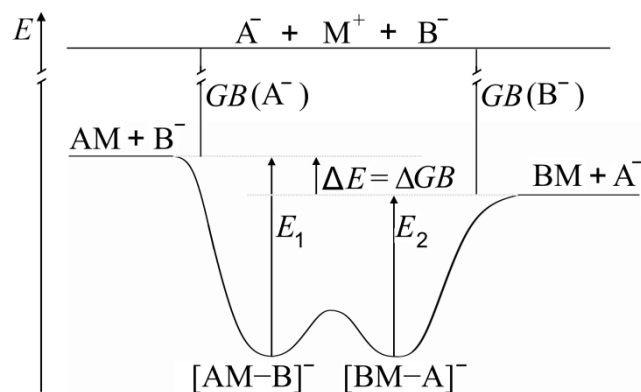
1.2.5 Kinetic Method

The kinetic method is a special experimental setup utilizing mass spectrometry and fragmentation experiments in order to determine thermodynamic parameters of gas-phase association reactions. The methodology was initially designed by Cooks in 1977 and has been improved upon since then.⁴⁵⁻⁴⁷ It is a relative method rather than an absolute method, so in order to obtain thermodynamic data on an absolute scale, already known species have to be used as references. This method is based on the fragmentation of heteroleptic complexes of the type [A-M-B]^{+/-}. Most commonly, M is a proton or another small cation, with A and B being neutral molecules, but anionic A and B or an anionic M with neutral or positive A and B are also possible. By supplying sufficient energy to this complex, smaller fragments are released. The fragments depend on the combination of charges in the initial complex, forming the free ions A^{+/-} and B^{+/-} (e.g. **eq. 1**) or, if A and B are neutral, the adducts AM^{+/-} and BM^{+/-}.



The ratio in which these ions are formed is highly dependent on the relative association energy towards M and the internal energy of the complex during the fragmentation, usually indicated by an effective temperature T_{eff} , which is formally not a temperature as the gas-phase ions do not follow a Boltzmann distribution, but instead corresponds to the temperature that would lead to the same product ratios.⁴⁸ By utilizing at least two similar calibrant species B_n , both the unknown T_{eff} and the absolute affinity scale can be anchored when fragmenting complexes of both with the same substrate A.

The product ratios can be linked to either the gas-phase affinity towards M, which is the negative enthalpy of the association reaction $\text{A}^- + \text{M}^+ \rightarrow \text{AM}$, or to the gas-phase basicity, which is the negative free energy of the same reaction, depending on assumptions and experimental details. For the initial derivation of either consideration, though, the same energetic scheme is used (**Scheme 1**). For the heteroleptic complex' potential surface, a double well potential with a negligible barrier in between is assumed.^{49,50}



Scheme 1: General energy diagram for the dissociation of a heteroleptic ionic complex of the type $[A-M-B]^-$ into a neutral salt and an anion.

In the initial experiment, the fragment ratios were correlated to the gas-phase affinity,⁴⁶ though today the derivation includes entropic components.⁴⁷ Independently from E_1 and E_2 , the fragment ratios can be equated to the difference in gas-phase basicity GB between A and B (**eq. 2**). As no relevant barriers need to be crossed along the reaction coordinates, the energies E_1 and E_2 can be treated as the activation energy of an Arrhenius equation (**eq. 3**).⁵¹ The ratio between the rate constants k , which in the case of irreversible fragmentation also corresponds to the ratio of the signal intensities I , is thereby linked to the difference in gas-phase basicity. The pre-exponential factor $A_{\text{Arrhenius}}$ is approximately equal for both reaction pathways, resulting in the displayed equation (**eq. 4**, molar units).

$$\Delta E = \Delta G_f(\text{BM}) + \Delta G_f(\text{A}^-) - \Delta G_f(\text{AM}) - \Delta G_f(\text{B}^-) = \Delta GB \quad \text{eq. 2}$$

$$\ln k_B = \ln A_{\text{Arrhenius}} - E_1/kT_{\text{eff}} \quad \text{eq. 3}$$

$$\ln k_B/k_A = \ln I_B/I_A = \Delta GB/RT_{\text{eff}} \quad \text{eq. 4}$$

When performing the experiments with a series of similar reference substrates B_n , the logarithmic intensity ratios can instead be written as a linear dependence of the known gas-phase affinity toward M (**eq. 5**). The term ΔG_M^{app} was introduced as an apparent affinity by Fenselau and contains both the target gas-phase affinity and a relative entropy term.⁵² It is obtained from the x -interception in a linear regression of the logarithmic intensity ratios against the reference gas-phase affinities. T_{eff} is obtained from the slope.

$$\ln I_{B_n}/I_A = \frac{\Delta H_M(B_i)}{RT_{\text{eff}}} - \frac{\Delta G_M^{\text{app}}}{RT_{\text{eff}}} \quad | \quad \Delta G_M^{\text{app}} = \Delta H_M(A) - T_{\text{eff}} \cdot \Delta(\Delta S) \quad \text{eq. 5}$$

The entropic term represents the difference between the substrate A and the average of the references B_n , which holds reasonably true for sufficiently similar reference structures. By varying the fragmentation energy, the internal energy of the complex can be changed. Plotting ΔG_M^{app} against T_{eff} , obtained from the slope, affords the separated enthalpic and entropic terms. This modification of the basic kinetic method was termed the extended method and is the overall preferred application today.⁵² If no change in the apparent affinity is observed upon increasing the internal temperature, the entropic differences are negligible and the apparent affinity equals the thermodynamic gas-phase affinity towards M. The first example of using multiple collision energies to differentiate entropic influences, later termed the authenticated method,⁵³ was applied by Cooks and Fulford roughly 10 years before the first application of the extended method.⁵² The accuracy of the extended method has been discussed over the years, with the general consensus being that the kinetic method provides accurate and easily accessible results, but only if entropic contributions are considered and determined when applicable.⁵⁴

As mentioned earlier, the most common application of the kinetic method is focused the determination of proton affinities of neutral molecules.⁵⁵ Other research focused on the proton affinity of anions⁵⁶ or affinities of neutral molecules towards alkali metal cations.⁵⁷ For inversed charges, bridging small anions like halides⁵⁸ or electrons⁵⁹ have been investigated, the latter being another way to determine electron affinities.

No matter the example, they all share a need for accurate reference compounds. By referencing results obtained from relative methods, whole ladders and rankings have been established, which at some point were based on thermodynamic values obtained from absolute methods. For less explored combinations, such as two anions bridged by a non-proton cation, reference values are usually not available and absolute methods may not be applicable to determine them. In those cases, quantum-chemical calculations may provide answers whose relative accuracy can be verified experimentally. One such case was published recently by Gal, in which the gas-phase alkali metal cation affinity and basicity of various benzoate anions were calculated and the quality of the relative values verified by the kinetic method.^{60,61}

1.3 Reactive Anionic Species

According to IUPAC recommendations, a species is considered to be reactive, when its rate constant for a specified reaction is larger than that of a reference compound.⁶² That means it is both a kinetic and a relative terminology. However, when talking about reactive species in a practical context, quite often neither the reaction nor the reference are specified. In those cases, “reactive” depends on the context and may indicate a short lifetime and/or a high susceptibility to impurities like oxygen or water.

For anions, the most common types of reactions are based on nucleophilicity, basicity and redox potentials. In a simple approximation, the reactivity is governed by the difference in stability between reactant and product, which can often be roughly predicted based on inductive and mesomeric effects. In general, a high delocalization of the negative charge results in less reactive anions. At the same time, the element on which the charge is primarily located on or steric considerations strongly influence the reactivity. These effects depend more strongly on the specific reaction than the charge delocalization, as indicated for example by the “hard and soft acids and bases” (HSAB)⁶³ concept. Similarly, the diisopropylamide anion is a strong base, so highly reactive towards protonation, but a weaker nucleophile due to the steric hindrance.⁶⁴

In order to quantitate reactivity, different metrics can be utilized. The most simple system is based on the equilibrium constant of the reversible (de)protonation reaction $AH \rightleftharpoons A^- + H^+$ in a specified solvent, the pK_a . This value is often determined from water, though this is not possible for very weak acids, for which other solvents are utilized. More common solvents are DMSO⁶⁵ or MeCN⁶⁶, for which large databases are available, but also alcohols, ethers or water mixtures were investigated. Efforts have been made to predict the pK_a of species in different solvents.^{67,68}

The prediction of nucleophilicity is less straight-forward due to the large number of different viable electrophiles. Successful reactivity scales include a purely empiric approach of measuring the kinetics of a multitude of reactant combinations, then generating electrophilicity and nucleophilicity parameters based on a least-squares basis,⁶⁹ the calculation of philicity parameters by density functional theory (DFT),⁷⁰ and a focus on the nucleophiles' highest occupied molecular orbital (HOMO) energy.⁷¹

For redox reactions, the direct measurement of the potential using cyclic voltammetry (CV) is sufficient to differentiate the reactivity as well as predict the number of electrons typically being transferred.⁷² However, results from CV do vary with the solvent, the working electrode material and other experimental conditions. As there is no unified standard regarding CV experiments, small deviations should be expected and accounted for when comparing species.⁷³ The second option for quantitating the reactivity towards redox reactions is the electron affinity (EA). Defined for the gas-phase electron attachment reaction, this thermodynamic parameter can sometimes be determined by the kinetic method as described in chapter 1.2.5.⁵⁹ Other methods include various forms of spectroscopy upon the attachment⁷⁴ or emission⁷⁵ of an electron and similar measurements based directly on that reaction.⁷⁶

Among the most reactive species commonly utilized in synthetic chemistry are lithium organyls, featuring extreme basicity.⁶⁵ Besides as strong bases, these simple carbanions can also be used for alkylation reactions⁷⁷ and were even reported to decay fast in comparatively inert solvents like THF.⁷⁸ On the other end of the basicity scale of carbanions are carbon acids carrying two or even three electron-withdrawing groups (EWGs) such as cyano or carbonyl groups, reaching single-digit pK_a values.⁷⁹ While technically still carbanions, these species mostly react as enolates or similar anions due to their functional groups' significant $-M$ -effect. A similar phenomenon of drastically increasing the acidity is caused by the resonance energy of completing the aromaticity of suitable ring systems such as cyclopentadienide or indenide.⁸⁰ By variation of the chemical environment, carbanions can thus be anything between stable and highly reactive and often occur as educts or intermediates in a multitude of reactions (**Figure 4**).

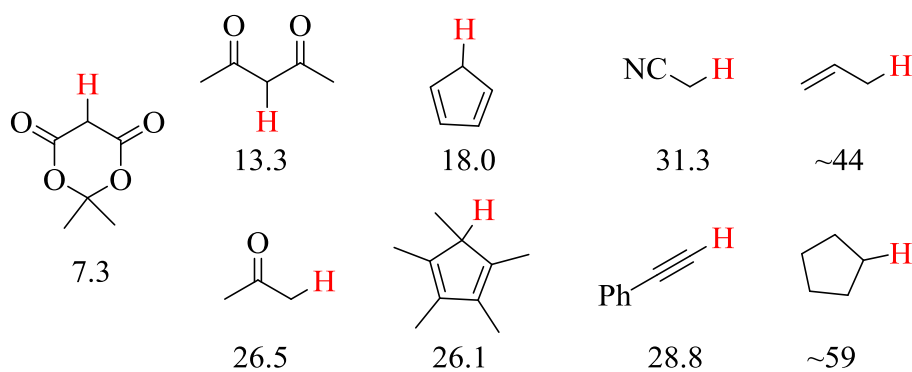
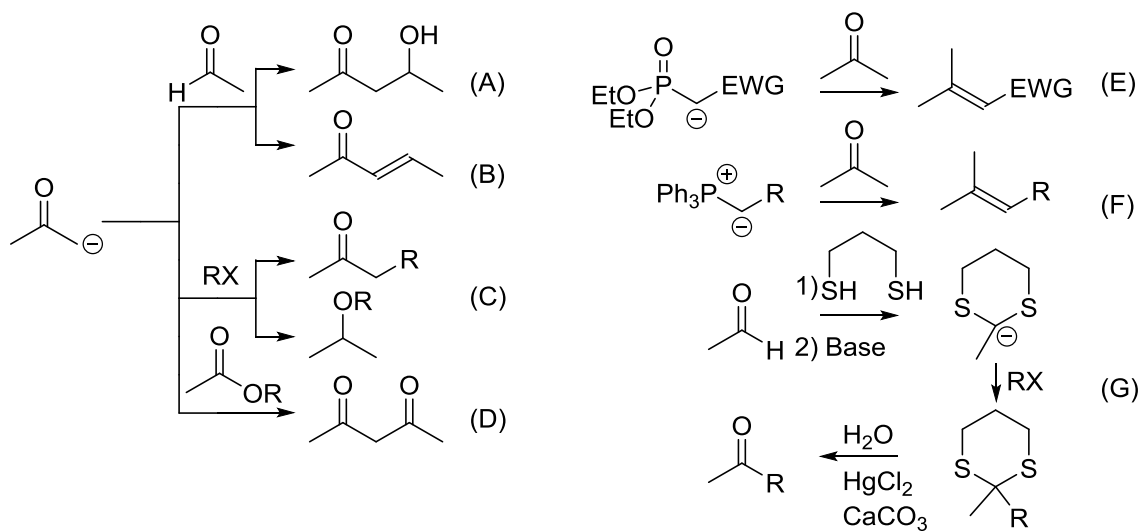


Figure 4: Various carbon acids and their pK_a values in DMSO.^{65,79-83}

The preparation of the various carbanions depends on the required reactivity, selectivity and the presence of other functional groups that may be affected by the activation. The most direct way is the deprotonation of a carbon acid containing suitable EWGs (**Scheme 2**). The formation of an enolate is the first step of metal-free aldol type reactions,⁸⁴ but they can also act as general nucleophiles for alkylation⁸⁵ or acylation⁸⁶ reactions. The base can be used catalytically or stoichiometrically, such as during the Claisen condensation.⁸⁷ Other carbanion intermediates formed by the direct deprotonation are found for example during the Horner-Wadsworth-Emmons reaction. In this particular case, the acidity of the neutral species is increased by the incorporation of a phosphonate.⁸⁸ Alternatively, the addition of a phosphine generates the phosphonium salt, which can once again be deprotonated to form a zwitterionic ylide as is used for the Wittig reaction.⁸⁹ Other types of ylides can be formed in a similar fashion. Another option to generate carbanions is to use polarity inversion to enable the abstraction of an otherwise unreactive proton, such as through the reversible formation of a thioacetal from an aldehyde during the Corey-Seebach reaction.⁹⁰ Polarity inversion is also employed to provide some of the most basic carbanions. For example, by mixing the halide with suitable metals, lithium organyls⁹¹ or Grignard reagents⁹² are generated.



Scheme 2: Examples for the reactivity of carbanions. A: Aldol addition. B: Aldol condensation. C: Alkylation/Acylation. D: Claisen reaction. E: Horner-Wadsworth-Emmons reaction. F: Wittig reaction. G: Corey-Seebach reaction.

The lifetime of these carbanions that are commonly encountered during synthetic organic chemistry is in many cases sufficient to detect and analyze them directly using various methods, spectroscopic or otherwise. Other reactions contain carbanions as short-lived

intermediates, such as enolates in protic solvents with lifetimes of $10^{-9} - 10^{-11}$ s.^{93,94} Examples of highly reactive carbanions being formed in solution are the Wolff-Kishner reduction⁹⁵ and the Shapiro-reaction⁹⁶. The stability of carbanions is heavily influenced by the coordination to metals. Lithium organyls tend to form larger aggregates,⁹⁷ which can be opened by the addition of complexing agents, increasing their reactivity.⁷⁸ Complexation by transition metals can increase the stability instead.⁹⁸

Radical anions are encountered less often during synthetic chemistry when compared to carbanions. The possibility of spontaneous electron detachment is present whenever the EA of a neutral species is negative or only slightly positive. As such, most organic radical anions are formed from mesomeric systems containing electronegative substituents or EWGs.^{99,100} Especially quinone-type species are of high relevance due to their tunability and extensive range of accessible EA and redox potentials.¹⁰¹ The single-electron reduction from benzoquinones to semiquinones has also been utilized during modern photoredox catalysis in particular, which is why the analysis of such species by as wide a variety of methods as possible is desirable.¹⁰² The conjugated system inherent to organic molecules able to form radical anions often also enables efficient light uptake, influencing the redox properties. This can be made use of in single-photon catalysis, in which the photoinduced excitement of the neutral organic catalyst enables a single electron transfer (SET) reduction through reductive quenching that would not occur otherwise.¹⁰³ Rather recently, examples of two-photon catalysis were reported, during which the radical anion is photoexcited once more in order to generate a highly reducing agent.^{104,105} The lifetime of excited states of photoredox catalysts after absorption of suitable light is measured in nanoseconds, decaying through fluorescence or various quenching processes.¹⁰⁶ Analytical methods are usually limited to various forms of spectroscopy, either in solution or in the gas phase.

1.4 Anionic Polymerizations

Synthetic polymers form a cornerstone of modern material science. They provide near endless options for variation and optimization based on the type and combination of monomers and the products mass distribution. In order to reliably produce polymers with well-defined properties, detailed knowledge of the reacting systems' kinetics is desirable. In most cases, the reactions leading to the formation of polymers can be separated into initiation, propagation, chain transfer and termination. The propagation describes the

addition of the next monomer to the growing chain. Chain transfer stops the growth of the current chain and starts a new one, keeping the total number of active chains constant but lowering the average chain length. Termination reduces the number of active chains, reducing the overall monomer consumption, unless fresh polymers are continuously provided by a sustained initiation reaction. A particularly high degree of manipulation is provided by controlled polymerization conditions. The requirements for that are a fast initiation reaction and no or slow transfer and termination reactions, both relative to the propagation.¹⁰⁷ For radical reactions, the termination by recombination can be sufficiently slowed by lowering the amount of active radicals through temporary deactivation by the reversible reaction with additives.¹⁰⁸ The true origin of controlled polymerization reactions, however, is found in living anionic polymerization.¹⁰⁹ When perfectly excluding all sources of impurities that may negatively interact with reactive anions, most importantly water and oxygen, this type of growing chain can have no termination reactions at all. The major benefits of preparing polymers in a living fashion are a constant growth speed, expressed in the linear increase in chain length, a narrow distribution of chain lengths and easy functionalization due to the reactive end groups.

The chain lengths of polymers are usually given as averages across all polymers of the sample. The average number of monomers per molecule is the degree of polymerization X_n . It is connected to the number-average molecular weight M_n by the molar mass of the individual monomers and the initiator (**eq. 6**). As some properties of the polymer depend directly on the individual size, the weight-average molecular weight M_w is an alternative display for the chain length (**eq. 7**). The ratio of M_n and M_w equals the polydispersity D of the polymer (**eq. 8**) and is often used to indicate the broadness of the mass distribution. A smaller polydispersity equals a more narrow distribution, with $D = 1$ being monodisperse, as is encountered for some biological polymers like enzymes. For ideal living polymerizations, the polydispersity follows a Poisson distribution.¹¹⁰

$$M_n = X_n \cdot M_{\text{Mono}} + M_{\text{Ini}} = \frac{\sum M_i \cdot N_i}{\sum N_i} \quad \text{eq. 6}$$

$$M_w = \frac{\sum M_i^2 \cdot N_i}{\sum M_i \cdot N_i} \quad \text{eq. 7}$$

$$D = M_w / M_n \approx 1 + \frac{X_n}{(X_n + 1)^2} \quad \text{eq. 8}$$

The vast majority of mass distributions are measured using size-exclusion chromatography (SEC), coupled to a suitable detector. Molecules are separated based on their hydrodynamic volume by a series of columns containing porous beads with different cavity sizes. Smaller molecules are able to enter a larger amount of cavities, retarding their progress through the column and therefore increasing the time required to reach the detector, whereas larger molecules can only enter the larger pores or in extreme cases bypass the beads completely. Suitable detectors are for example based on IR absorption or refractive index (RI) changes. For sufficiently large polymers, the properties of the end groups are negligible compared to the actual chain, resulting in the detector response to be based almost entirely on the monomer. The total amount of monomer passing by the detector to any specific retention time is recorded, independent of the number of molecules. The complete chromatogram affords the weight-average molecular weight directly, but the number-average can also be derived from the data.^{111,112}

SEC is a relative method, comparing the hydrodynamic volume of the sample polymer to the hydrodynamic volume of calibration polymers of known molecular weight. As the ratio of molecular weight to hydrodynamic volume depends on the intermolecular and intramolecular interactions based on the type of monomer, other analytical methods may be required to adjust for this difference. One option for this would be nuclear magnetic resonance (NMR) spectroscopy, in which the intensity of selected signals of the monomer are compared to the intensity of an end group signal, affording M_n . Alternatively, the post-separation SEC solution can be passed directly to an ESI mass spectrometer or other analytical instrument in order to assign exact masses to the retention times.¹¹³ Still the IR or RI intensities are used for the final spectrum due to those being more reliable for the quantification of polymers.¹¹⁴

MS is a strong and versatile tool for the analysis of polymers due to the ability to easily differentiate end groups. It has for example been used to differentiate the relative initiation efficiency of various photoinitiators¹¹⁵ or to investigate post-polymerization modifications.¹¹⁶ Limiting the amount of species to similar masses by coupling MS to SEC increases the accuracy.¹¹⁷ However, the reason why MS is rarely used as the sole analytical method to determine the mass distribution of polymers, despite theoretically affording quantitative results, is the common occurrence of mass bias effects. Aside from effects inherent to the type of mass spectrometer in general, the largest issue is a chain-length dependent ionization. Different surface activities and an increasing number of

functional groups that can form adducts or be (de)protonated influence the ionization efficiency, though the extent depends on the ionization method.¹¹⁸ These differences also extend to a differing amount of multi-charged species, which is further favored by a larger possible distance between two charges in the same molecule. Other aspects during the ionization process may also be different, such as the release of the charged analyte from microdroplets during ESI-MS, though such effects are case-specific and difficult to predict. Nevertheless, MS for polymers was attempted over the years with varying amounts of success. The usually most suitable instrument utilizes a matrix-assisted laser desorption/ionization (MALDI) ion source with a TOF analyzer, though other methods have been applied as well.¹¹⁹ Both MALDI and TOF are suitable for rather high masses. Other requirements to the instrument pertain the softness of the method (as polymers usually share common fragment ions), a low amount of multi-charged species (for most applications), and a low mass bias. The latter can be influenced by calibration with internal standards and custom sample preparation steps.¹²⁰ A narrow mass distribution of the polymer increases the accuracy of MS, as mass bias becomes less significant.¹²¹

The successful application of ESI-MS to polymers would open up a series of advantages. For free polymerization processes, it would serve as a faster alternative to SEC, both in sample preparation and actual measurement time. More importantly, for living polymerizations or condensation polymerizations, in which the average molecular weight increases with time, the ability to perform in-situ measurements affords a new level of control over the reaction, facilitates kinetic measurements, and potentially reveals new mechanistic aspects of the growing chain. First steps in that direction have for example been taken by the groups of Chen, Metzger and Junkers.

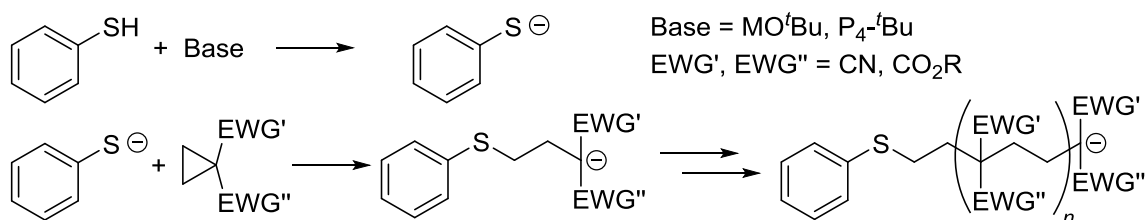
By coupling a microreactor to ESI-MS, Junkers was able to record the changes in the mass distribution by altering the residence time and the experimental conditions inside the microreactor for a reversible addition-fragmentation chain transfer (RAFT) polymerization of *n*-butyl acrylate.¹²² RAFT is a controlled radical polymerization method, exhibiting linear growth in molecular weight with time.¹²³ The polymer of sizes between 1100 and 2700 *m/z* was detected in positive-ion mode in form of Na⁺-adducts and was differentiated into those capped by the initiator and those capped by the RAFT agents leaving group. Calibration curves were recorded for the different types of polymer, though changes due to chain length were not considered explicitly.¹²²

Metzger similarly coupled ESI-MS to a microreactor, though one optimized for vastly shorter reaction times. Solutions containing ethylene and a methyl aluminoxane-activated zirconium-catalyst were mixed and, after a short reaction time, quenched through the addition of MeCN. Species corresponding to the active catalyst during a Kaminsky-type¹²⁴ single-site catalyzed polymerization were found. During fragmentation experiments, the active species was formed by eliminating the coordinating MeCN molecule. The reactivity was proven by ion-molecule reactions in the gas phase, in which ethylene was incorporated into the ion subsequently. Fragmentation behavior of different species was investigated and their reactivity with ethylene tested.¹²⁵

In early works by Chen, direct ESI-MS of catalytic solutions containing multiple palladium-catalysts and ethylene was used to screen for optimal reactivity. For this, the higher molecular weight products were isolated and fragmented, revealing a fragment characteristic for the most reactive catalyst.¹²⁶ Later they also fit reaction rates to the MS mass distribution, obtaining rate constants for initiation, propagation and transfer reactions.¹²⁷ With a polydispersity of ~ 2 , the mass distribution obtained from MS could be expected to be significantly biased. However, they were likely aided by one particular effect, even though it is not explicitly stated: Every active polymer carries exactly one permanent charge throughout the reaction. The polymers need not be ionized during the ESI process, which would introduce significant bias dependent on their chain length. Other mass bias effects likely still affect the results, including the transfer from solution to gas phase, but the accuracy of the resulting mass distribution is expected to have been significantly improved.

Aspects of this thesis were based on the prospect that a persistent charge throughout the polymerization process enables at least an approximate analysis of the mass distribution. Suitable reaction systems are anionic, cationic and, depending on the active species, some coordinative polymerizations, provided that transfer and termination reactions are sufficiently slow compared to the propagation. Furthermore, the accessible systems are limited in their reactivity by the available mass range and, most likely, by their susceptibility towards impurities. The conditions required for living anionic polymerization of olefins are unlikely to be achievable when linking the reaction flask directly to a mass spectrometer. In the context of potential carbanionic polymers, Penelle has performed extensive work on the ring-opening polymerization of monomers based on 1,1-disubstituted cyclopropanes featuring two EWGs. His research includes an optimized

strategy to enable effective anionic polymerization,¹²⁸ as well as an improved monomer synthesis that removes traces of reactant, which may otherwise serve as a transfer agent.^{129,130} The polymerization strategy consists of the initiation by thiophenolate with an alkali metal cation or a large phosphazene cation as the counterion in THF as solvent at a temperature of 60 °C. Earlier iterations included DMSO as the solvent, which allowed temperatures of 80-130 °C, reducing the time required for full conversion. The product polymer achieved chain lengths of up to $X_n = 200$.¹²⁸ During the polymerization, comparatively stable carbanions reminiscent of methylmalonate ($pK_a \approx 18$)⁷⁹ are formed, which are resistant to common impurities that terminate most anionic polymerizations. The anionic functionality remains throughout the polymerization, showing no transfer or termination reactions, while being amenable to easy end-group functionalization, for example by alkyl halides (**Scheme 3**).¹³¹



Scheme 3: Anionic ring-opening polymerization of 1,1-disubstituted cyclopropanes initiated by thiophenolate anion (PhS[⊖]).

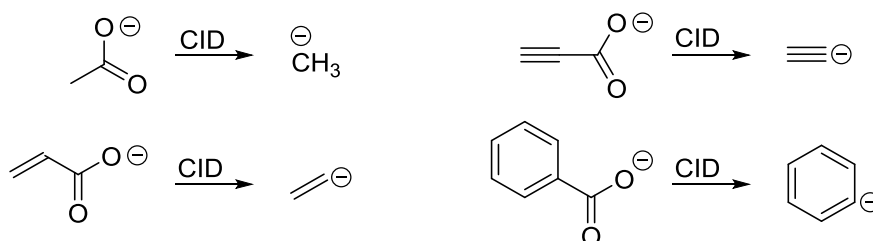
The polymer itself consists of propane subunits, breaking away from the majority among polymers of ethylene subunits due to their accessibility through modified ethylenes. The high density of functional groups that can easily be altered further allows for specialized polymers.¹³² In this, they resemble products derived from cyanoacrylates or methylenemalonates, though the slower propagation affords a higher level of control and favors lower average molecular weights.¹³³ This reduced reaction rate potentially makes them ideal candidates for an exemplary in-situ investigation of an anionic polymerization by ESI-MS.

In regards to metal-coordinated polymerization reactions, the examples by Metzger¹²⁵ and Chen^{126,127} provide a solid base for further explorations into the topic. One potential example is the integration of multiple units of isoprene into cobaltate catalysts generated by the reaction of CoCl₂ with lithium organyls or Grignard reagents observed by Kreyenschmidt and Koszinowski.¹³⁴

1.5 Mass Spectrometry of Reactive Anionic Species

Previous works on reactive species analyzed by MS can be divided in those detected from solution, produced during the ionization process and those intentionally generated through fragmentation experiments or similar gas-phase reactions. In almost all cases, the intention was to analyze the behavior of the gas-phase ion, for example by performing equilibrium measurements to determine gas-phase basicities, performing spectroscopic experiments, or observing rearrangement or ion-molecule reactions free from solvation, aggregation, and counterion effects.

One of the easiest methods of generating even highly reactive carbanions is the decarboxylation of suitable precursors. Carboxylates can easily be generated by deprotonation and transferred into the gas phase by conventional ionization sources. Once there, CID can be used to generate even pure alkyl anions (**Scheme 4**).^{135,136}



Scheme 4: Decarboxylation for the generation of gas-phase carbanions.¹³⁷

The reverse reaction was used to differentiate between isomers of substituted phenolate anions in the gas phase.¹³⁸ Alternative pathways such as the removal of a trimethylsilyl group in ion-molecule reactions by gas-phase fluoride anions were explored for cases where the decarboxylation was accompanied by rearrangement.¹³⁹ In other cases, the intramolecular reactivity itself was subject of the study.¹⁴⁰ Similar strategies of decarboxylation or silyl abstraction were applied to generate carbon-based radical anions.^{141,142} The additional electron was lost either spontaneously or via reaction with elementary fluorine.

An alternative method to generate radical anions is through direct attachment of a low-energy electron. Requirement is a positive EA and a lifetime that is long enough to enable stabilization through collisions or photon emission. Energy can also be lost through dissociative processes, such as the dissociative electron attachment to N₂O, forming the oxygen radical anion O^{•-}.¹⁴³ This ion is then able to perform ion-molecule reactions and

can produce new radical anions by abstracting a proton together with a hydrogen atom.¹⁴⁴ Alternatively, the molecular oxygen radical anion $O_2^{\bullet-}$ can transfer the electron directly to neutral substrates.¹⁴⁵ The targeted generation of $O_2^{\bullet-}$ is utilized in negative-ion mode atmospheric pressure chemical ionization (APCI). It is the most efficient method to generate radical anions in the gas phase for species with higher EA than O_2 .¹⁶ Both electron capture and electron transfer are commonly used as fragmentation methods in biomolecular analysis.¹⁴⁶

In some cases, ESI-MS was also reported to afford radical anions of the analyte directly. A notable example is tetrachloro-1,4-benzoquinone, whose solution in MeCN afforded a mass spectrum containing $M^{\bullet-}$ and a product formed upon reaction with water ($C_6O_3Cl_3^-$). The gas-phase ion was then analyzed by time-resolved photoelectron imaging.¹⁴⁷ The unsubstituted 1,4-semiquinone was generated starting from both benzoquinone¹⁴⁸ and hydroquinone,¹⁴⁹ indicating a reductive or an oxidative process respectively. The reduction was suggested to occur for analyte redox potentials of -0.8 V to $+1.0$ V vs SCE in CH_2Cl_2 .¹⁴⁸ The oxidative process is unexpected as the electric current applied during negative-ion mode ESI-MS suggests the reduction to occur exclusively. However, the authors gave evidence for the formation of $O_2^{\bullet-}$ during the ESI process due to corona discharge, which is the formation of plasma next to a highly charged conductor or electrode, at sufficiently high capillary voltages. While generally unwanted, in this case the ESI source was changed into a composite APCI-ESI by applying suitable conditions.¹⁴⁹ Corona discharge occurs more commonly for negative-ion mode ESI-MS than for positive-ion mode and is favored by a high capillary voltage, a high desolvation temperature, and increased distances between the capillary tip and both the nebulizer tube and the opposing MS inlet.¹⁵⁰ This process was suggested to also support the formation of the semiquinone anion starting from benzoquinone,¹⁵¹ though considering its reduction potential,¹⁵² a purely electrochemical generation should be possible.

Previous studies on reactive species and intermediates directly from solution are for the most part limited to metal-bound complexes, with a focus on determining previously unknown intermediates and confirming hypotheses. This is especially helpful for metals that change their oxidation state throughout a catalytic cycle, which can often be assigned by MS. Tandem MS can help elucidate their microscopic reactivity. The complexes often carry highly basic ligands, such as alkyl, allyl or phenyl anions. Examples are the works by McIndoe¹⁵³, Chen^{126,127} and the Koszinowski working group.^{134,154-157}

For metal-free species, occasionally carbanions and other reactive anions were assigned in ESI mass spectra,¹⁵⁸⁻¹⁶¹ but no targeted attempt had been made to investigate the scope and limitations of generating such species directly from solution. Only very recently and in parallel with this work was the detection of carbanionic intermediates during suitable reactions by desorptive ESI (DESI) reported.¹⁶² Aliquots of a reacting solution were placed on a glass slide and bombarded with negatively charged water droplets from an ESI source (**Figure 5**). The resulting secondary droplets generated by this impact proceed to provide gas-phase anions similar to the regular ESI process. The investigated species include enolates, an acetylide and trichloromethanide. The decrease in reactant concentration with time was in some cases represented by the resulting DESI-MS ion intensities, though the sample preparation of taking aliquots at defined times conflicts with the advantages usually provided by in-situ measurements. The signal intensity profile reaching a maximum after minutes was interpreted as showing the intermediacy of the carbanion, though when considering the lifetime of enolates in water, the timeframe seems odd. A distinctly non-zero baseline of the same species in control experiments instead indicates proton transfer taking place in the gas phase, where the proton affinity of hydroxide anions is comparatively large.¹⁶³ As such, the limitations of detecting carbanionic species directly from solution are as of yet unknown.

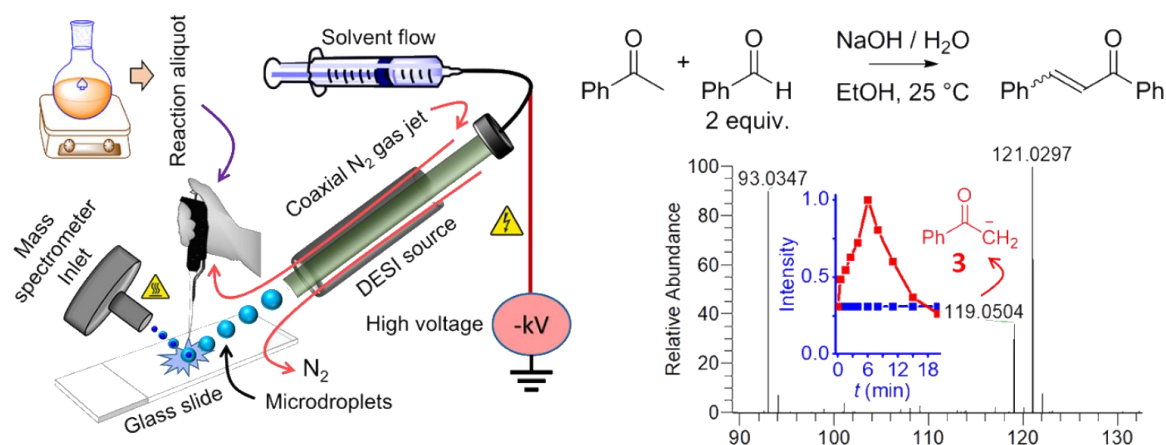


Figure 5: Experimental setup for capturing reactive carbanions using DESI (left) and mass spectrum taken from aliquots during the reaction of benzaldehyde and acetophenone in the presence of base (right). The inset represents the time course of the signal intensity of the deprotonated acetophenone anion during the reaction (red) and control experiment (blue). Reprinted with permission from Ref. 162. Copyright 2022 American Chemical Society.

2 Objective

Electrospray-ionization mass spectrometry (ESI-MS) enables in-situ measurements, which have the potential to provide fast, reliable, and detailed information about reacting solutions. However, the reliability and limitations when attempting to analyze small carbanions, many of which are highly reactive, have not been tested systematically. In this work, the detection of carbanions and carbon-based radical anions directly from solution will be investigated in order to identify the conditions, regarding both the structure of potential analytes and external factors like solvent, counterion, and additives, which facilitate or prevent the successful in-situ analysis. All experiments were conducted using a standard ion trap mass spectrometer with no custom alterations, making the conclusions more applicable to other working groups.

Based on the results, exemplary applications will be demonstrated. Starting with a simple system, rate constants for a Michael addition reaction will be determined by a direct kinetic investigation of the reacting solution. For more complex systems, the anionic oligomerization of ethyl 1-cyanocyclopropane-1-carboxylate and the coordination polymerization of isoprene on an anionic Co(I) complex will be monitored on-line, providing detailed data that is not available from alternative methods. This makes use of the ability of mass spectrometry to easily distinguish charged oligomers and provides rate constants depending on the chain length. Both systems contain persistent anionic species, avoiding a chain length-dependent ionization that is known to cause significant mass bias.

Slightly more removed from solution phase chemistry, an observed tendency to form aggregates containing two anions and one cation under the chosen experimental conditions will be made use of for the determination of alkali metal cation affinities for a series of carbanions by the kinetic method.

Finally, the potential of ESI-MS for in-situ measurements will be discussed in relation to other commonly applied analytical techniques.

3 Results and Discussion

3.1 ESI-MS for the In-Situ Detection of Carbanions

In the following, an attempt has been made to systematically identify the scope and limitations for the direct detection of carbanions from solution. In addition to the molecular structure of carbanions, and thereby their reactivity, external influences such as solvents or preparation methods have also been examined.¹⁶⁴

To ensure an easy adaption of the method by other working groups, no specialized or unique features, setups or preparation were used beyond those available to regular laboratories. All experiments were performed using a non-specialized, commercial mass spectrometer featuring an ESI ion source and a 3D ion trap mass analyzer. Techniques that were used are Schlenk techniques using argon as protective gas, as well as pressurized sample infusion (PSI)¹⁶⁵ when performing time-dependent experiments.

The highest reactivity among carbanions is usually shown by simple alkali metal organyls, acting mostly as strong bases but also as nucleophiles.^{65,77} Previous work in this group has shown that free alkyl anions or those bound by simple alkali metals cannot be detected directly from solution. In order to find the threshold between detection and non-detection, a total of 15 carbon acids have been chosen (**Figure 6**), using their pK_a (in dimethylsulfoxide, DMSO) as a likely indicator of reactivity and detectability. The pK_a range covers 18 orders of magnitude with a maximum at 29.5 and includes species with one electron-withdrawing group, those with two such groups, and those forming aromatic compounds upon deprotonation.

The general procedure was to prepare a 2-mM solution of the carbon acid AH in acetonitrile (MeCN), then deprotonating by addition of 1 equivalent of potassium *tert*-butoxide (KO^tBu) as a solution in tetrahydrofuran (THF). The pK_a of HO^tBu in DMSO is 32.2,¹⁶⁶ which can be expected to be sufficiently high to deprotonate all of the chosen carbon acids completely or at least mostly. Slight deviations might occur due to the differences between DMSO and MeCN, the latter of which has no sufficiently expansive collection of pK_a values available, and will be discussed where appropriate. No inversion of the acidity order is expected as both solvents are similarly polar aprotic.¹⁶⁷

* Results published in: N. F. Eisele, K. Koszinowski*, *J. Org. Chem.* **2021**, 86, 3750-3757

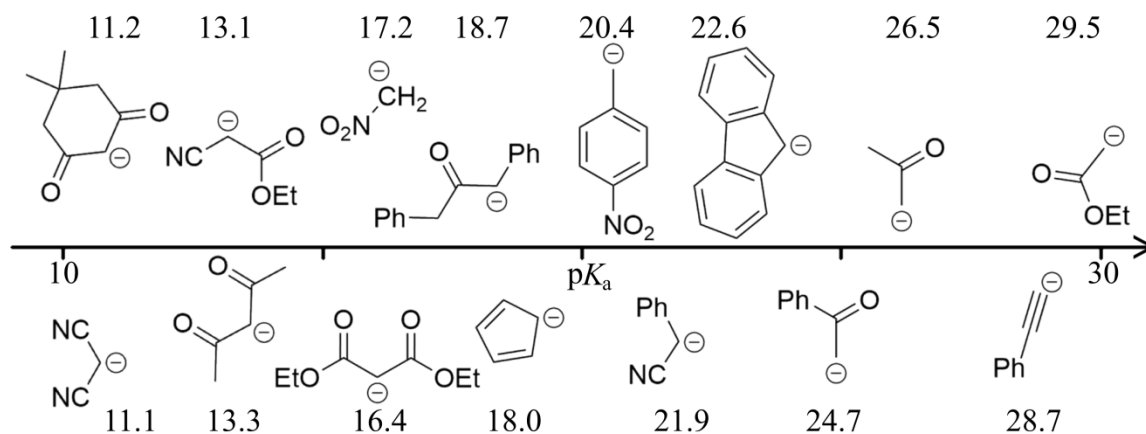


Figure 6: Carbanions, sorted by the pK_a of their corresponding acids in DMSO, whose detectability by ESI-MS was investigated.

The thus-prepared solution of a carbanion in MeCN was then infused into the ESI source of the mass spectrometer using a syringe pump and gastight syringes. The instrument settings were adjusted to a method that provides good signal intensities for small molecules and all samples were measured using the same settings (e.g. **Figure 7**, left). In order to reduce the counterion effect¹⁶⁸ and possibly increase the signal intensity of the free carbanion, the same experiment was repeated with the addition of 1 equivalent of the crown ether 18-crown-6 (18C6, **Figure 7**, right).

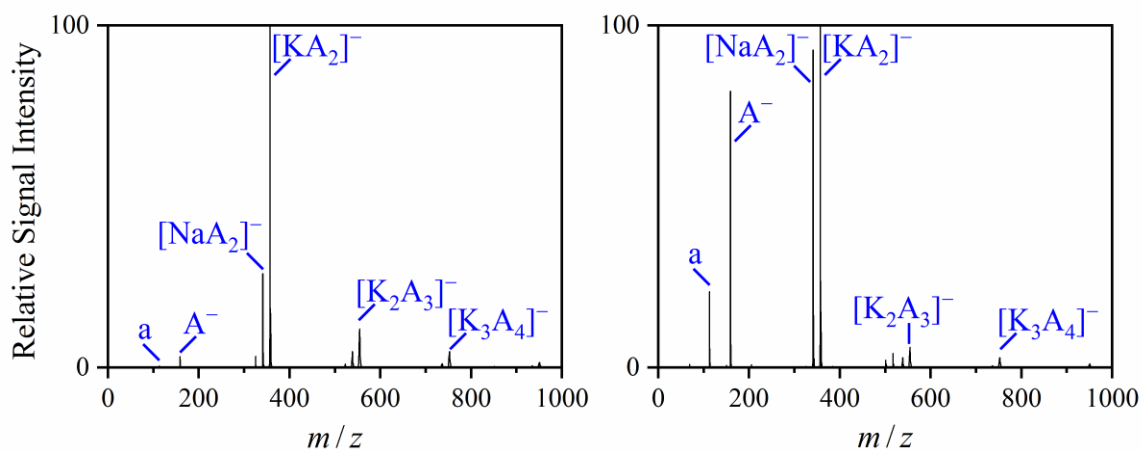


Figure 7: Negative-ion mode ESI mass spectra of 2-mM solutions of diethyl malonate (AH) / KOtBu in MeCN without (left) and with 1 equivalent of added 18C6 (right). a = $[A-EtOH]^-$.

The negative-ion mode ESI mass spectrum obtained from the solution of diethyl malonate with no added crown ether contained the free carbanion (m/z 159) in low signal intensity. The base peak was the aggregate formed from two carbanions and one potassium cation, $[KA_2]^-$ (m/z 357). Other signals mostly consisted of higher aggregates $[K_{x-1}A_x]^-$, as well

as sodium aggregates, but also a fragment ion after the loss of one ethanol unit, presumably from in-source fragmentation. The aggregates may already exist in solution, but their formation is also favored by the ESI process. The gradual evaporation of solvent from charged microdroplets formed in the spray process increases the effective concentration, shifting the equilibrium towards higher aggregates according to the mass action law.^{169,170} The presence of sodium aggregates is unintended, though not unexpected as sodium cations may for example have been taken up from the glassware.

The addition of 18C6 to the sample solution drastically increased the relative signal intensity of the free anion, while also reducing the relative amount of higher aggregates. No aggregates incorporating 18C6, such as $[(\text{KC}_{12}\text{H}_{24}\text{O}_6)_2\text{A}_2]^-$ (m/z 621), were observed. The ratio of sodium to potassium aggregates was also increased, in line with the higher affinity towards potassium of this particular crown ether, leaving a higher ratio of sodium in the remaining free cations that can be coordinated by the anion.¹⁷¹

The ESI mass spectra of the investigated carbon acids could be sorted into one out of three categories. One category contains mass spectra similar to that observed for diethyl malonate (**Figure 7**), featuring high signal intensities of the alkali metal-bound species. This was usually accompanied by a low but significant intensity of the free anion. The second category is composed of those species with high intensity of the free anion, but a low degree of aggregation (e.g. **Figure 8**, left). Finally, the third group shows a low signal intensity of both the free and bound carbanion, in most cases also featuring a high number of unknown species (e.g. **Figure 8**, right). The differences between the individual carbanions will be made apparent in the following section.

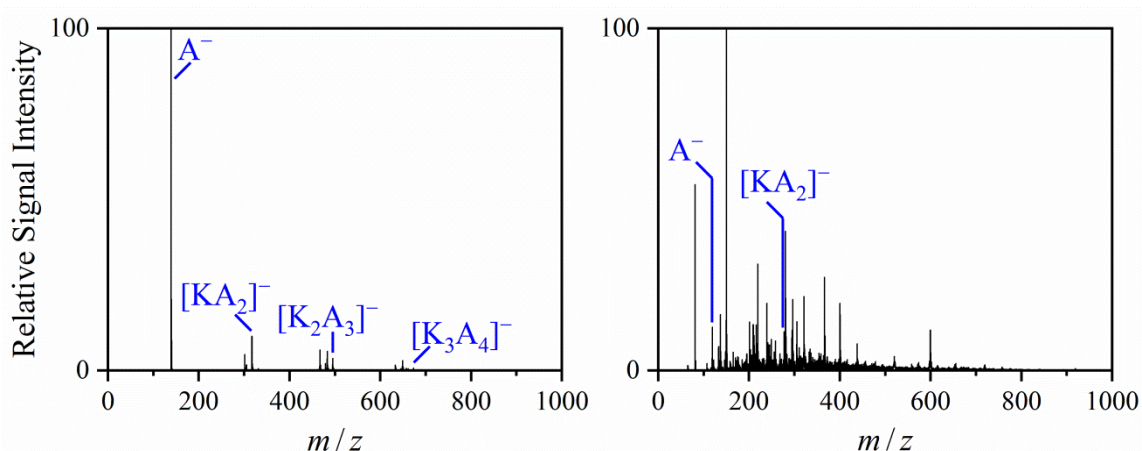


Figure 8: Negative-ion mode ESI mass spectra of 2-mM solutions of dimedone / KO^tBu (left) and acetophenone / KO^tBu (right) in MeCN. A⁻ = [dimedone-H]⁻ (left), [acetophenone-H]⁻ (right).

3.1.1 Influence of Structure and Acidity

The 15 deprotonated carbon acids AH in anhydrous MeCN were measured both with and without 18C6 using negative-ion mode ESI mass spectrometry and their relative signal intensities were evaluated (**Table 1**). The substrates are sorted by the pK_a of the conjugate acid. While the pK_a values correspond to DMSO as a solvent instead of MeCN, the relative order of acidity can be expected to be the same and the available data should be sufficient to identify existing trends in the ESI-mass spectrometric response. The gas-phase proton affinity of the carbanions $\Delta_{\text{acid}}H$ is also included as an alternative parameter that may influence the suitability of ESI-MS for the analysis of the substrate.

In order to best compare the species with each other, the signal intensities of the free carbanion and the first three aggregates $[K_{n-1}A_n]^-$ ($n = 1-4$), as well as the most intense signal not corresponding to an aggregate (*Other*) have been categorized into high (>80%, +++)), medium (25-80%, ++), low (3-25%, +) and no (<3%, -) relative signal intensity. The same sorting was applied to sample solutions containing 18C6, the relative signal intensities of which are displayed using brackets. In some cases, the *Other* signal could be traced back to the carbanion, such as in-source fragmentation or other reactions during the ESI process or in solution. In other cases, especially for the more basic carbanions, the signal most likely arises from unspecified interactions and reactions between the base, solvent and the ESI process and could not be related to the carbon acid or the carbanion.

When approaching the upper end of the pK_a range, the signal intensities of the free and bound carbanions decrease in favor of other signals, which for the most part could not be identified. The most basic carbanion that could be detected, at rather low signal intensity, was the acetone enolate, featuring a pK_a of 26.5⁶⁵ and $\Delta_{\text{acid}}H^\circ$ of 1544 kJ/mol.¹⁶³ This species could easily be confirmed by repeating the experiment using acetone-*d*6 instead (**Figure 9**). The mass signal m/z 57 was shifted by $\Delta m = 5$, corresponding to the 5 remaining deuterium atoms. Furthermore, there is clear evidence for H/D-exchange in the form of mixed species in between m/z 57 and 62, even when measuring shortly after preparing the solution. This distribution of signals shifted towards the non-deuterated species with increasing reaction time, precluding the reaction occurring primarily within microdroplets during the ESI process.¹⁷⁰

Table 1: Relative signal intensities of free and potassium-bound carbanions $[K_{n-1}A_n]^-$ observed upon negative-ion mode ESI mass spectrometric analysis of solutions of carbon acids AH (2 mM) and KO^tBu (1 equiv.) in MeCN. Values in brackets refer to the relative signal intensities observed for solutions containing 18-crown-6 (1 equiv.).

Structure A ⁻	pK _a ^a	Δ _{acid} H [kJ mol ⁻¹] ^b	[A] ⁻	[KA ₂] ⁻	[K ₂ A ₃] ⁻	[K ₃ A ₄] ⁻	Other
	11.1 ^c	1405 ± 9	+ ^d (++)	+ ^e (+)	++ ^{e,f} (++)	+++ ^{e,g} (+++)	+ (+)
	11.2 ^h	1418 ± 9	+++ (+++)	+ (+)	+ (+)	- ^l (+)	+ (+)
	13.1 ^j	1422 ± 10	+ (++)	+++ (+++)	++ (+)	++ (+)	+ (+)
	13.3 ^h	1438 ± 9	++ (+++)	++ ^e (+++)	++ ^e (++)	+++ ^e (++)	+ ^k (+)
	16.4 ^h	1457 ± 10	- (++)	+++ ^e (+++)	++ ^e (+)	+ ^e (-)	- (-)
	17.2 ^c	1491 ± 9	- (-)	+ (+)	+ (+)	+ (++)	+++ (++) ^k
	18.0 ^l	1481 ± 9	- (+)	++ (++)	++ (+++)	+++ (++)	+ (+)
	18.7 ^m		+++ (+++)	+ (+)	- (+)	- (-)	++ (+)
	20.4 ⁿ	1475 ± 9	++ (+++)	++ (++)	- (-)	- (-)	+++ (++)
	21.9 ^o	1467 ± 10	+++ (+++)	+ (+)	+ (+)	- (-)	++ (+)
	22.6 ^c	1472 ± 9	+++ (+++)	+ (++)	- (-)	- (-)	++ (+)
	24.7 ^o	1512 ± 9	+ (+++)	+ (++)	- (+)	- (+)	+++ (++)
	26.5 ^o	1544 ± 9	+ (+)	- (-)	- (-)	- (-)	+++ (+++)
	28.7 ^o	1551 ± 10	- (-)	- (-)	- (-)	- (-)	+++ (+++)
	29.5 ^p	1555 ± 17	- (-)	- (-)	- (-)	- (-)	+++ (+++)

a) Of the corresponding acid in DMSO. b) Gas-phase acidity, Ref. 163. c) Ref. 83. d) Species observed in low signal intensities (3-25%). e) Including aggregates with sodium counterions. f) Species observed in moderate signal intensities (25-80%). g) Species observed in high signal intensities (>80%). h) Ref. 82. i) Species not observed (<3%). j) Ref. 172. k) Highest signal intensity for $[K_4A_5]^-$. l) Ref. 80. m) Ref. 173. n) Ref. 174. o) Ref. 65. p) Ref. 175.

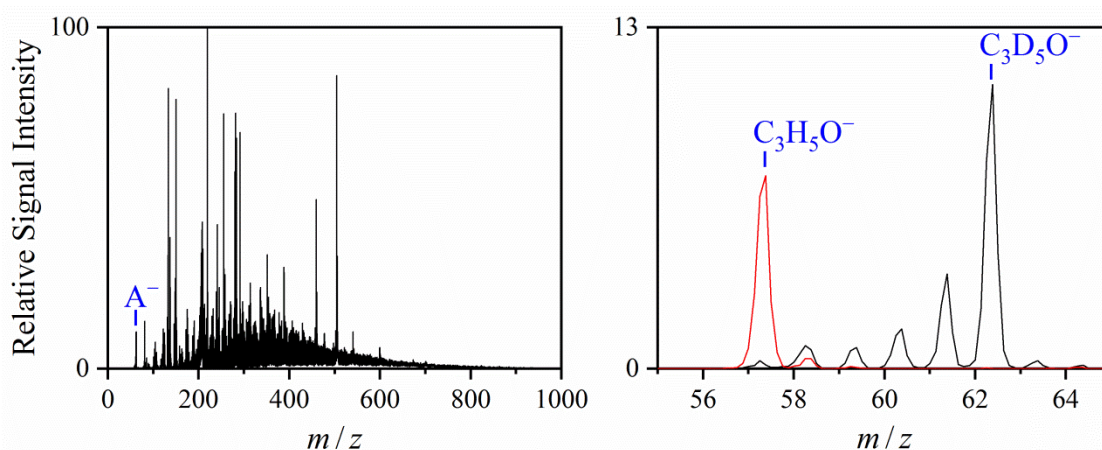


Figure 9: Negative-ion mode ESI mass spectrum of a 2-mM solution of acetone-*d*₆ / KO^tBu in MeCN (left) and zoomed in overlay of the same solution measured after 140 min (right, red).

The reaction partner capable of donating protons in this case was either the solvent MeCN or traces of water remaining in the solvent or entering during the preparation of the sample solution. Signals of m/z 40 and 81 observed from solutions of KO^tBu in MeCN without the addition of an acid indicate deprotonation of the solvent. The large excess compared to the sample acetone may enable a reversible proton transfer despite the large difference in acidity (pK_a (in DMSO) 26.5 vs 31.3 of MeCN⁸³). Considering this, the pK_a value of a substrate may constitute an upper limit of what can be detected using this combination of solvent, base and instrument. Any carbanion with a higher pK_a of the corresponding acid will be reprotonated by the solvent. Due to the logarithmic nature of the pK_a scale, the transition from detectable to not detectable can be expected to be rather sharp.

At the same time, proton transfer during the spray process may enable the detection of species depending on their gas-phase proton affinity instead, which does not always strictly correlate with the pK_a . One possible example for this is deprotonated nitromethane. The moderate acidity (pK_a 17.2) suggests it to be fully deprotonated, but the absolute and relative signal intensity of the free and metal-bound carbanion was much lower than other substrates with comparable basicity in the condensed phase. Possibly the higher proton affinity of the anion, in combination with an increased internal energy, enabled a proton transfer from MeCN ($\Delta_{acid}H = 1491$ kJ/mol vs ~ 1560 kJ/mol of MeCN¹⁶³) during the ESI process, thus reducing the signal intensity.

Besides the general detectability, the structure of the substrate also influences the amount of aggregate formation to a large degree. The main factor contributing to high signal

intensities of aggregates appears to be the ability to form chelate complexes. For every species containing two flexible electron-withdrawing groups, such as diethyl malonate anion or acetylacetonate, the free anion was observed in minor quantities only. The dimedone anion is similarly structured, containing two carbonyl groups, but predominately occurred in its free form instead due to the geometrical constraints. Other carbanions containing only one functional group suitable to forming complexes with alkali metals tended towards the free carbanion as well. A special role is occupied by the cyclopentadienyl anion, which featured one of the highest tendencies to aggregate among all investigated structures. This apparently mirrors the formation of stable multidecker complexes, similar to those found for solid KCp.¹⁷⁶

The increase in signal intensity of the free anion observed for diethyl malonate upon the addition of crown ether was shared by the other structures as well and is therefore a good option when attempting to maximize the amount of free carbanions in the gas phase. The second observed effect was a general increase in signal intensity compared to the *Other* signals. This was most noticeable for acetophenone, but other samples were affected as well. For acetone, no such effect was observed and neither could the less acidic carbon acids be detected through the addition of crown ether. This second effect is likely caused by changing the association equilibrium in solution.⁸² By decreasing the formation of neutral KA, the ratio of A⁻ to other anions in the solution undergoing the ESI process is increased, which is reflected in the ion ratios inside the resulting microdroplets.

3.1.2 Influence of Concentration and Water

After determining the limits of which structure can be reasonably detected from 2-mM solutions in MeCN using KO^tBu as a base, the next step was to investigate the limits of detection by reducing the concentration. This was expected to have a strong influence on the aggregation behavior as well. For that reason, this investigation was focused on diethyl malonate, showing high signal intensities and aggregation tendencies, and on acetophenone as one of the least signal intensive substrates. The reason for choosing acetophenone over acetone was the option to utilize gas-phase fragmentation in a MS² step, reducing the effect of isobaric impurities that may overlap with the signal of interest. Diethyl malonate and its aggregates were similarly fragmented. The fragmentation method utilized here was collision-induced dissociation (CID), in which the mass-selected ions are elevated to higher kinetic energy and allowed to collide with a target

gas, which in this case was helium. The excitation energy depends on the amplitude of the excitation voltage V_{exc} , with typical values being 0.3-0.8 V.

When subjecting aggregates $[K_{n-1}A_n]^-$ to CID, the loss of one unit KA occurred easily for all carbanions A^- . For the free carbanion, the fragmentation was rather variable. The ion derived from diethyl malonate readily and efficiently lost one unit of EtOH at relatively low excitation energies. Compared to that, deprotonated acetophenone required a much higher energy and lost much of the original signal intensity to fragments outside the detection range. CID was applied to all species of interest to prevent isobaric interference while reducing the concentration of both carbon acid and base to a minimum of 2 μM (**Figure 10**). Blank samples confirmed the assignment and the successful application, as no signals were detected at the expected m/z of the fragments.

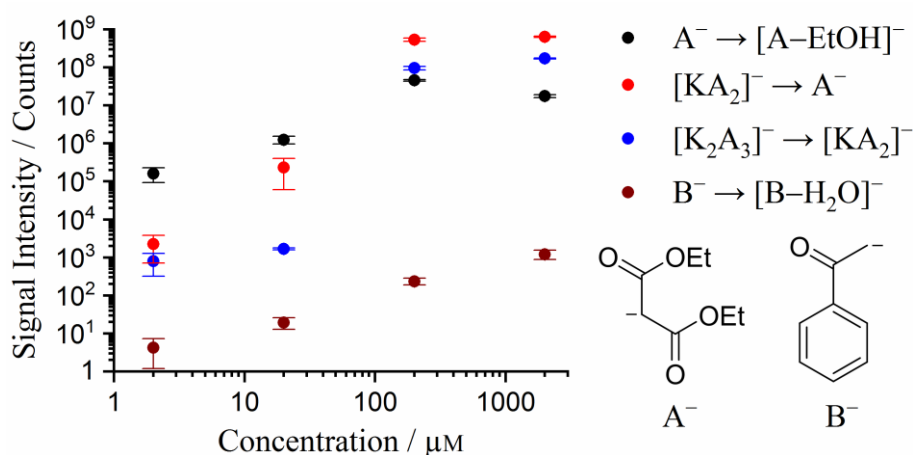


Figure 10: Concentration dependence of the absolute carbanion signal intensities observed upon negative-ion mode ESI-mass spectrometric analysis of solutions of diethyl malonate or acetophenone, deprotonated using 1 equiv. KO^tBu in MeCN. The free anions and aggregates were mass-selected and fragmented using CID in order to avoid isobaric interference.

For the benzophenone anion, the linear decrease in signal intensity when reducing the concentration precludes reactions with impurities like water lowering the effective concentration. The fragment ion generated through CID of deprotonated acetophenone was observed even at the lowest concentration of only 2 μM . At this point, the signal intensity was very low and the species would likely not be measureable when decreasing the concentration even further. The use of fragmentation techniques was necessary here, as the non-fragmented signal was approximately equal to the background noise when measuring blank samples. Due to the linear response, the signal intensity from ESI-MS experiments may be used to approximate concentrations of the anion in solution.

For diethyl malonate and similar substrates, the use of ESI-MS to determine concentrations is more complicated. The presence of aggregate signals mandates a non-linear calibration curve that includes the signal intensity of every relevant species $[M_{n-1}A_n]^-$. In most cases, alternative methods such as quantitative NMR spectroscopy¹⁷⁷ would be better suited for this task, though ESI-MS may be used for sufficiently low concentrations. At this point, the aggregates will be reduced according to the mass action law, leaving the free carbanion as the base peak whose intensity is approximately proportional to the concentration. The addition of crown ether may once again be useful by increasing the limit in concentration below which the free anion predominates.

Similarly to acetophenone, there was no indicator for reactions occurring with diethyl malonate in the used concentration range. The signal intensity at 2 μM was higher than that of the acetophenone fragment ion at 2 mM, mostly due to the efficient fragmentation. Considering the signal intensities of both substrates, the detection limit of diethyl malonate may be as low as single-digit nM, though this has not been investigated further.

Remnants of water did not appear to affect the intensities in mass spectra of diluted carbanion sample solutions. This is not unexpected, as the acidity of water is drastically reduced in aprotic solvents such as DMSO and MeCN.¹⁶⁶ However this situation may change when the acidity of water increases along with the water content. To investigate this, fixed amounts of water up to 10 vol% were added to sample solutions of both acetone and acetophenone (**Figure 11**). For the latter, CID was employed once again. Acetone has no accessible fragment ion, so the free carbanion signal intensity is shown.

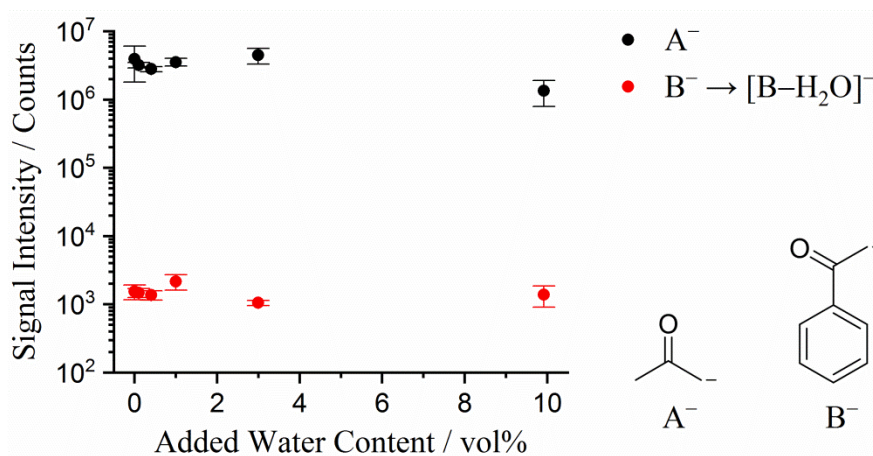


Figure 11: Absolute carbanion signal intensities observed upon negative-ion mode ESI-mass spectrometric analysis of 2-mM solutions of acetone (AH) or acetophenone (BH), deprotonated using 1 equiv. KO^tBu in MeCN after addition of fixed amounts of water. The acetophenone anion (m/z 119) was mass-selected and fragmented using CID in order to avoid isobaric interference.

Both carbanions behaved similarly when increasing the water content of the solvent up to 10%. The signal intensity was not affected strongly, decreasing by a factor of 3 for acetone and even less for acetophenone after the addition of the full 10% water. At this point, the acidity of water can be expected to be at least similar to the substrates and should affect the effective sample concentration in solution drastically. The reason for the unexpectedly high signal intensity is most likely the reduced stabilization of the hydroxide anion by hydration, with the proton affinity of the free gas-phase anion being ~80 kJ/mol larger than that of deprotonated acetone.¹⁶³ While proton transfer from water to the carbanions in solution is expected, the reverse reaction may occur during the ESI process, where hydroxide anions collide with neutral sample molecules in the gas phase. This possibility needs to be considered when performing negative-ion mode in-situ measurements from solutions containing water. The potential ion-molecule reaction in the gas phase may generate additional analyte anions, leading to an overestimation of the approximate anion concentration in solution. It also means the limitation in species that can be detected in a chosen solvent/base system most likely depends on both condensed-phase and gas-phase acidity rather than on the pK_a alone.

Based on the results of changing concentrations and the water content, ESI-MS should be capable of in-situ monitoring of reactions concerning carbanions. The linear response observed for different concentrations of deprotonated acetophenone suggests it may be used for estimating conversions and for kinetic analysis, at least in the case of non-aqueous solutions. For simple systems, a pseudo-first order exponential decay curve may be traced directly. More complex systems that contain multiple types of ions simultaneously require more care to ensure no suppression effects occur. The formation of aggregates prevents the linear ESI-MS response and needs to be suppressed, either by decreasing the concentration the experiment is run at, or by changing the counterion.

3.1.3 Influence from Changing the Solvent

MeCN was initially chosen as one of the most commonly used solvents for ESI-MS, along with MeOH. Its polarity is sufficient for efficient ion transfer into the gas phase, while also featuring an advantageous combination of viscosity, volatility and availability. Both MeCN and MeOH are usually mixed with water in order to facilitate proton transfer or to improve solubility of simple salts.¹⁷⁸ As all species investigated here are deprotonated specifically using a strong, soluble base, the addition of water is not

necessary, leading to pure MeCN being used as the solvent. As mentioned above, it is aprotic polar and as such similar to DMSO in nature, which allows for the evaluation of trends using pK_a values recorded for solutions in DMSO. Alcohols are more acidic than MeCN and their pK_a values can be expected to decrease similarly to water when comparing a dilute solution in aprotic solvents with the pure alcohol. Nevertheless, the gas-phase proton affinity of the methoxide anion is higher than that of deprotonated acetonitrile¹⁶³ and as such both solvents have been tested for diethyl malonate, fluorene and acetophenone. For the final solvent tested regarding the detectability of carbanions, THF was chosen as an example for less polar, but also drastically less acidic solvents (Figure 12).¹⁶⁷

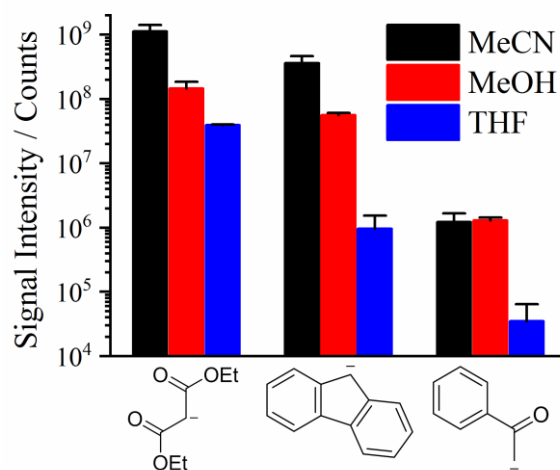


Figure 12: Absolute carbanion signal intensities observed upon negative-ion mode ESI-mass spectrometric analysis of solutions of diethyl malonate, fluorene or acetophenone, deprotonated using 1 equiv. KO^tBu in MeCN, MeOH or THF as solvent. Aggregates were summed up where applicable, accounting for their stoichiometry.

The absolute signal intensity of the different carbanions varied strongly with the solvent. MeOH and MeCN were comparable for acetophenone, but for the substrates more amenable to ESI-MS, MeCN offered a clear improvement over MeOH, with differences in signal intensity being one order of magnitude. When using THF, the detection remained successful for every sample, but led to a drastic reduction in signal intensity by a factor of ~30 or more. Noise and unknown signals experienced a similar reduction in signal intensity, as the difference in ESI response stems from the lower polarity which affects all species to a similar degree.¹⁷⁹ No particular advantage for the detection of acetophenone due to the reduced acidity was observed.

The choice of solvent also influenced the aggregation behavior of the analyte. For diethyl malonate in MeCN, the signal corresponding to $[\text{KA}_2]^-$ predominated the spectrum, with larger aggregates present in smaller amounts, followed by even less of the free anion. A similar spectrum was generated from a solution in THF, though the relative signal intensity of the free carbanion was reduced even further. In MeOH on the other hand, both the free anion signal and aggregates containing more than 2 anions were recorded at comparatively higher relative signal intensities. Furthermore, the bridging cation in aggregates primarily consisted of Na^+ instead of K^+ (Figure 13).

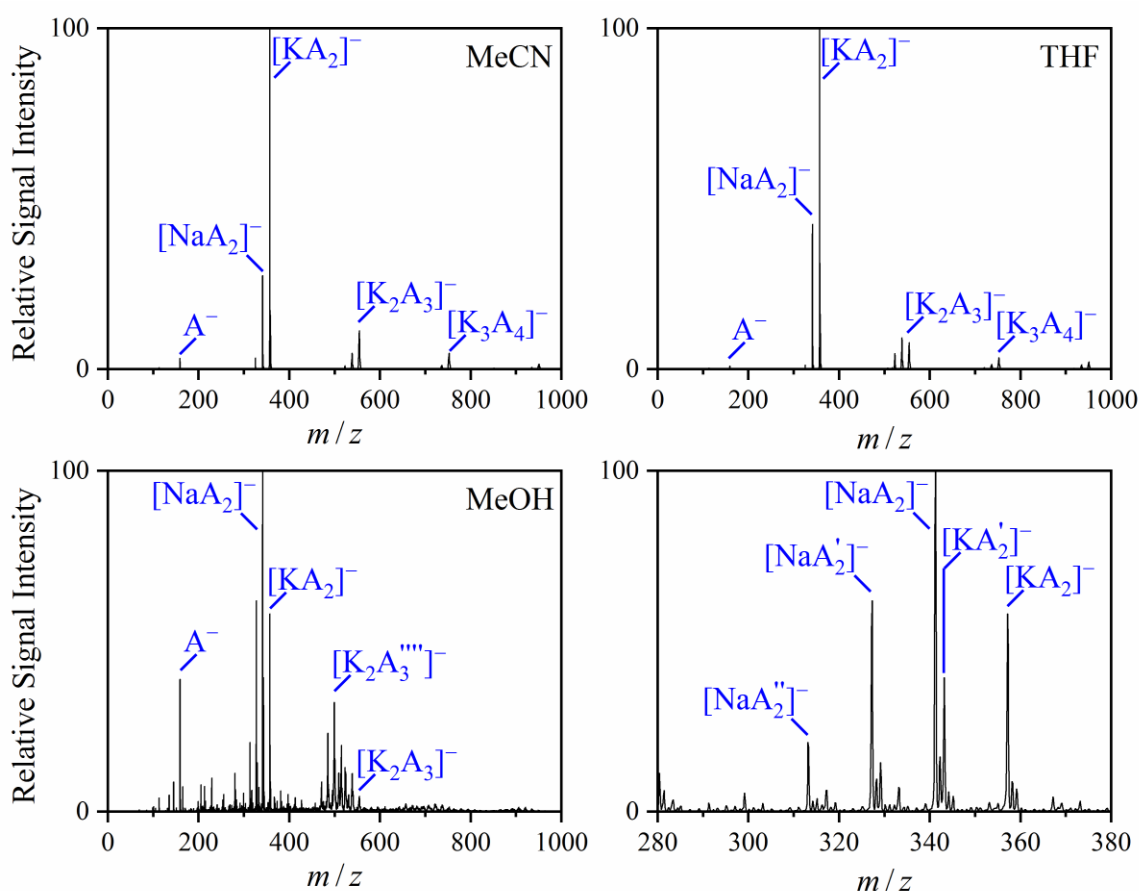


Figure 13: Negative-ion mode ESI mass spectra of 2-mM solutions of diethyl malonate / KO^tBu in MeCN (top left), THF (top right) and MeOH (bottom). A close-up view of the spectrum taken from MeOH (bottom right) highlights an Et/Me ester exchange, the amount of ' indicating the number of Me esters in the ion (formal loss of CH_2 each, $\Delta m = 14$).

The higher polarity of MeOH and its protic nature presumably shifts the association equilibrium of carbanion and alkali metal cation towards the free ions. The ability of MeOH to form hydrogen bonds in particular may contribute to this effect by stabilizing both the free enolate anion and the cation. This effect may be desirable when attempting to maximize the amount of free carbanion in the gas phase, but is mostly compromised by

the generally lower signal intensity. Furthermore, for some substrates such as diethyl malonate, MeOH is non-innocent as a solvent. In this case, it leads to the exchange of ethyl for methyl groups in the ester, resulting in a formal loss of CH₂ and increasing the complexity of the mass spectrum significantly (**Figure 13**, bottom). As reactions involving MeCN are far less likely to occur than those involving MeOH, the former will usually be the preferred solvent of choice. THF and similar solvents may be useful when analyzing species that are too basic for MeCN, despite the generally lower signal intensity.

3.1.4 Influence of Base and Counterion

Other than KO^tBu, lithium diisopropylamide (LDA) as a solution in THF/hexanes and sodium hydride (NaH) as a solid have also been used for the deprotonation of diethyl malonate, fluorene and acetophenone in MeCN. The detection was successful for every case, but differences in signal intensity and aggregation behavior were evident (**Figure 14**).

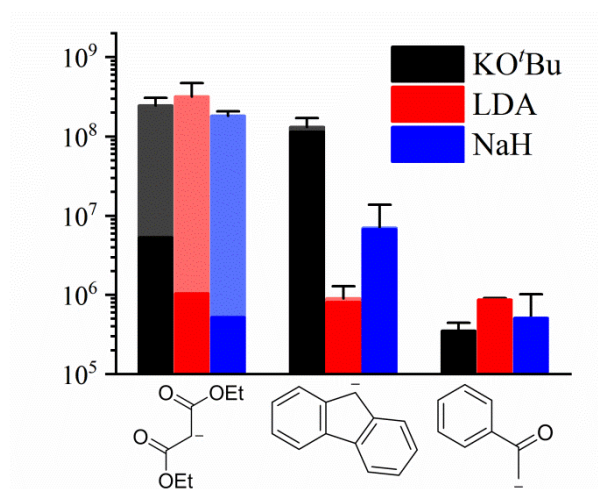


Figure 14: Absolute carbanion signal intensities observed upon negative-ion mode ESI-mass spectrometric analysis of 2-mM solutions of diethyl malonate, fluorene or acetophenone, deprotonated using 1 equiv. KO^tBu, NaH or LDA in MeCN. Semi-transparent bars indicate summed-up signal intensities of aggregates up to [M₂A₃]⁻.

Regarding the absolute signal intensity, none of the chosen bases can be considered a clear favorite for the detection of carbanions. LDA provided the highest signal intensity for acetophenone and, when including both the free anion and metal-bound aggregates, for diethyl malonate. For fluorene, the intensity was drastically reduced compared to the other bases. NaH produced average results, but led to the highest uncertainties. This may

be connected to the experimental procedure, in which the base did not fully dissolve in the solvent. Any reactions would have to occur on the solid-liquid interface, thus being more strongly affected by stirring and the reaction time before the measurement. A full deprotonation is not guaranteed and therefore, NaH should not be considered for any quantitative or time-dependent experiment. KO^tBu, the base used thus far, produced the most reliable results, which is a quality more important than higher but fluctuating signal intensity. It also facilitates the detection of free diethyl malonate carbanions at the cost of the aggregate signals. This, however, is most likely the result of changing the counterion and unrelated to the change of the base in itself.

In order to fully separate the effect of counterion and base in regards to aggregation behavior, diethyl malonate was deprotonated using hydroxide salts MOH with M = K⁺, Na⁺, Li⁺, NBu₄⁺. Due to the low solubility of the salts in MeCN, they were first dissolved in MeOH and then added to the solution of the carbon acid (**Figure 15**). Due to the low amount of MeOH in the solvent mixture, no significant ester exchange reactions or similar issues occurred.

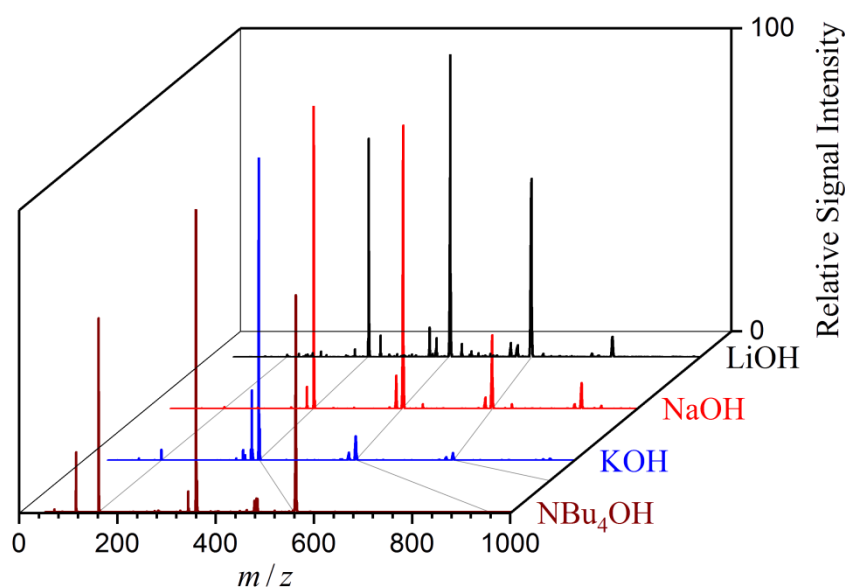


Figure 15: Negative-ion mode ESI mass spectra of 2-mM solutions of diethyl malonate, deprotonated using 1 equiv. MOH (M = K⁺, Na⁺, Li⁺, NBu₄⁺) in MeCN. Grey lines indicate the expected m/z of aggregates of the type $[M_{n-1}A_n]^-$ ($n = 1 - 4$).

Within the alkali metal cations, the tendency to form aggregates increased with decreasing size of the cation. The mass spectrum produced from KOH contained predominately $[KA_2]^-$, accompanied by a low amount of both $[K_2A_3]^-$ and the free anion A^- . For lithium and sodium, the free anion signal intensity approached zero, in favor of

larger aggregates. NBu_4^+ on the other hand formed only a very limited amount of aggregates and instead facilitated the detection of the free carbanion. The base peak was $[\text{KA}_2]^-$, likely caused by traces of K^+ from previous measurements, further emphasizing the difference in aggregation behavior between the organic cation and the alkali metal cations investigated here. For maximizing the free anion signal, greater care to remove traces of other metals needs to be taken before employing NBu_4OH . The hydroxide may not be suitable for less acidic species, though in general the use of large, organic counterions is a promising option to simplify mass spectra of carbanions. When attempting to reduce the aggregation in order to estimate the carbanion concentration in solution, other large bases may be preferable, as hydroxide anions may cause ion-molecule reactions to generate additional carbanions as mentioned above. Depending on the required basicity, large amines or phosphazene bases may be suitable.¹⁸⁰

Overall, ESI-MS is a solid option for the detection of carbanions with up to medium basicity. The most sensitive species detected was deprotonated acetone. The optimization of the solvent/base system may facilitate the analysis of further carbon acids, though it is unlikely that the most reactive species such as alkyl anions will be amenable to analysis from solution without coordinating to a transition metal. For quantitative interpretation of mass spectrometric data, it may be necessary to reduce the amount of aggregation by reducing the concentration or by employing large, organic counterions. The latter effect can also be achieved through the addition of crown ethers to solutions containing alkali metal cations. Finally, gas-phase fragmentation methods can be used to reduce isobaric interferences. Considering these points, the mass spectrometric analysis of reactive intermediates should be possible in some cases, but likely the live monitoring of reactions with carbanionic reactants and/or products is of higher practical importance and will be explored further in chapter 3.3.

Another application makes use of the formed aggregates in order to determinate the thermodynamics of cation association through the kinetic method.⁴⁷ The dissociation of heterodimeric aggregates $[\text{A-M-B}]^{+/-}$ has often been utilized, though it has mostly been used for two neutral molecules associating with one ion instead of the combination of two anions and one cation, and even less so for carbanionic species. An example for this will be given in chapter 3.4.

3.2 ESI-MS for the in-situ Detection of Radical anions

The preparation of gaseous radical anions can usually be achieved through negative atmospheric pressure chemical ionization (APCI), in which a highly reactive radical anion is generated through corona discharge or dissociative electron attachment, which can then transfer the electron to the gaseous, neutral analyte.¹⁸¹ However, for the transfer into the gas phase and subsequent mass-spectrometric analysis of radical anions present in a sample solution, there has been no systematic investigation so far. The following approach was performed similarly to the investigation of carbanions (chapter 3.1), in which the neutral analyte precursor in MeCN is mixed with the reducing agent cobaltocene (CoCp₂), which is a strong single-electron-donor,¹⁸² instead of a base. Of note is that some species do not require the addition of a reducing agent to form a radical anion A^{•-}, as the ESI process itself can result in redox reactions (**Figure 16**).

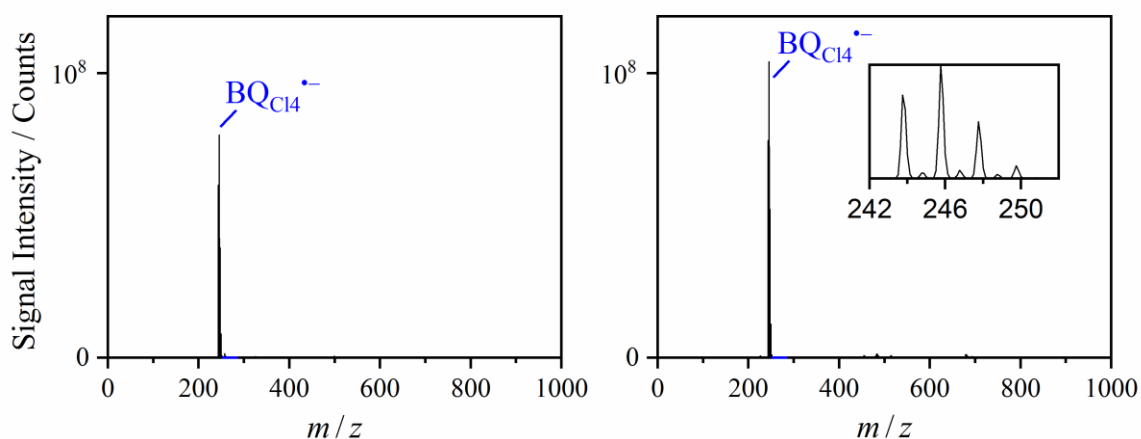


Figure 16: Negative-ion mode ESI mass spectra of 2-mM solutions of chloranil (BQCl₄) in MeCN, without (left) and with (right) 1 equiv. CoCp₂.

Chloranil (BQCl₄) is one such species that could be recorded without the addition of a reducing agent and produced a very clean mass spectrum with high signal intensity due to its extreme EA of 2.78 eV¹⁸³. The spectrum upon addition of CoCp₂ contained no aggregates of the type [CoCp₂(BQCl₄)₂]⁻, which would be the analogue to [KA₂]⁻ observed for the carbanionic species. This may be due to the counterion CoCp₂⁺ not interacting with the anions as alkali metal cations would, in combination with the radical anions charge delocalization across the whole molecule. In this it can in some ways be compared to deprotonated fluorene, which did not show a propensity to aggregation. This holds true for most radical anions, in contrast to many regular anions produced by

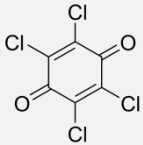
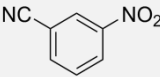
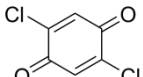
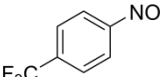
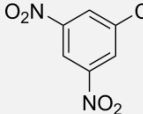
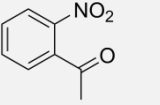
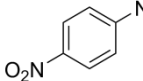
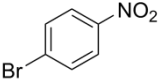
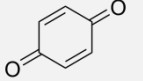
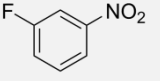
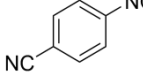
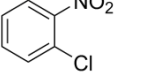
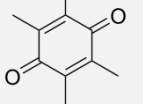
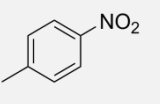
deprotonation, whose negative charge often can be assigned to a specific site and few functional groups in direct vicinity.

3.2.1 Influence of Structure and Redox Properties

The descriptor most likely to influence whether a radical anion can be detected from solution using ESI mass spectrometry is expected to be the electron affinity of the neutral precursor, which is a gas-phase thermodynamic property, or the electrochemical potential associated with the redox pair determined in solution. The two values are closely connected, though the determination of redox potentials through cyclic voltammetry is often inconsistent due to variation in solvents, concentrations and reference electrodes.⁷³ As such, the gas-phase EA was used for selecting suitable analytes. A total of 14 species were chosen, ranging from EA = 0.95 eV to 2.78 eV.¹⁸³⁻¹⁸⁵ Due to the internal energy introduced into the ions during the ionization process,^{186,187} radical anions of lower stability were not expected to be accessible by ESI-MS. All species were either benzoquinones (BQ) or nitrobenzenes (NB), which are some of the prevalent classes of small, organic molecules capable of forming radical anions within the EA range of interest.

The 14 radical anion precursors are listed in order of their EA. The suitability of ESI-MS for the detection of radical anions from solution, both with and without added reducing agent CoCp₂, is indicated by sorting the species into one of three categories (**Table 2**). Good detectability (++) means the radical anion signal is both the base peak of the spectrum and stable over several minutes at least. Species of moderate detectability (+) are present in the mass spectra, but either their signal intensity decreases significantly over a short amount of time or the signal intensity is lower than other, unknown signals in the mass spectra from the start. Finally, no detection (–) means no signal of the *m/z* ratio corresponding to the radical anion was observed upon ESI-mass spectrometric analysis. All of the detected NBs shared a characteristic fragmentation upon CID, which could be used to confirm the assignment and, in one case, prevented a false positive due to isobaric interference.

Table 2: Detection of radical anions BQ^{•-} or NB^{•-} from solutions of a neutral precursor A (2 mM) in MeCN with and without the addition of the reducing agent CoCp₂ (1 equiv.) by the use of negative-ion mode ESI mass spectrometry.

Neutral precursor	EA / eV	Without CoCp ₂	With CoCp ₂	Neutral precursor	EA / eV	Without CoCp ₂	With CoCp ₂
	2.78 ¹⁸³	++ ^a	++		1.56 ¹⁸³	+	++
	2.44 ¹⁸⁴	++	(+) ^b		1.47 ¹⁸⁵	- ^d	++
	2.16 ¹⁸³	+ ^c	++		1.38 ¹⁸⁵	-	++
	2.00 ¹⁸³	+	++		1.29 ¹⁸³	-	-
	1.91 ¹⁸³	+	+ ^b		1.23 ¹⁸³	-	- ^e
	1.72 ¹⁸³	+	++		1.14 ¹⁸³	-	-
	1.62 ¹⁸⁴	+	++		0.95 ¹⁸³	-	-

a) Stable 100% relative signal intensity. b) Decreasing signal intensity due to reactions. c) Constantly low signal intensity. d) No signal intensity at the corresponding *m/z*. e) Low signal intensity at the corresponding *m/z*, but does not show the expected fragmentation pattern.

The detection of radical anions from solutions without an added reducing agent was most pronounced at the upper end of the EA scale, though it did occur for species with moderate EA as well. In every case, the signal intensity was drastically reduced when compared to solutions containing CoCp₂. For the generation of these radical anions, two different processes may occur during the ESI step. The first is a reduction of the analyte within the steel needle of the ESI sprayer, while the other is the formation of less electron-affine radical ions by corona discharge in the gas phase, followed by electron transfer.

For the species and conditions utilized in this series, a reduction within the spray needle is the more likely scenario to occur and, in the case of BQ, has been reported already.¹⁴⁸ BQ_{Me4} in MeCN has a half-wave potential of -0.84 V vs SCE¹⁸⁸ and is barely outside the range of -0.8 V to +1.0 V vs SCE that was predicted for CH₂Cl₂ as a solvent.¹⁴⁸ Considering that *m*-nitrobenzonitrile (NB_{*m*CN}) was also detected, the actual limit in redox potential for the reduction to occur appears to be lower, though this may also change with solvent, flow rate, temperature, and instrument settings.¹⁸⁹ The general premise holds true. Electron transfer from plasma on the other hand can be dismissed. As seen from the stable, high signal intensity of the various species upon addition of CoCp₂, the radical anions appear to be persistent once formed and are not lost during the transfer into the gas phase and into the mass analyzer. The lack of signal intensity for less electron-affine molecules therefore means that they were not generated in the first place. As all experiments were conducted using the same conditions, the amount of O₂^{•-} formed would be roughly the same across all experiments if corona discharge were to occur. All species were sufficiently strong electron acceptors for efficient transfer to occur from O₂^{•-} (EA = 0.45 eV)¹⁹⁰, so any species detected after reduction with CoCp₂ should also be accessible by chemical ionization through corona discharge-generated plasma.

Of greater interest than the already known reduction of analytes during the ESI process is the detection of radical anions from solution that were preformed through the addition of a reducing agent. A sudden shift from good to no detected signal intensity was observed when going from *o*-nitroacetophenone (NB_{*o*COCH₃}) to *p*-bromonitrobenzene (NB_{*p*Br}). Both species should be able to be reduced by CoCp₂, which was also confirmed by both solutions reaching the same signal intensity of CoCp₂⁺ in positive-ion mode ESI-MS. The radical anion NB_{*p*Br}^{•-} was lost either in solution or during the ESI process, the latter of which being more likely. NB_{*p*Br} and NB_{*o*COCH₃} are sufficiently similar in structure and electronic properties that no drastic shift in reactivity is expected. As such, a threshold in their EA is the most likely explanation for the sudden change in detectability, as the internal energy of the ion exceeds its EA.⁴⁸ The internal energy of ions can be measured using thermometer ions.¹⁸⁶ For this, a set of similar ions undergoes fragmentation during the mass-spectrometric analysis, with the ratio of precursor and fragment ions being dependent on the substitution of the ion and the internal energy being imparted. In a previous study, the internal energy imparted by an instrument similar to the one used in this study had been measured.¹⁸⁷ The mean internal energy was found to be ~2 eV with a

broad distribution. This means that the majority of the radical anions transferred into the gas phase may be expected to undergo spontaneous electron detachment, lowering their signal intensity. Only a small fraction of ions has an internal energy of less than 1.3 eV, which may be insufficient for the detection of species such as $\text{NB}_{p\text{Br}}^{\bullet-}$.

Attempting to detect $\text{NB}_{p\text{Br}}^{\bullet-}$ by lowering the internal energy through changing the instrument parameters was unsuccessful. This was done by decreasing the drying temperature to 60 °C, using the *Smart Parameter Settings* available to the instrument to decrease trap drive Level or compound stability to 10% (usually 100%), or combinations of these settings. Intentionally increasing the internal energy by setting the compound stability to 300% when measuring a solution of $\text{NB}_{o\text{COCH}_3}$ with CoCp_2 reduced the signal intensity of $\text{NB}_{o\text{COCH}_3}^{\bullet-}$ by more than 95%. Employing the same instrument settings for *p*-nitrobenzotrifluoride (NB_{pCF_3}) with CoCp_2 only led to a reduction in signal intensity by 60%. Both species were observed at similar signal intensities when measuring under standard conditions. This behavior is an indicator for the interplay of internal energy and EA determining the detectability of radical anions.

3.2.2 Influence of Concentration

Radical anions in solution are usually only encountered in small concentrations, therefore it is important to investigate the ESI-MS response at low concentrations and, if possible, estimate the detection limit for different species. To this matter, BQ_{Cl_4} , $\text{NB}_{o\text{COCH}_3}$ and NB_{pCF_3} were chosen for further investigation. In order to avoid isobaric interference, fragmentation of the signals of interest was utilized when possible. All nitrobenzene radical anions $\text{NB}^{\bullet-}$ used in this study shared a common fragmentation pathway when subjected to CID. Neutral NO is lost, resulting in even-electron phenolate anions with $\Delta m = 30$ (eq. 9).



This fragmentation occurs readily and efficiently at comparatively low excitation energies (Figure 17). For $\text{QB}_{\text{Cl}_4}^{\bullet-}$, no readily accessible fragmentation pathway was observed. Due to the generally high signal intensity, isobaric interference can be expected to be negligible up to very low concentrations. At that point, the characteristic isotope pattern inherent to species containing Cl_4 (Figure 16) can be used to determine the extent of isobaric interference by comparing the experimental and the theoretical isotope ratios.

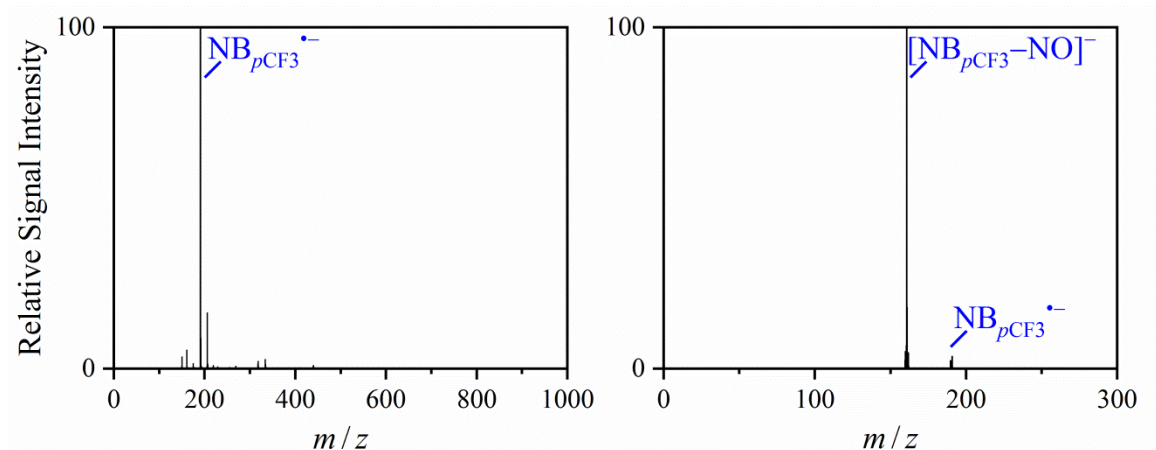


Figure 17: Negative-ion mode ESI mass spectrum of a 2-mM solution of *p*-nitrobenzotrifluoride (NB_{pCF₃}) / CoCp₂ in MeCN (left) and fragmentation pattern upon CID of mass-selected NB_{pCF₃}^{•-} (*m/z* 191) with $V_{\text{exc}} = 0.5$ V (right).

The concentration dependence of the signal intensity of the radical anions was investigated by preparing a 2-mM solution of the precursor and CoCp₂ in MeCN, then after a short mixing period a defined amount of this solution was added to more solvent using gastight Hamilton syringes. The dilute solution was then immediately subjected to ESI-MS, keeping the time delay between preparation and analysis as short as possible (**Figure 18**). Samples were prepared in order of increasing concentrations to avoid carry-over effects. The initially prepared stock solution was measured last.

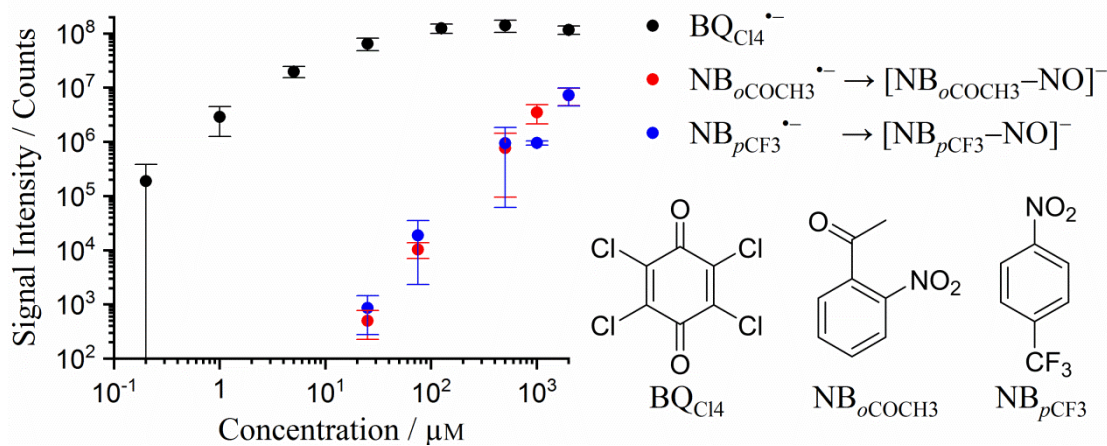


Figure 18: Concentration dependence of the absolute signal intensity of radical anions observed upon negative-ion mode ESI-mass spectrometric analysis of solutions of chloranil (BQ_{Cl4}), *o*-nitroacetophenone (NB_{oCOCH₃}) or *p*-nitrobenzotrifluoride (NB_{pCF₃}) with CoCp₂ (1 equiv.) in MeCN. For the nitrobenzenes, the fragment ion resulting from the use of CID is displayed.

From the progression of the signal intensity of BQ_{Cl4}^{•-}, it is apparent that the mass spectrum of the 2-mM solution was drastically oversaturated. The signal intensity did not decrease significantly even after diluting the solution by a factor >10. Only past this point

was there a roughly linear correlation between concentration and signal intensity. This change in behavior occurs for a concentration that is similar to the estimated excess charge concentration in microdroplets during ESI of $\sim 10 \mu\text{M}$.¹⁹¹ For the lowest concentration of $0.2 \mu\text{M}$, the characteristic isotope pattern was still distinguishable, but was visibly affected by noise (**Figure 19**). This, in combination with the small amount of liquid that had to be handled for the dilution, resulted in significant deviations across the experiments, which is expressed in the standard deviation.

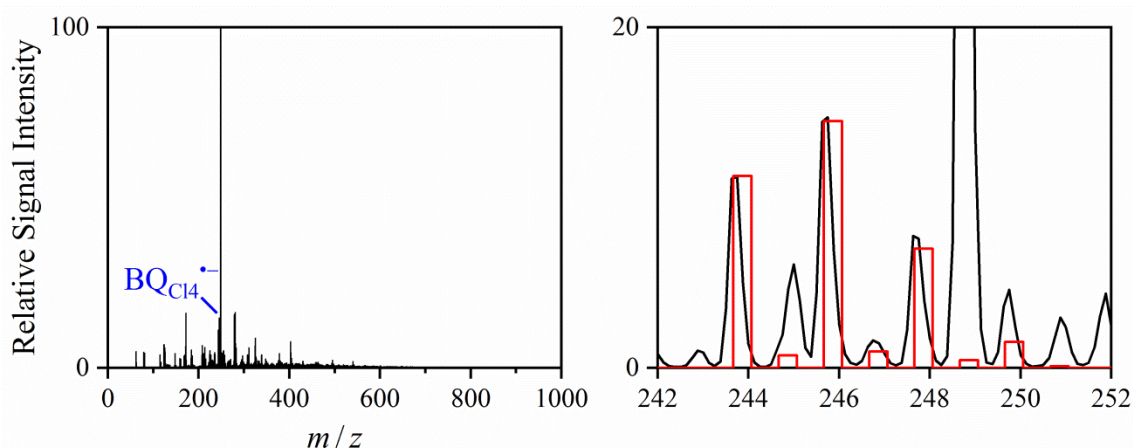


Figure 19: Negative-ion mode ESI mass spectra of a 0.2- μM solution of chloranil (BQ_{Cl_4}) / CoCp_2 in MeCN (left) and close-up overlay of the experimental (black) and theoretical (red) isotope patterns (right).

For the NBs, the high propensity to fragmentation enabled the elimination of such noise, allowing the detection of low-intensity signals that would not be accessible otherwise. The signal intensities of both NBs after CID were near-identical at high concentrations and even when reducing the concentration by up to 1/80, the species behaved similarly in their ESI-MS response. At low concentrations, $\text{NB}_{p\text{CF}_3}^{\bullet-}$ appeared to prevail slightly, which may be connected to the higher EA of the precursor when compared to $\text{NB}_{o\text{COCH}_3}$. However, the difference is not sufficiently large to draw conclusions. The concentration-intensity-correlation for both NBs was allometric, so the ionization process or the ion transfer was less efficient for lower concentrations. This may indicate side reactions, as the ratio of impurity to analyte increases, though the signal intensities were stable during the measurement, meaning that reactions in solution are unlikely. Instead, the experimental conditions like humidity or the amount of oxygen inside the spray chamber may have influenced the results, which may also have increased the standard deviation across multiple experiments to the extent observed here. Automation of the sample preparation and liquid handling may help to increase the reliability of the data.

3.2.3 Influence of Water Content in the Solvent

Remnants of water in the solvent did not outright prevent the detection of radical anions even at low concentrations, where the ratio of water to analyte is drastically shifted. This means the radical species may tolerate larger amounts of water as well and possibly even benefit from it, considering how the solvents used for ESI-MS most commonly consist of a mixture of MeOH/H₂O or MeCN/H₂O.¹⁷⁸

In order to investigate this, 2-mM solutions of 3 neutral precursors were prepared in mixtures of MeCN and water in ratios ranging from 250/1 to 1/1. The reducing agent CoCp₂ was added and, after a short mixing time, the solutions were analyzed by ESI-MS (**Figure 20**). For the NBs, CID was used to prevent isobaric interference.

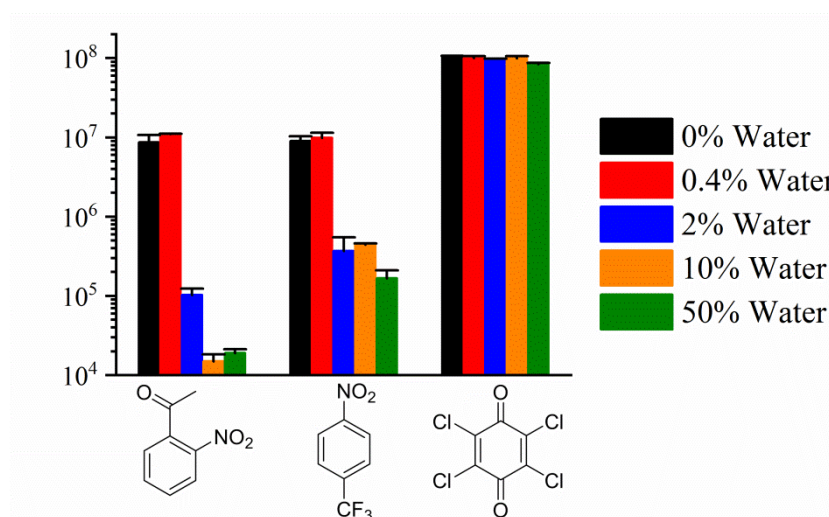


Figure 20: Absolute signal intensities observed upon negative-ion mode ESI-mass spectrometric analysis of 2-mM solutions of *o*-nitroacetophenone, *p*-nitrobenzotrifluoride or chloranil with CoCp₂ (1 equiv.) in MeCN/Water mixtures. For the nitrobenzenes, the signal intensity of the fragment ion resulting from CID is displayed.

Setting the water content to 50% resulted in a decrease in signal intensity by approximately half for BQ_{Cl4}. A similar decrease in signal intensity was achieved by reducing the concentration to 1/80. A stable signal intensity during the ESI-mass spectrometric measurement means that any reactions occurring with water are either concluded or have reached an equilibrium at the time of the measurement. The former would indicate a competitive reaction during the addition of the reducing agent. No new signals have been identified that may result from either possibility, as they most likely were outside the applied mass range (m/z 50 – 1200). However, the actual concentration of BQ_{Cl4}⁻ is not necessarily as low as indicated by the signal intensity, as the change in

solvent properties, in combination with the saturation effects observed earlier, likely affected the results of the analysis. Therefore, side reactions are not guaranteed to have occurred.

The reducing agent being completely consumed by side reactions, leaving no preformed radical anions in the solution, may also be an option for BQ_{Cl4}, where the observed signal intensity may be generated by redox processes during the ESI process exclusively instead. However, this is precluded by the detection of NB^{•-}, which were previously shown to require a reducing agent for the successful detection, in mixtures containing 50% water. For these species, adding a small amount of water seemed to improve the signal response. In a more practical context, a small tolerance towards water as seen here may be sufficient to eliminate the need for dry solvents, as 0.4% is already above water contents typically encountered for HPLC grade MeCN.¹⁹²

When increasing the water content further, a drastic reduction in signal intensity was observed. The less electron-affine NB_oCOCH₃ was affected more strongly than NB_pCF₃. In both cases, the signal intensity remained stable across the duration of the measurement. Similarly to BQ_{Cl4}, an initial reaction or the establishment of an equilibrium is expected, with the EA of the precursor influencing the final concentration of the radical anions. The initial signal intensity increase for a low amount of water, followed by a drastic decrease for higher amounts may be the result of changing properties of water depending on the concentration and environment, such as a drastic difference in pK_a when comparing diluted water in an aprotic solvent with pure water.¹⁶⁶

3.2.4 Influence from Changing the Solvent

So far, all measurements were focused on solutions of radical anions in MeCN or MeCN/H₂O. The choice of solvent was influenced by achieving the best results for the detection of carbanions using MeCN (chapter 3.1.3). Many properties of the solvent can be expected to result in similar interactions for both classes of analytes, such as reduced signal intensity when using less polar solvents like THF. Nevertheless, reactions between reducing agent and solvent may change the outcome and result in another solvent being the preferred choice. For this reason, BQ_{Cl4}, NB_oCOCH₃ and NB_pCF₃ were measured from MeOH and THF and compared with experiments from MeCN (**Figure 21**). THF was dried over sodium/benzophenone, while MeOH was dried using molecular sieve 3 Å.

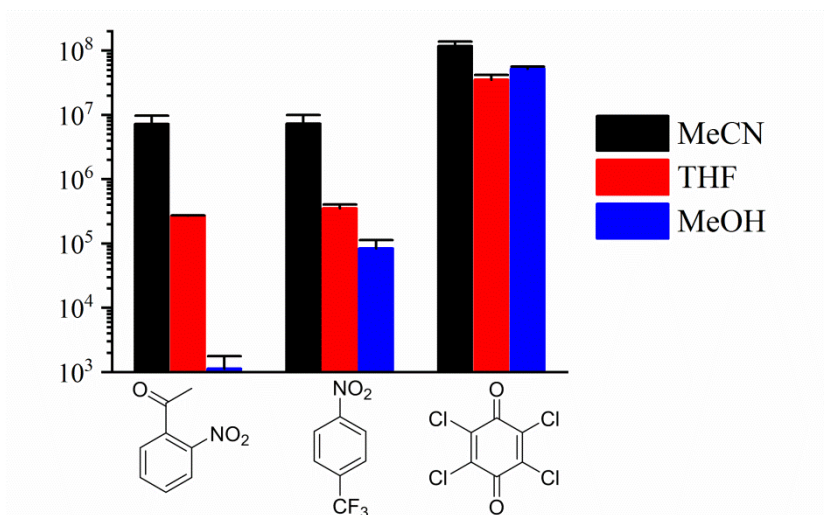


Figure 21: Absolute signal intensities observed upon negative-ion mode ESI-mass spectrometric analysis of 2-mM solutions of *o*-nitroacetophenone, *p*-nitrobenzotrifluoride or chloranil with CoCp₂ (1 equiv.) in different solvents. For the nitrobenzenes, the signal intensity of the fragment ion resulting from CID is displayed.

As for the detection of carbanions, MeCN appears to be the most suitable solvent for the analysis of radical anions. In all cases, the best signal intensity was achieved using MeCN. The use of THF resulted in a reduction in signal intensity across all species, which affected both NBs to the same degree. This indicates that no side reactions occurred. Instead the reduced signal intensity was the result of the lesser polarity of THF compared to the usual ESI solvents.¹⁷⁹ BQ_{C14} was seemingly less affected than the NBs, which may be the result of the oversaturation recorded for concentrations of 2 mM.

For MeOH, the results were rather mixed when compared to MeCN or THF. The addition of CoCp₂ to a solution of BQ_{C14} in MeOH resulted in the precipitation of a dark green solid, which did not fully dissolve with time. Despite that, the achieved signal intensity of the radical anion exceeded those of THF solutions due to the higher polarity of the solvent. For NBs, the signal intensity was reduced drastically, though by different amounts. Most likely, MeOH acted as a non-innocent solvent in these cases, being a reaction partner for CoCp₂ more reactive than even water. Once again, the signal intensities remained stable throughout the measurement. Overall, MeCN remains the solvent of choice due to the high signal intensity observed for corresponding solutions and due to it being seemingly non-reactive with the reducing agent CoCp₂.

3.2.5 Influence of the Reducing Agent

In addition to CoCp₂, dissolved in toluene, other reducing agents were also used to perform the radical anions. As a weaker reducing agent,¹⁸² FeCp₂ was added to solutions of the radical precursors, but in all cases, the result was equal to adding no reducing agent. No signal intensity was observed for NBs and comparatively moderate signal intensity for BQ_{C14}^{•-}. Other reducing agents were tetrakis(dimethylamino)ethylene (C₂(NMe₂)₄) as a mixture with MeCN and sodium naphthalenide (Na⁺C₁₀H₈^{•-}), prepared in THF shortly before the addition to the precursor solutions (**Figure 22**). The latter is a reducing agent stronger than CoCp₂ and should easily facilitate the transfer of the excess electron to more affine species.¹⁸² The former is an organic reducing agent that is slightly weaker than CoCp₂ (solvent-dependent $-(0.6-0.8)$ V vs SCE¹⁹³ compared to -0.9 V vs SCE¹⁹⁴ for CoCp₂), but should be sufficiently strong to quantitatively reduce the precursor analytes. It is known to undergo single-electron transfers, but has the potential to donate a second electron as well.¹⁹³ All reducing agents were prepared as ~ 0.25 -M solutions and added to the sample solutions using gastight syringes.

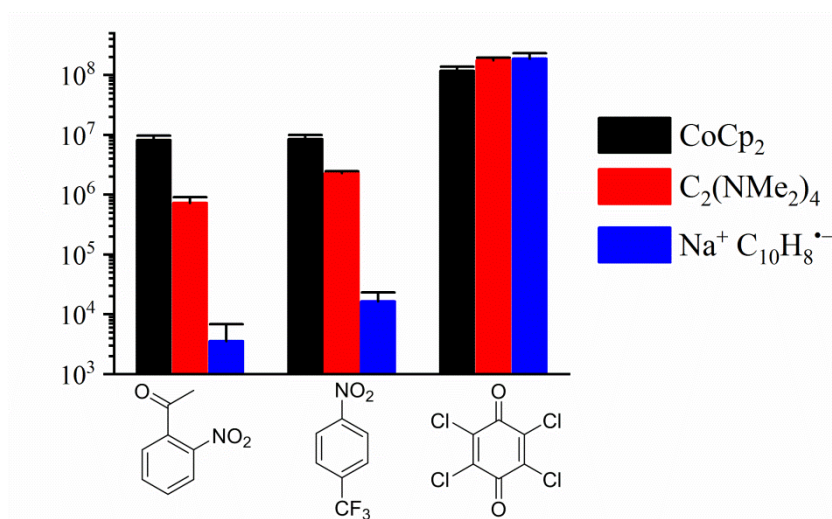
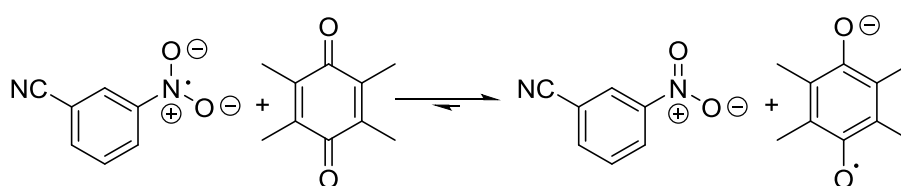


Figure 22: Absolute signal intensities observed upon negative-ion mode ESI-mass spectrometric analysis of 2-mM solutions of *o*-nitroacetophenone, *p*-nitrobenzotrifluoride or chloranil with various reducing agents (1 equiv.) in MeCN. For the nitrobenzenes, the signal intensity of the fragment ion resulting from CID is displayed.

For BQ_{C14}, the radical anion signal intensity was higher when using reducing agents other than CoCp₂. As BQ_{C14} is essentially guaranteed to be quantitatively reduced in every case, the difference most likely stems from the counterion and its interaction with the anion during the ESI process, especially in regards to the oversaturation of the anion signal.

The NBs experienced a reduction in signal intensity by a factor of ~ 10 when using $C_2(NMe_2)_4$ instead of $CoCp_2$, and a drastic reduction when using $C_{10}H_8^{\bullet-}$ instead. In both cases, the less electron-affine NB_{oCOCH_3} was affected more. For $C_2(NMe_2)_4$, the slightly lesser reduction potential may perhaps lead to incomplete formation of $M^{\bullet-}$, thus reducing the signal intensity. As most purely organic reducing agents are weaker than $C_2(NMe_2)_4$, it may seem preferable to rely on metal complexes such as $CoCp_2$ or even $CoCp^*_2$ instead.¹⁸² For $C_{10}H_8^{\bullet-}$, two options are likely. The first is a reaction with the solvent or certain impurities due to the stronger reduction potential compared to the other additives. Due to the high EA of BQ_{Cl_4} , it may react with products of said side reaction or compete directly, in contrast to the NBs. The second option is the decay of $C_{10}H_8^{\bullet-}$ during the transfer to the sample. The large variance across experiments for the NBs indicates the latter possibility. In both cases, the reduced concentration of $BQ_{Cl_4}^{\bullet-}$ may not be represented by the mass spectrum due to the oversaturation observed under standard conditions.

The fact that electron transfer from one radical anion to a neutral molecule occurs has been confirmed by adding 1 equivalent of duroquinone (BQ_{Me_4} , EA = 1.59 eV) to a solution of *m*-nitrobenzonitrile (NB_{mCN} , EA = 1.56 eV) and $CoCp_2$ in MeCN (**Scheme 5**). In the time delay between addition of BQ_{Me_4} to the solution and the measurement, an equilibrium had already been established, reaching stable signal intensities at a ratio of 25:1 for $BQ_{Me_4}^{\bullet-}$ and $NB_{mCN}^{\bullet-}$ respectively.



Scheme 5: Fast electron transfer from $NB_{mCN}^{\bullet-}$ to the more electron affine BQ_{Me_4} .

3.2.6 Reactivity of Radical Anions in Solution

Among the species tested regarding their behavior during ESI-mass spectrometric measurements, some were observed to undergo reactions, thus reducing their signal intensity over time. One of the advantages of ESI-MS is the identification of new species produced by side reactions, provided they are ionic. This was, as an example, the case for 2,5-dichlorobenzoquinone (BQ_{Cl_2}). The mechanism was initially thought to be a radical

recombination, resulting in the condensation of two radical anions to produce $[(\text{BQ}_{\text{Cl}_2})_2-\text{Cl}]^-$ and Cl^- . However, reducing or increasing the amount of added reducing agent led to drastically different reactivities (**Figure 23**).

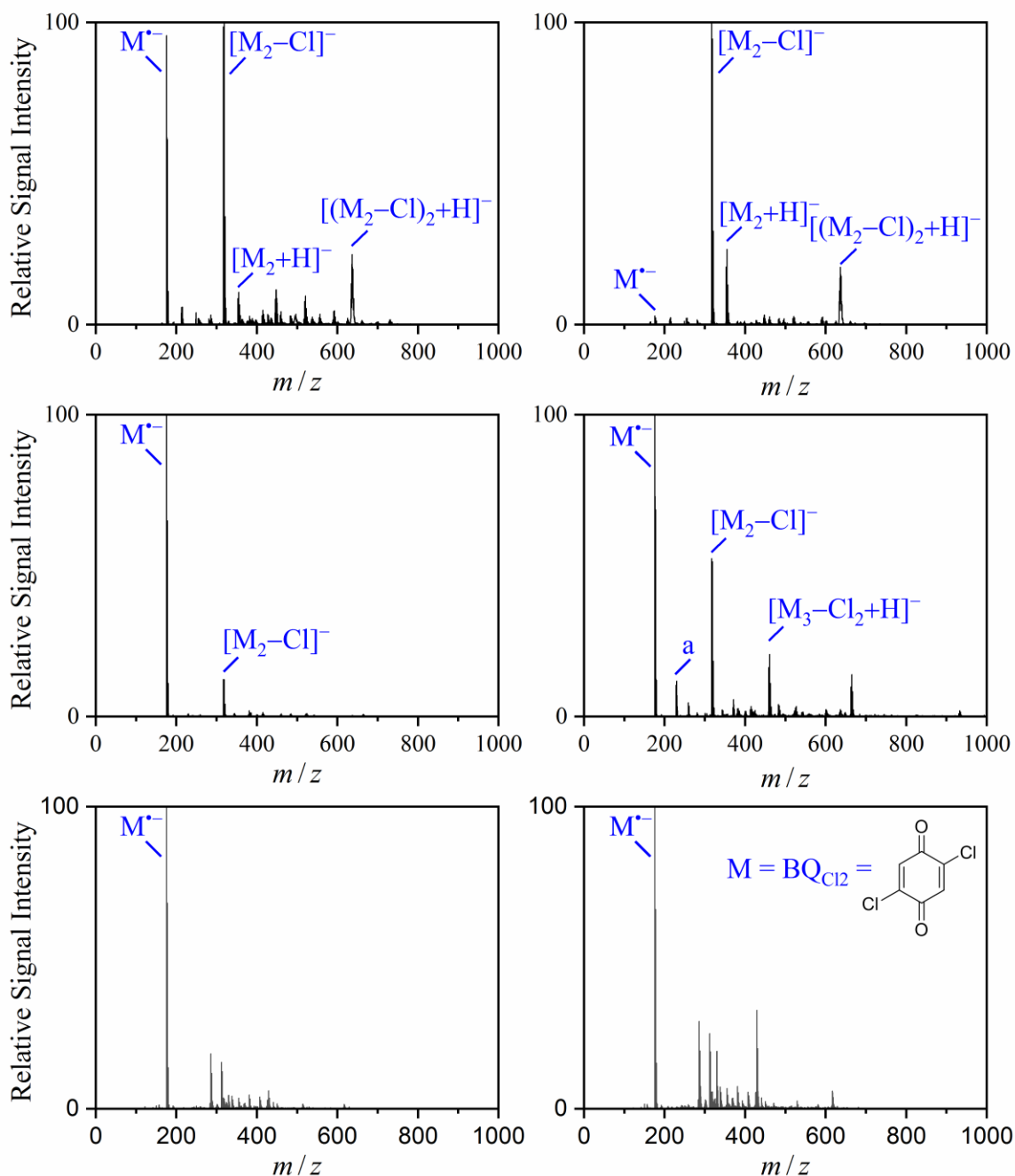
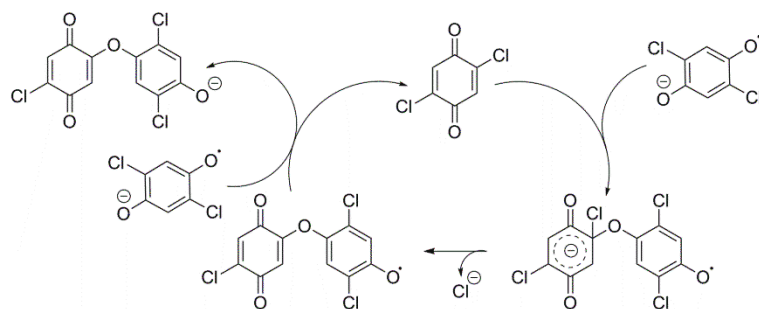


Figure 23: Negative-ion mode ESI mass spectra of 2-mM solutions of 2,5-dichlorobenzoquinone (BQ_{Cl_2}) with 0.5 (top), 1 (middle) and 2 (bottom) equiv. CoCp_2 in MeCN. Spectra were recorded immediately after the addition of CoCp_2 (left) and after 5 min of stirring (right). $a = [\text{M}_3-\text{Cl}_2]^{2-}$.

After the addition of 1 equiv. of CoCp_2 , the reaction was observed to occur at a moderate rate. After 5 min, the radical anion signal of $\text{BQ}_{\text{Cl}_2}^{\bullet-}$ remained the most prominent signal, but both dimers and trimers had been formed in significant amounts, having lost one and

two Cl^- , respectively. By increasing the amount of CoCp_2 , this condensation reaction could be prevented. Some new signals appeared, likely due to the excess of reducing agent, but none that could be attributed to BQ_{Cl_2} directly. When decreasing the amount of CoCp_2 to 0.5 equivalents instead, the dimerization reaction proceeded much faster, with the radical anion being almost non-existent in the mass spectrum after a reaction time of 5 min. No trimers were observed, but other forms of dimers could be assigned. It is unknown whether these consist of covalent bonds or if, for example, the association of HCl to a dimer resulted in $[(\text{BQ}_{\text{Cl}_2})_2 + \text{H}]^-$. Its only fragment ion upon CID was $[(\text{BQ}_{\text{Cl}_2})_2 - \text{Cl}]^-$.

Considering these reactivity changes, it is unlikely a radical recombination occurred here. Instead, the radical anion reacted as a nucleophile with the neutral BQ in an $\text{S}_{\text{N}}\text{Ar}$ reaction. By quantitatively reducing the BQ to its semiquinone form with an excess of reducing agent, the reaction is deprived of one component and does not occur. The addition of 1 equivalent of reducing agent should result in a similar spectrum, but presumably small differences in the stoichiometries were sufficient to enable the reaction. The net result of the reaction according to the suggested mechanism is a dimerization of two radical anions, catalyzed by the neutral BQ_{Cl_2} (**Scheme 6**).



Scheme 6: Suggested reaction mechanism for the dimerization of 2,5-dichlorosemiquinone.

The kinetics of ionic reactions can often be determined using the mass spectrometric change in signal intensity over time for both reactant and product.¹⁹⁵ The analysis of this particular reaction, however, is hindered by the relevant molecules being present both as anionic and as neutral species. Without the ability to monitor both at the same time, the reactions can be identified by interpreting the mass spectra qualitatively, but the signal intensities cannot be linked to concentrations, as in-source ionization of neutral species is likely to occur, in addition to potential reactions with impurities like water or oxygen.

The difficulty of distinguishing radical anions present in solution and those formed during the ESI process can be expected to be encountered during many of the potential applications. The signal intensity can only be linked to the concentration of radical anions in solution if in-source reduction can be precluded. This is the case when the radical anion is formed quantitatively or if the neutral species has a sufficiently low EA. The second option may be expanded upon by changing the experimental conditions to disfavor this reduction process, but a drastic reduction in scope of potential applications is to be expected nevertheless. The generally fast reaction of radicals and radical anions further reduces the potential uses of ESI-MS, whose timescale is usually limited to seconds or longer. In these cases, use of electron paramagnetic resonance (EPR) spectroscopy is preferred, which performs on a much faster scale.^{196,197}

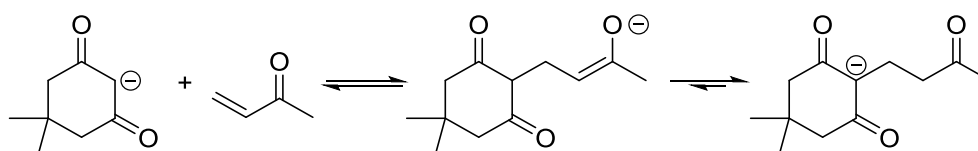
For the cases in which in-source ionization does not interfere with the results, ESI-MS is a good alternative to other analytical techniques for the analysis of radical anions in solution. While limited to species of sufficient EA, those anions can be detected easily and efficiently. The sample preparation is straightforward, with the species investigated here even tolerating small amounts of water. The simultaneous detection of non-radical anions helps identify and quantify reactions that would be inaccessible to EPR spectroscopy. Finally, the utilized ESI-MS instrument required no particular set-up in order to transfer preformed radical anions into the gas phase and has the potential to be an easier alternative to chemical ionization, which may require specialized instruments, when the objective is the generation of gas-phase species for further analysis by spectroscopic means.

3.3 Reaction Monitoring and Kinetic Observations

A highly effective and relevant application of ESI-MS is the time-resolved, on-line monitoring of reacting solutions.¹⁹⁸ By tracking the concentrations of individual species, exact kinetic information can be gathered. This requires a known correlation between signal intensities and concentrations. During the direct detection of carbanions from solution by ESI-MS, this correlation was shown to be linear when the degree of aggregation is low. The formation of aggregates depends strongly on the species, counterion, and concentration. It may be influenced further by the addition of, for example, crown ethers, though this affects the reaction rates as well.¹⁹⁹ Other requirements were shown to be a moderate basicity of the carbanion and moderate reaction rates, preferably below $pK_a \sim 25$ and a half-life of minutes, respectively. The latter can be adjusted by changing the initial concentrations of the reactants. When these conditions are fulfilled, ESI-MS may be used to determine kinetics directly from solution. In the following, examples will be demonstrated, beginning with a simple Michael addition reaction and followed by two oligomerizations featuring suitable anionic active species.

3.3.1 Michael-Addition of Dimedone to Butenone

As an example for the kinetic analysis of reacting carbanions, the Michael-addition²⁰⁰ between butenone and deprotonated dimedone was chosen (**Scheme 7**). Being an efficient way of forming C-C-bonds, this type of reaction has always been of great importance in organic chemistry. Deprotonated dimedone was chosen as the carbanion due to its low propensity to aggregation.²⁰¹



Scheme 7: Michael-addition of deprotonated dimedone to butenone.

The above-mentioned second-order reaction was simplified to a pseudo first-order reaction by adding 20 equivalents of butenone to a 2-mM solution of dimedone and KO^tBu in MeCN while being stirred at room temperature under a constant pressure of argon. Shortly after, the ESI inlet line was placed in the solution, completing the standard

pressurized sample infusion (PSI)¹⁶⁵ setup that transfers the sample solution directly to the ESI source. The expected reaction took place, as seen by the decreasing signal intensity of dimedone (m/z 139) in favor of the product ion (m/z 209). The intensity ratios shifting with time (**Figure 24**) precludes the possibility of the reaction occurring exclusively or primarily within the generated microdroplets.¹⁷⁰ Instead, this phenomenon of accelerated reaction rates was treated as a time-offset, which does not interfere with the analysis due to the simplification to pseudo first-order.

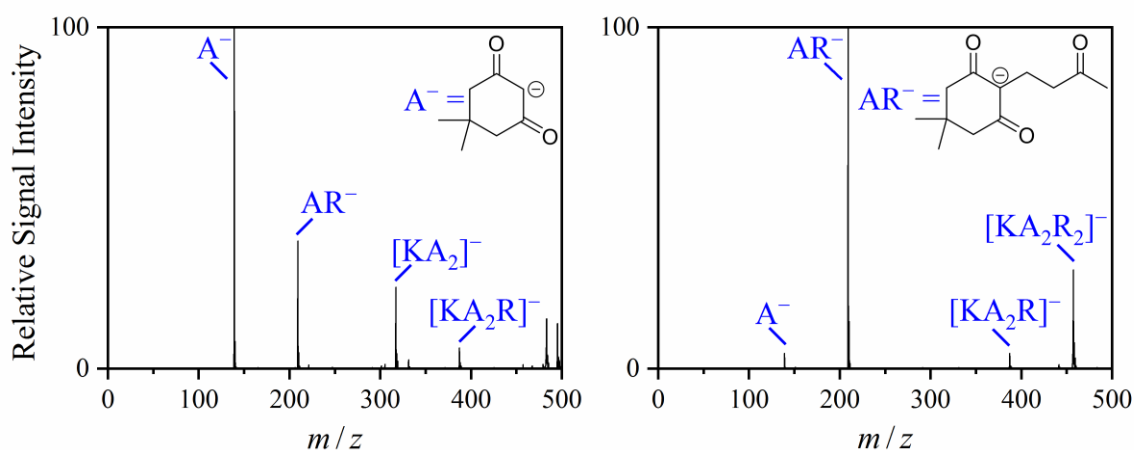


Figure 24: Negative-ion mode ESI mass spectra of a 2-mM solution of dimedone / KO^tBu and butenone (20 equiv.) in MeCN at room temperature after 0.5 min (left) and 20 min (right).

The signal intensities of educt and product were traced separately, each affording an individual rate constant by fitting an exponential curve to the mass spectrometric data. The relevant ions were not fragmented in this case, as two signals had to be traced simultaneously and significant isobaric interference was unlikely judging by the ESI-mass spectrometric measurement of deprotonated dimedone. In order to compare the results gained in this way with an alternative method, the reaction was repeated and aliquots, taken after defined times, were quenched with NH₄Cl before quantitating the neutral reactant and product using HPLC equipped with an positive-ion mode ESI-MS detector (**Figure 25**). Further analysis was the same as for the direct negative-ion mode ESI-MS.

In the ESI mass spectra, reactant and product had different ESI activities, as seen by comparing the initial reactant's signal intensity with the final product signal intensity. This prohibits using their relative intensities and instead requires a separate analysis of reactant and product as described earlier. The rate constants determined by ESI-MS and HPLC mostly agree (**Table 3**).

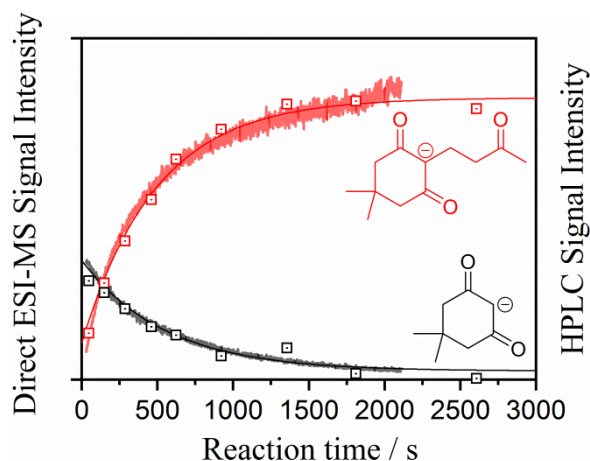


Figure 25: Time profiles of reactant (black) and product (red) during the Michael-addition of deprotonated dimedone (2 mM) to butenone (20 equiv.) in MeCN at room temperature observed live by direct negative-ion mode ESI-MS (lines) and by positive-ion mode HPLC-ESI-MS of aliquots (squares), along with logarithmic fits of the direct ESI-MS data.

Table 3: Experimental second-order rate constants derived for the Michael-addition of deprotonated dimedone to butenone in MeCN at room temperature.

Method	$k / (\text{L mol}^{-1} \text{s}^{-1})$	
	Derived from reactant	Derived from product
Direct ESI-MS(-)	$47 \pm 13 \times 10^{-3}$	$52 \pm 15 \times 10^{-3}$
HPLC-ESI-MS(+)	$33 \pm 12 \times 10^{-3}$	$45 \pm 10 \times 10^{-3}$

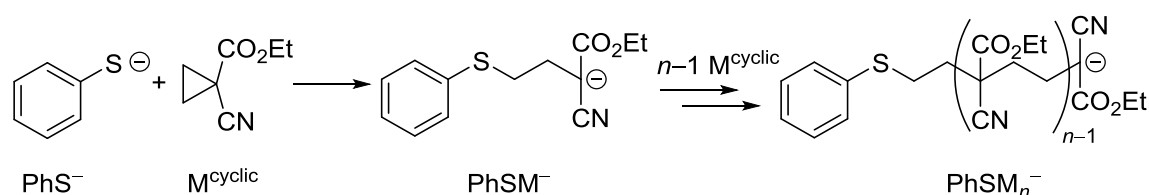
The difference in rate constants derived from reactant and product was smaller for ESI-MS than for HPLC, though the standard deviations in general were in an acceptable range for kinetic measurements. Factors reducing the accuracy for ESI-MS may be the formation of aggregates that was not prevented fully, as well as a non-perfect linear relation between signal intensity and concentrations. The most extreme case for this would be oversaturation, for which there was no evidence in this case, but the observed deviation from an ideal exponential decay curve may have been the result of smaller deviations from the linear correlation. The non-zero baseline approached by the deprotonated dimedone's signal intensity likely resulted from in-source fragmentation of the product.

Nevertheless, the comparison between direct ESI-MS and HPLC shows the suitability of the former for kinetic analysis of metal-free ionic reactions, combining the advantages of in-situ measurements with the selectivity inherent to mass spectrometric methods.

3.3.2 Anionic Polymerization of 1,1-Substituted Cyclopropane

A more complex example for the application of direct ESI-MS for kinetic analysis is the monitoring of an anionic polymerization. Simple reactions like the Michael addition can be investigated using other methods as well, affording comparable results. For polymerizations, however, a method capable of in-situ mass distribution determination may provide information that is otherwise inaccessible and thus is highly desirable.

The model reaction chosen to investigate the suitability of ESI-MS for kinetic monitoring of anionic living polymerizations was the ring-opening polymerization of ethyl 1-cyanocyclopropane-1-carboxylate (M^{cyclic}), initiated by a thiophenolate anion (PhS^- , generated from PhSH and KO^tBu) in the presence of 18-crown-6 (18C6) in THF (**Scheme 8**). This type of monomer, a cyclopropane featuring two electron-withdrawing groups in a 1,1-substituted fashion, has been extensively investigated by Penelle and coworkers.^{128-132,202} The polymerization of this type of monomer features a rather stable end group, reminiscent of carbanions shown to be readily accessible by ESI-MS above.



Scheme 8: Anionic ring-opening polymerization of ethyl 1-cyanocyclopropane-1-carboxylate (M^{cyclic}) initiated by thiophenolate anion (PhS^-).

A solution of PhSH (2 mM), KO^tBu (1.3 equiv.) and 18C6 (1.7 equiv.) in dry THF was heated to 70 °C bath temperature under an argon atmosphere. The slight excess of base prevented proton transfer from neutral PhSH to growing chains. 18C6 was added to reduce counterion-effects and aggregation that may negatively impact the analysis of the mass distribution. A defined amount of monomer was added via syringe and after a short delay the inlet line to the ESI source was introduced into the solution to complete the PSI^{165} setup. The mass spectra were recorded for up to 4 h (**Figure 26**). The main feature in the mass spectra was a series of equidistant peaks beginning at m/z 109, with the distance between two signals being $\Delta m = 139$. These m/z ratios correspond to those expected for PhSM_n^- . A shift towards higher masses with increasing reaction time indicates the successful polymerization.

* Results published in: N. F. Eisele, M. Peters, K. Koszinowski, *Chem. Eur. J.* **2023**, e202203762.

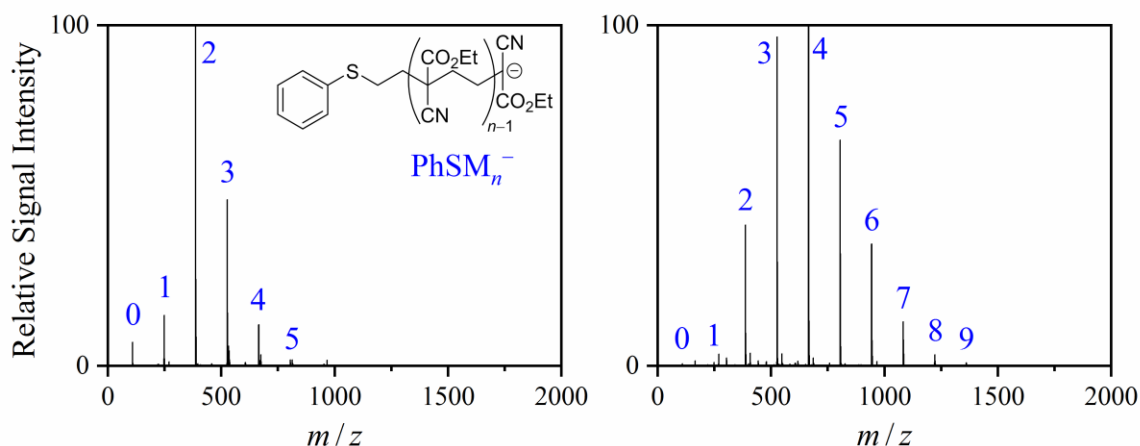
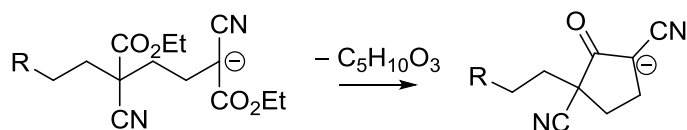


Figure 26: Negative-ion mode ESI mass spectra of a solution of PhSH (2 mM), KO^tBu (1.3 equiv.), 18C6 (1.7 equiv.) and M^{cyclic} (27 equiv.) in THF at 70 °C bath temperature after 50 min (left) and 240 min (right) reaction time. Numbers indicate the degree of polymerization n .

The reaction rate of this particular polymerization and under the chosen conditions is very slow compared to typical anionic polymerizations, due to the high stability of the end group and the low reactivity of cyclopropanes compared to oxiranes and other comparable structures.²⁰³ The spectrum does not contain any species of another series of oligomers that would indicate transfer reactions or a direct initiation of M^{cyclic} by the base, such as ^tBuOM_{*n*}⁻ or HOM_{*n*}⁻. It does, however, contain a second series with $\Delta m = -118$ when approaching long reaction times. This series was revealed to be the product of an intramolecular termination reaction, in which the active center backbites onto the previous ester functionality (**Scheme 9**). The product of this reaction contains a stable anionic charge, as it is also being stabilized by two electron-withdrawing groups. This results in the product being easily detectable by ESI-MS.



Scheme 9: Suggested slow termination reaction of PhSM_{*n*}⁻ via backbiting.

The structure of the side reaction product was suggested based on the fragmentation pattern of PhSM_{*n*}⁻ with $n = 1$ compared to $n \geq 2$, of which only the latter predominately fragments into the second observed series of $\Delta m = -118$ when subjected to CID (**Figure 27**). Further fragmentation of this anion results in the dissociation of either PhS⁻ or PhSH, with the ethylcyclopentanone subunit being unable to be fragmented any further.

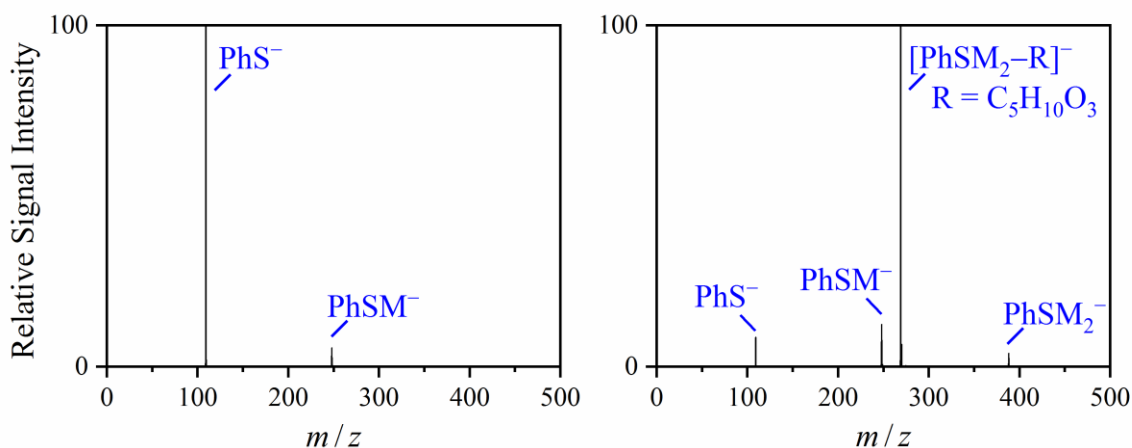


Figure 27: Negative-ion mode ESI-mass spectrometric analysis of the fragmentation patterns of mass-selected PhSM^- ($m/z = 248$, left) and PhSM_2^- ($m/z = 387$, right) when subjected to CID with $V_{\text{exc}} = 0.4$ V.

The increase of said species with time precludes the possibility of in-source fragmentation being the main contributor to the signal intensity. Nevertheless, the termination rate is slow compared to the propagation, so the reaction can for the most part still be considered to behave like a controlled polymerization. This holds true especially when performing the reaction at higher concentrations, where a high degree of conversion is reached after comparably short reaction times.²⁰² Purposefully increasing the reaction time to multiple days resulted in a spectrum containing exclusively this termination product. Addition of new monomer did not result in an increase in chain length, thus confirming this reaction to be an actual termination reaction.

3.3.2.1 Mass Bias Considerations

The most common approach when using mass spectrometry for polymers is to analyze the isolated product using MALDI-TOF-MS.¹¹⁹ Fewer examples exist for ESI-MS and most of those use ESI-MS coupled to size-exclusion chromatography (SEC), in order to assign exact masses to the retention times.¹¹³ The reason why ESI-MS is rarely used to determine mass distributions directly is the risk of significant mass bias.¹¹⁸ One of the main reasons contributing to this effect is a chain length-dependent ionization.¹¹⁹ Under regular ESI conditions, analyte ions are usually formed by association of, for example, alkali metal cations. A longer chain equals more functional groups that a cation may attach to, resulting in higher ionization efficiency and an increased tendency to form multi-charged ions that complicate the estimation of the mass distribution. This is a non-issue when using ESI-MS for living anionic polymerizations, as all species share the same type of permanent charge. On a related note, the high stability of the anionic center during

the polymerization of M^{cyclic} means that proton transfer from traces of water or similar impurities does not occur. Every chain that was initiated can be expected to keep exactly one charge until the time of the measurement.

A second effect that may introduce mass bias is the ESI efficiency of the different chain lengths. It is known that the transfer of ions into the gas phase is facilitated by long, non-polar residues, which increase the surface activity of the analyte.²⁰⁴ The magnitude of this effect is difficult to quantify. For this particular model system, however, the effect is expected to be greatly diminished. The monomer contains a large amount of polar functional groups, while the solvent is less polar than the most common ESI solvents. By aligning the polarity of analyte and solvent, the increase in surface activity with increasing degree of polymerization should be largely mitigated.

The third aspect to be considered regarding a possible mass bias is the mass analyzer. Ion traps are known to more efficiently capture ions of particular m/z depending on the current instrument settings.²⁹ Usually, when not directly comparing multiple species with each other, this effect does not influence the capability of ESI-MS to monitor concentrations as long as the instrument settings are kept constant. For polymers though, multiple species have to be compared to each other in order to obtain a roughly accurate molar mass distribution. Additionally, as the mass distribution shifts over the course of the reaction, any individual setting that may approximate the actual mass distribution would do so only within a specific time frame.

In order to approximate the molar mass distribution across the whole time frame of the polymerization, an approach was attempted that contrasts regular mass spectrometric analysis. Using the *Smart Parameter Settings* function of the used instrument, the parameters can automatically be adjusted to be optimized for the detection of species near a *Target Mass*. For the detection of oligomers of the type PhSM_n^- , the *Target Mass* was tuned to equal the individual n successively. This was done for a full cycle of $0 \leq n \leq 20$. Then, the absolute signal intensity of the individual oligomers was extracted only when *Target Mass* equals the expected mass of the specific PhSM_n^- and compared with the other species within this cycle. A new cycle was then started immediately or after a defined delay. Using this methodology, the continuous measurement by ESI-MS was changed to be semi-continuous, with a separate mass distribution obtained for each cycle.

The above-mentioned methods to reduce the impact of mass bias, using a polar monomer in a less polar solvent and successively changing the parameter settings, are expected to improve the accuracy of mass distributions obtained via ESI-MS, but a complete mitigation of both effects is unlikely. In order to estimate the accuracy of said mass distributions, polymer samples were isolated and analyzed by ESI-MS after dissolution in THF with KO^tBu and 18C6, by NMR spectroscopy and by SEC (**Table 4**). As the oligomers from the diluted solutions used for ESI-MS analysis did not precipitate, the isolated samples were produced using higher concentrations. This enabled reaching high conversion within a time short enough to not be affected by the slow termination reaction, so samples were prepared using 5 and 10 equivalents of M^{cyclic}.

Samples prepared using 5 equivalents of monomer could be fully dissolved and subsequently analyzed, but the longer-chained samples did not fully dissolve in THF, CHCl₃, MeCN or DMSO, even at elevated temperatures. This results in an underestimation of the mean molar mass by ESI-MS and NMR spectroscopy, the magnitude of which not necessarily being equal. The mean molar mass from NMR was obtained by comparing the signal integrals of the aromatic initiator end group with a characteristic signal of the alkyl group of the ester. SEC measurements were performed externally, using a refractive index detector and DMF as the liquid phase.

Table 4: Number-average molar masses M_n and ratio of weight-average to number-average molar masses M_w/M_n of isolated oligomer samples determined by ESI-MS, NMR spectroscopy and SEC.

		ESI-MS ^a	NMR ^a	SEC
$c(\text{M}^{\text{cyclic}})/c(\text{PhS}^-)$	$M_n / (\text{g mol}^{-1})$	835 ± 14	822 ± 42	$1205 \pm 5^{\text{b}}$
= 5	M_w/M_n	1.071 ± 0.003	–	1.19^{b}
$c(\text{M}^{\text{cyclic}})/c(\text{PhS}^-)$	$M_n / (\text{g mol}^{-1})$	1339 ± 27	1331 ± 34	– ^c
= 10	M_w/M_n	1.064 ± 0.007	–	– ^c

a) Average of 4 samples for each ratio of concentrations. b) Average of 2 samples. c) Not attempted due to insoluble components.

The number-average molar masses determined by ESI-MS and by NMR spectroscopy overlap very well. This agreement for both the short- and the longer-chained samples is an indicator that the steps taken to ensure an accurate depiction of the mass distribution across a larger mass range were successful. The molar mass obtained from SEC was larger by ~50%, though this stems from the difference in hydrodynamic volume of the

poly(methyl methacrylate) used as calibrant compared to the sample oligomers and does not contradict the other methods. On the other hand, the ratio of weight-average to number-average molar masses, commonly referred to as polydispersity \mathcal{D} , shows a discrepancy that may implicate further analysis.

A direct comparison between the mass distributions obtained from ESI-MS and from SEC illustrates the difference in broadness (**Figure 28**). For this, the SEC data display was adjusted. The mass scale was calibrated using the M_n obtained from NMR experiments. The refractive index detector signal increases linearly with the mass of the sample that is being detected, so the signal intensity was divided by the molar mass in order to approximate concentration-based signal intensity. Finally, the resulting signal intensity was divided by the mass difference to the next data point, in order to transform the logarithmic x -scale into a linear scale as was obtained from mass spectrometry.

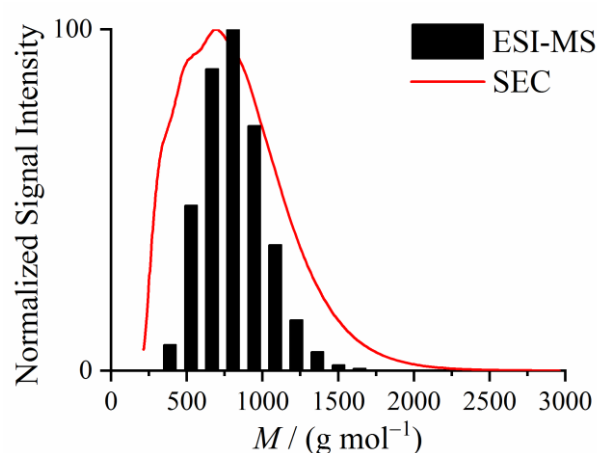


Figure 28: Overlay of mass distributions of an isolated oligomer sample PhSM_nH obtained from SEC using a refractive index detector and from ESI-MS of the deprotonated sample. The x -scale of the SEC distribution was adjusted according to the NMR results and the signal intensity was adjusted to represent a number-average mass distribution.

The differences between the methods can be attributed to multiple different effects, though the individual magnitudes of these effects could not be determined. The first possibility is a mass bias when recording ESI-MS data. This would require both low and high masses to be suppressed in favor of the moderate mass oligomers. The good agreement between NMR and ESI-MS for both samples with different M_n conflicts with this possibility, but the presence of a small amount of insoluble components in both NMR and ESI-MS sample solutions precludes a concluding argument. The second effect is an insufficient separation of the species using SEC, leading to peak broadening. The very small mass range the oligomer samples occupy may exacerbate this effect further.

Similarly, the short size may affect the response efficiency of the detector. Refractive index detectors are usually used for longer polymers, in which the detector response increases linearly with the molar mass. Such polymers can be approximated to be purely the connected monomers, as the end groups occupy sufficiently small a fraction of the total composition as to be negligible. For the oligomers tested here, the end groups may still influence the detector response, impacting the linear correlation of chain length to signal intensity.²⁰⁵

The polydispersity values obtained from both methods are not conclusive. An ideal living polymerization, with the same rate constant for the initiation as for each propagation step afterwards, has a polydispersity depending on the degree of polymerization with $D = 1+n/(n+1)^2$, resulting in ~ 1.14 for samples prepared from a fivefold excess of monomer.¹¹⁰ This, however, does not hold true when the early propagation steps occur faster than the later ones, compressing the mass distribution.

3.3.2.2 Reaction Kinetics obtained from ESI-MS Measurements

As the mass distributions obtained from ESI-MS so far appear to be consistent, the described method was used for further analysis, potentially resulting in further arguments for or against either side. For a kinetic investigation, 2-mM initiator solutions were prepared, to which M^{cyclic} was added, reaching concentrations of 32, 54, 107 or 211 mM. The molar mass distribution was tracked according to the above-mentioned method (**Figure 29**).

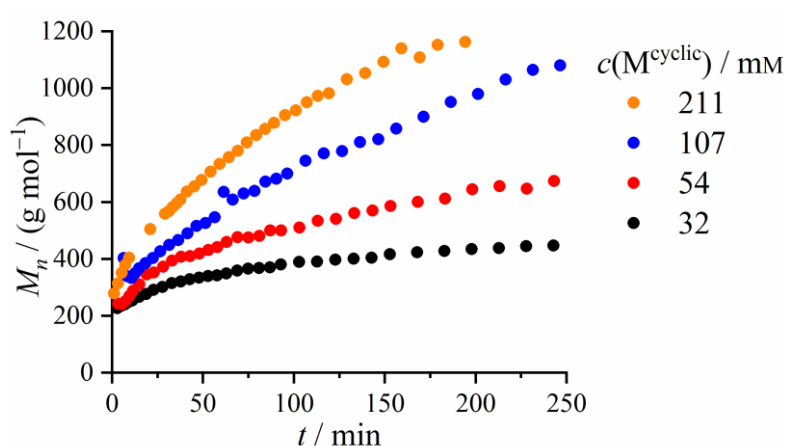


Figure 29: Time profiles of the number-average molar mass of PhSM_n^- during the polymerizations of M^{cyclic} at various concentrations initiated by PhSH (2 mM), KO^tBu (1.3 equiv.) and 18C6 (1.7 equiv.) in THF at 70 °C bath temperature.

The time profiles of the number-average molar mass across all experiments follow the same trend. During the initial stages of the reaction, a steeper increase in molar mass is observed. Shortly afterwards, the average molar mass increases linearly as is expected for a living polymerization, with the slope depending on the concentration of the monomer. The behavior in the low mass range can be the result of a significantly faster initiation reaction compared to the later propagation, or it may be caused by a drastically lower ESI efficiency of very short oligomer species. The former option would play into the polydispersity from SEC being overestimated, while the latter would result in the polydispersity obtained from ESI-MS to be underestimated, as the measured distribution would be compressed. As the average molar mass determined by ESI-MS agrees with that from NMR experiments, an underestimation of low-mass chains would need to be compensated by a similar underestimation of the higher-mass chains. This does not seem to be the case, judging by the molar mass evolution at long reaction times when using high initial concentrations of the monomer. However once again, neither option can be ruled out completely based on these observations.

For an estimation of the rate constants of initiation and propagation, the program COPASI (Complex Pathway Simulator) was used.²⁰⁶ The goal was the determination of rate constants for the individual reaction steps, contrasting the usual approach to polymerization kinetics of assigning a singular rate constant each for the initiation, propagation, transfer and termination steps. This procedure is enabled by the ability of ESI-MS to monitor not only the average molar mass or the overall number of active species, but the whole mass distribution within a limited mass range. Furthermore, by combining multiple runs with different initial concentrations in a single simulation, a successful estimation of the rate constants would indicate the mass distributions obtained from ESI-MS to be mostly accurate as well.

For the simulation, the following assumptions were made:

- 1) The relative signal intensities of the various PhSM_n^- correspond to the relative concentration in solution. All species have the same ESI efficiency.
- 2) The total concentration of all PhSM_n^- equals the initial concentration c_0 of PhS^- . There are no transfer or termination reactions.
- 3) Every monomer addition step follows an irreversible second-order rate law with an individual rate constant k_n for the reaction $\text{PhSM}_{n-1}^- + \text{M}^{\text{cyclic}} \rightarrow \text{PhSM}_n^-$.

The first assumption is based on the method of successively changing the *Target Mass* to the individual species and extracting the signal intensity accordingly. It is an approximation that is necessary in order to connect the detected signal intensities in the mass spectra with the species' concentrations in solution.

The second assumption is not strictly true, as seen by the backbiting termination reaction observed for long reaction times, but is justified by the low amount of side reaction products observed even after 4 h reaction time. Due to differing ESI efficiencies of the active and the terminated form, the signal intensities could not be linked to concentrations without this or a similar limitation.

A total of 14 experiments were included in the simulation as experimental data, with concentrations in the range of $32 \text{ mM} \leq c_0 \leq 211 \text{ mM}$. An individual time offset was included in the simulation for each experiment. This includes not only the time delay between addition of the monomer and the first data point, but also mitigates a slower reaction due to a lower temperature immediately after the addition of the monomer and within the tubing of the ESI source inlet, as well as the faster reaction that may occur within microdroplets during the electrospray process.¹⁷⁰

According to the mass distributions of the available data, the simulation was limited to the 1st to 11th addition step (**Figure 30**). The apparent concentration of the initiator PhS^- was not included in the simulation, due to its low signal intensity even at the first data point, a risk of in-source fragmentation of PhSM^- feeding into said concentration, and the different structure of the charged center that leads to a significant possibility of differences in ESI efficiency. Instead, the reaction rate of the initiation was obtained exclusively from the concentration of PhSM^- . Its time course deviates from an ideal exponential decay expected of a pseudo-first order reaction due to simultaneously being generated by the remaining PhS^- . This leads to a higher uncertainty for the initiation rate constant, but should more accurately represent the true value.

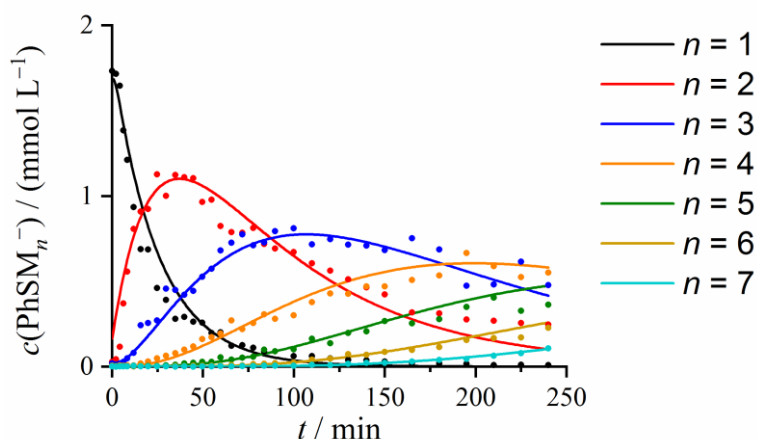


Figure 30: Experimental (dots) and simulated (lines) time profiles of the individual apparent concentrations of PhSM_n^- obtained from ESI-mass spectrometric analysis of a solution of PhSH (2 mM), KO^tBu (1.3 equiv.), 18C6 (1.7 equiv.) and M^{cyclic} (27 equiv.) in THF at 70 °C bath temperature.

The agreement between simulation and experimental data is good, with no evidence of the assumptions being insufficient to accurately display the course of reaction. Despite using a total of 14 separate experiments, including various concentrations, the individual rate constants were obtained with standard deviations below 10%, excluding k_{11} due to not all experiments reaching non-zero concentrations of PhSM_{11}^- . The final rate constants show a steep decline after the initiation, decreasing from $0.25 \text{ M}^{-1} \text{ s}^{-1}$ to $0.003 \text{ M}^{-1} \text{ s}^{-1}$ within the first 4 steps, after which the rate constants remain at the same level for the further propagation reactions (**Figure 31**).

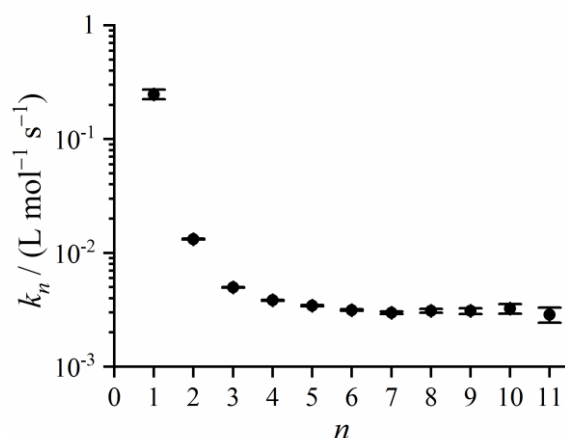


Figure 31: Individual rate constants k_n for the reaction of $\text{PhSM}_{n-1}^- + \text{M}^{\text{cyclic}} \rightarrow \text{PhSM}_n^-$ at 70 °C bath temperature in THF as obtained from a parameter estimation using the experimental data.

The observed decline in reaction rates with increasing chain length reflects the observations made from the time profiles of the average molar masses. The difference in

reaction rate between initiation and the later steps of propagation is in line with the higher nucleophilicity recorded for thiophenolate compared to deprotonated ethyl cyanoacetate and similar anions.^{207,208}

The contrast between PhSM^- and PhSM_n^- is rather large, despite containing the same type of active center. This being a result of mass bias, leading to the underestimation of the concentrations of very short species, cannot be fully ruled out. However contradicting this is the constant reaction rate for species with $n \geq 5$. This behavior is expected for polymerizations where the addition of a single monomer does not significantly change the reaction behavior of the molecule and suggests no mass bias affecting the signal intensities in the upper mass range. This, in combination with the good agreement in average molar mass between ESI-MS and NMR experiments, infers that no large mass bias occurs in the low mass range either. Assuming the rate constants to be qualitatively correct, the change in reactivity can be caused by a combination of various effects. The electronic structure of the active center may be affected by the distance between the active center and the sulfur, though this effect should be rather small as the system is not conjugated and even in PhSM^- the C_2 -unit between the charged moiety and the initiator acts as a spacer, isolating the electronic structure. Steric considerations, accessibility and speed of diffusion can be expected to decrease the reaction rates, as the large relative increase in hydrodynamic radius decreases the diffusion coefficient. Finally, the polar functional groups of the incorporated monomers in PhSM_n^- may influence the reactivity. For example, the oxygen of an ester group nearby the active center could support the coordination of a counterion, thus temporarily blocking a portion of the active centers and reducing the overall reaction rates. Overall, these results should not be used to infer a general trend for the reactivity of very short oligomers, as the differences between IniM^- and IniM_n^- ($n = 2-4$) can be assumed to depend strongly on the exact system.

In order to compare the results of the kinetic simulation of rate constants from in-situ monitoring of the oligomerization reaction with experimental results reported in the literature, the monomer conversion of this system was simulated using the same concentrations as those used by Penelle and coworkers.²⁰² A rate constant of $0.003 \text{ M}^{-1} \text{ s}^{-1}$ was assumed for every propagation step past the 11th. Besides the drastically lower concentration, further differences between the reported polymerization and this reaction monitored by ESI-MS were the addition of a crown ether and changing the solvent from a small amount of DMSO to a large amount of THF. The bath temperature was increased to

70 °C, as the difference between bath temperature and actual temperature was expected to be much larger for the experimental setup used for this study. Considering these changes, the simulated monomer conversions agree remarkably well with those reported by Penelle and coworkers. While the simulation reaches a monomer conversion of 44% after 15 min and 87% after 1 h, they reported experimental yields of 39% and 84% respectively.²⁰²

The qualitative agreement between reported and simulated conversions confirms that in some cases the rate constants for polymerization reactions may already be derived from the in-situ monitoring of the oligomerization instead. The effect of single monomer additions on reaction rates for very short chains is a field that was previously mostly unexplored, with few exceptions like the esterification of lactic acid oligomers with ethanol, where comparable differences between M , M_2 and M_3 were observed.²⁰⁹ ESI-MS enables this analysis for ionic oligomerizations to be faster and easier than any other method. It is, however, limited in scope of the system, regarding both the reactivity and occurring species. To obtain representative signal intensities in a low mass range and to prevent multi-charged species, a permanent charge is required that is sufficiently stable to survive the transfer from solution into the gas phase. The reactivity of the active species is limited by the scan rate of the instrument. While the oligomerization of the model system was sufficiently slow that scans could be performed at multiple settings in order to reduce mass bias, this will not always be the case. For faster reactions, other methods of mitigating mass bias may be required, first of which being changing the mass analyzer. As an example, a time-of-flight (TOF) mass analyzer is less prone to introducing mass bias than an ion trap.²⁹ Nevertheless, mass spectrometry will approach a limit in reactivity dependent on the scan rate and the available mass range. Reducing the concentration of both monomer and initiator may enable faster reactions to be monitored but increases the risk of impurities compromising the experiment.

For systems that fall within these limitations, most of which depend strongly on the utilized instrument and can be expected to change with further technological advancements, ESI-MS was shown to be a viable method for obtaining unprecedentedly detailed kinetic information of oligomerizations by providing a method that can measure mass distributions in-situ. By significantly slowing down the propagation by the use of low concentrations, side reactions can be identified that would go unnoticed when analyzing the system using more traditional methods. Finally, the option to fragment mass-selected ions provides another avenue of insight into the behavior of the system.

3.3.3 Anionic Coordination Polymerization of Isoprene on Cobalt(I)

The following results are a continuation of a project initiated by Dr. F. Kreyenschmidt. New experiments were performed and extensive existing data was reanalyzed.

The limits regarding the reacting system that were inferred for the direct analysis of anionic oligomerizations by ESI-MS for the most part do not apply when the oligomer to be analyzed is coordinated by a metal ion. For neutral polymers that are ionized by attachment of a smaller ion, the accuracy of the method is greatly diminished by chain length-dependent coordination behavior. However, this is not the case when considering living coordination polymerizations. During those, all growing chains are either permanently bound to the metal ion during both the reaction and the analysis, or have an equal chance to be coordinated to the metal at all times via a reversible chain transfer. Either effect results in an ionization efficiency that is chain length-independent. This can also include non-controlled polymerizations, though the larger polydispersity may negatively affect the accuracy of the mass distributions. This way, the accessible systems are greatly expanded, also including some with non-polar monomers.

The viability of ESI-MS to generate detailed kinetic information for this type of reaction was demonstrated for the system of isoprene (DE^{I}) mediated by the combination of CoCl_2 and PhLi in THF at room temperature. The reaction solution was prepared by adding PhLi to a solution of CoCl_2 in dry THF at $-78\text{ }^\circ\text{C}$, stirring for 10 min, then adding the monomer DE^{I} to the mixture at the same temperature. The solution was drawn up in a gastight syringe and injected into the inlet of the ESI source of the mass spectrometer. By drawing up a small volume compared to the mass of the glass syringe, the solution was allowed to reach approximately room temperature within a short time frame, with the temperature raise marking the initiation of the polymerization reaction. The mass spectra were recorded for up to 30 min using an ESI-TOF-MS, so no additional steps regarding the instrument settings, like those applied to the previously used ion trap, were taken to prevent mass bias (**Figure 32**).

* Results published in: F. Kreyenschmidt⁺, N. F. Eisele⁺, V. Hevelke, R. Rahrt, A.-K. Kreyenschmidt, K. Koszinowski*, *Angew. Chem. Int. Ed.* **2022**, *61*, e202210211.

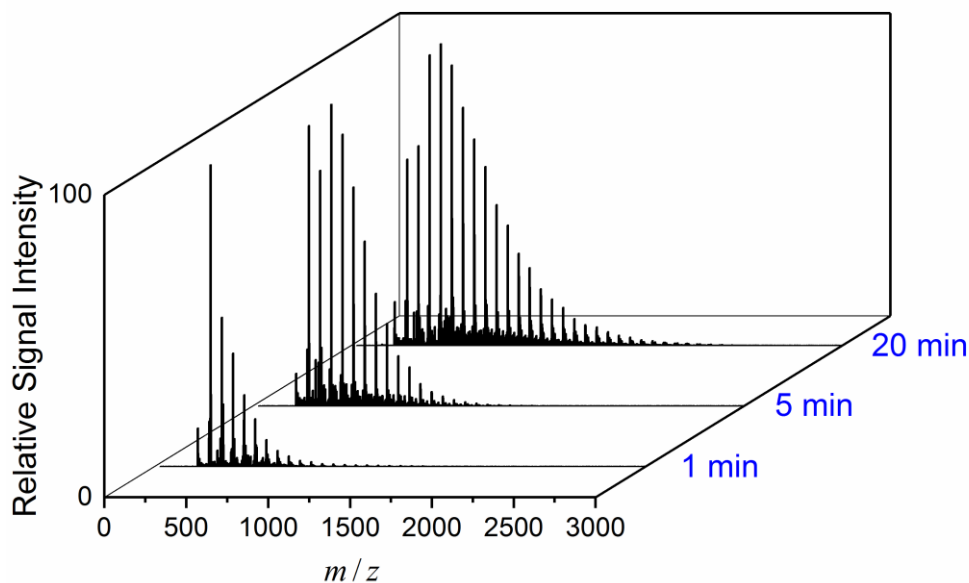


Figure 32: Negative-ion mode ESI mass spectra of a 13-mM solution of CoCl_2 with PhLi (4 equiv.) and isoprene (20 equiv.) in THF at room temperature after increasing reaction times.

The mass spectrum obtained from the sample solution predominately consisted of equidistant ions with a mass difference of $\Delta m = 68$ between neighboring signals that could be assigned to the series $\text{Co}(\text{DE}^{\text{I}})_n\text{Ph}_2^-$. A second series of $\text{LiCo}_2(\text{DE}^{\text{I}})\text{Ph}_4^-$ was observed at much lower signal intensities, consisting of two mononuclear cobalt species connected by a bridging Li^+ cation. No signals were found that would indicate a termination or chain transfer reaction, such as β -hydride elimination.²¹⁰

The spectrum shifted towards a higher mass area within the first 15 min reaction time, after which the relative signal intensities remained mostly constant. The largest species observed after 20 min reaction time and with a monomer excess of 20 equivalents in relation to CoCl_2 was $\text{Co}(\text{DE}^{\text{I}})_{28}\text{Ph}_2^-$. Notably, even at the maximum reaction time, a high signal intensity of species with $n = 2$ remained. While in the initial stages shorter species were consumed to form larger ones, as is expected for polymerizations with persistent active species,²¹¹ the shorter species do not approach a signal intensity of zero. Instead, all species, both short and long, seem to approach a plateau after long reaction times.

Assuming equal ESI efficiencies of all species, the degree of polymerization after 20 min was estimated to be $X_n = 8.7$, indicating incomplete conversion. Increasing the amount of monomer from 20 to 30 equivalents proportionally increased the average chain length to $X_n = 18.6$ (slightly underestimated as species larger than $\text{Co}(\text{DE}^{\text{I}})_{40}\text{Ph}_2^-$ were cut off due to the available mass range), with $\text{Co}(\text{DE}^{\text{I}})_2\text{Ph}_2^-$ remaining still (**Figure 33**). This

behavior is suggested to result from a reversible propagation, resulting in the establishment of an equilibrium after long reaction times. Similar mass spectra were recorded when using other lithium organyls RLi or when using 1,3-butadiene instead of isoprene, though the Li^+ -bridged species $\text{LiCo}_2(\text{DE})_n\text{R}_4^-$ were much more prevalent and in some cases, β -hydride elimination occurred.²¹²

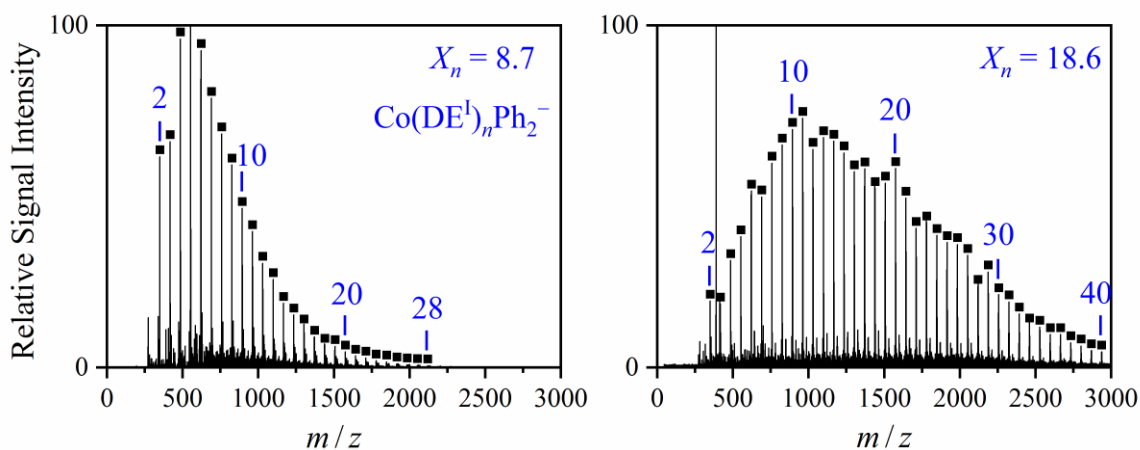
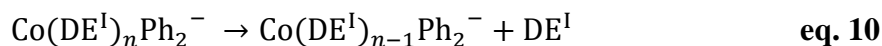


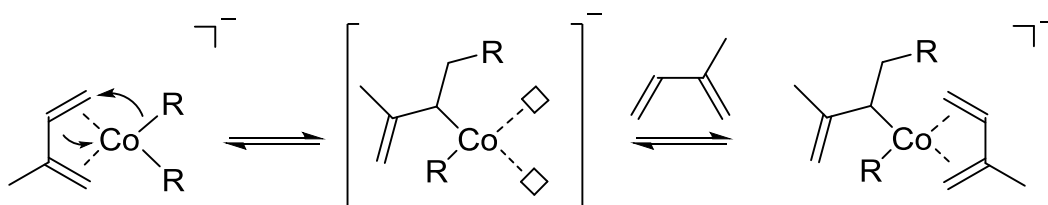
Figure 33: Negative-ion mode ESI mass spectra of 13-mM solutions of CoCl_2 with PhLi (4 equiv.) and 20 equiv. (left) or 30 equiv. (right) isoprene in THF at room temperature after a reaction time of 20 min.

Other experimental evidence indicating a reversible propagation was found during copolymerization experiments. Adding 1,3-butadiene to a mixture of CoCl_2 , PhLi and isoprene that had already been reacting for 30 min resulted in a broad distribution of species incorporating both monomers. This confirmed the catalytic species to be active after half an hour of reaction time, precluding the incomplete conversion to result from a termination due to mass-neutral rearrangement. Secondly, species containing exclusively 1,3-butadiene were present in the mass spectrum drawn from the copolymerization experiment. These can only result from a reversible propagation or by cleaving off the preexisting isoprene oligomer, though no evidence was found for the latter to occur.

Further supporting this claim of a reversible polymerization were fragmentation experiments. Collision-induced activation of mass-selected species belonging to the series $\text{Co}(\text{DE}^{\text{I}})_n\text{Ph}_2^-$ predominately resulted in cleaving off a single monomer unit (eq. 10). This means that most likely one diene is not integrated covalently into either of the growing chains but rather is coordinated to the cobalt center. From an electronic point of view, this behavior is expected as it allows the molecule to form a square-planar $16 e^-$ complex, reminiscent of nickel or palladium catalysts that are able to polymerize olefins.²¹³

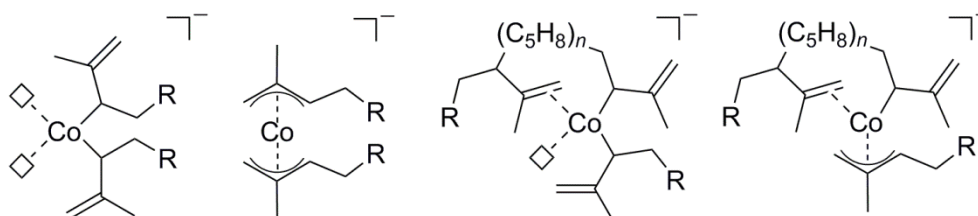


The migratory insertion, which from comparing this system to other polymerization catalysts is the most likely mechanistic pathway for the chain growth to occur,²¹⁴ being reversible would allow the empty coordination sites to be filled again, stabilizing the post-fragmentation complex. In solution, where the free coordination sites can be filled up either by the reversed insertion or by coordination of new monomer from the solution, an equilibrium is established (**Scheme 10**). According to the degrees of polymerization estimated for 20 and 30 equivalents of monomer and under the chosen reaction conditions, the remaining monomer concentration should be about 140-160 mM.



Scheme 10: Suggested mechanism for the reversible propagation reaction during the polymerization of isoprene mediated by CoCl_2 and RLi .

The displayed resting state of the active center with one diene coordinating twice to the metal is mostly based on the fragmentation behavior. Other configurations are possible, either exclusively or as a mixture of multiple forms. As the smallest species observed at the beginning of the reaction was $\text{Co}(\text{DE}^{\text{I}})_2\text{Ph}_2^-$, two separate dienes coordinating with a single double bond each is an option as well. After the first insertion of the diene, the organyl may coordinate as η^1 - or η^3 -allyl ligand. Similarly, the mid-chain double bonds may coordinate to free coordination sites and stabilize the intermediate, reducing the risk of β -hydride elimination that would be expected to occur otherwise (**Scheme 11**).



Scheme 11: Stabilization of the suggested intermediate (left) by η^3 -allyl coordination, coordination of a mid-chain double bond, or a combination of both.

3.3.3.1 Kinetic parameter estimation from reaction modeling

Similarly to the oligomerization of substituted cyclopropanes, the signal intensity time profiles of the various $\text{Co}(\text{DE}^{\text{I}})_n\text{Ph}_2^-$ species from the in-situ monitoring of the

coordination polymerization of isoprene was suitable to parameter estimation using kinetic modeling. Using COPASI,²⁰⁶ the following approximations were made:

- 1) The relative signal intensities of the various $\text{Co}(\text{DE}^{\text{I}})_n\text{Ph}_2^-$ correspond to the relative concentration in solution. All species have the same ESI efficiency.
- 2) The total concentration of all $\text{Co}(\text{DE}^{\text{I}})_n\text{Ph}_2^-$ equals the initial concentration c_0 of CoCl_2 . There are no transfer or termination reactions.
- 3) Every monomer addition step follows a reversible second-order rate law for the reaction $\text{Co}(\text{DE}^{\text{I}})_n\text{Ph}_2^- + \text{DE}^{\text{I}} \rightarrow \text{Co}(\text{DE}^{\text{I}})_{n+1}\text{Ph}_2^-$ for all species with $2 < n < 40$. The first 3 propagation steps are assigned individual rate constants k_2 , k_3 and k_4 , while every further addition step shares the same rate constant k_n .

Once again, the first two assumptions are not entirely accurate. As the reaction system features a non-polar monomer, the increased chain length is expected to come with increasing surface activity, thus potentially leading to an overestimation of the concentrations in the high-mass area. This effect is reduced by using THF as a comparatively non-polar solvent, though it is unlikely to be mitigated entirely. Regarding the second approximation, no products indicating termination or transfer reactions were found, but the aggregation to form $\text{LiCo}_2(\text{DE}^{\text{I}})_n\text{Ph}_4^-$ may occur more frequently for certain chain lengths, thus reducing the estimated concentration of said species. For the reaction system of PhLi and isoprene, this assumption may still be made as the corresponding aggregates occur in comparatively low abundances. For systems containing 1,3-butadiene or other organyls, this approximation would not be reasonable.

Due to the large number of species, the consideration of individual reaction rates for every step was not feasible. Instead, a distinction was made between the very first reaction steps and the later propagation. This distinction was taken as the reactivity of the initial species is expected to differ significantly when compared to species that already incorporated multiple units of monomer. This includes changes both to the electronic structure, due to the difference between phenyl ligands and allyl ligands, and the availability of mid-chain double bonds. As the active center features two organyls, each of which may initiate an individual oligomer chain, the corresponding rate constant k_3 represents the average of the monomer insertion into, for example, $\text{Co}(\text{DE}^{\text{I}}_2\text{Ph})\text{Ph}^-$ and $\text{Co}(\text{DE}^{\text{I}}\text{Ph})_2^-$. The exact species may differ depending on configuration of the metal complex as described earlier.

Due to their generally higher signal intensity, the first 10 insertion steps were assigned a weighting of 1 when fitting the simulated concentrations to the experimental ones, whereas the later steps were assigned a weighting of 0.5. No further steps were taken to equalize the unequal weighting between k_n and k_{2-4} that resulted from assigning a multitude of reactions to the former. Due to this, deviations between the simulated concentrations and the experimental data were more likely to occur within the first few species, though even for those the agreement between experiment and simulation was satisfactory (**Figure 34**). For the later species, the agreement was excellent despite the wide range of species covered by one rate constant.

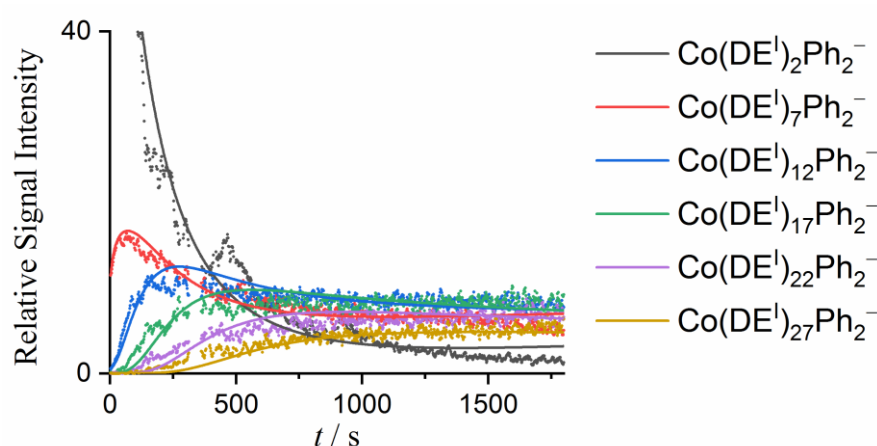


Figure 34: Experimental (dots) and simulated (lines) time profiles for the individual apparent concentrations of $\text{Co}(\text{DE}^1)_n\text{Ph}_2^-$ obtained from ESI-mass spectrometric analysis of a solution of CoCl_2 (13 mM), PhLi (4 equiv.) and isoprene (30 equiv.) in THF at room temperature.

The simulated concentrations successfully reflect the plateaus the various species reach after long reaction times. For $\text{Co}(\text{DE}^1)_2\text{Ph}_2^-$, the final plateau is overestimated by the parameter estimation, so the actual equilibrium constant can be expected to be higher than calculated. Reasons for this deviation are the unequal weighting during the parameter estimation, but also the fact that $\text{Co}(\text{DE}^1)_2\text{Ph}_2^-$ covers the widest range of concentrations. Potential mass bias effects have the strongest influence on species on either extreme of the spectrum. Furthermore, due to the experimental setup, where the reaction is initiated by letting the cooled solution warm up to room temperature, the temperature likely has not equalized completely during the initial stages where $\text{Co}(\text{DE}^1)_2\text{Ph}_2^-$ approximately follows an exponential decay of its concentration, which greatly impacts the calculated rate constant. Despite these imperfections, the calculated rate constants for k_{2-4} were obtained with low standard deviations, reinforcing the conclusion that the chosen kinetic system and approximations were suitable to perform this parameter estimation (**Table 5**).

Table 5: Rate constants for the propagation step $\text{Co}(\text{DE}^{\text{I}})_n\text{Ph}_2^- + \text{DE}^{\text{I}} \rightarrow \text{Co}(\text{DE}^{\text{I}})_{n+1}\text{Ph}_2^-$ (k_{+1}) and the reverse reaction (k_{-1}) in THF at room temperature derived from kinetic modeling.

$n / n+1$	2/3	3/4	4/5	$n / n+1^{\text{a}}$
$k_{+1}^{\text{b}} / (\text{L mol}^{-1} \text{s}^{-1})$	0.023	0.12	0.11	0.20
$k_{-1}^{\text{b}} / \text{s}^{-1}$	0.004	0.013	0.011	0.032

a) $5 < n < 40$. b) Relative standard deviation obtained from kinetic modeling $\Delta k/k < 3\%$.

The estimated rate constants suggest that under the current reaction conditions, the equilibrium will be reached once ~ 160 mM of monomer is remaining. By performing the reaction with a larger excess of monomer or by continuously replenishing the consumed monomer, the system can be driven towards longer polymers, though the reactivity may change when approaching longer species, e.g. due to precipitation.

The reaction rates for both the forward and the reverse reaction are slowed by a factor of ~ 8 for the initiation (in this case the addition of monomer to $\text{Co}(\text{DE}^{\text{I}})_2\text{Ph}_2^-$) when compared to the general propagation to $\text{Co}(\text{DE}^{\text{I}})_n\text{Ph}_2^-$. The second and third insertion steps proceeds at a rate that is roughly the average between the initiation and the later propagation. This may be a difference in the insertion into a Co-Ph bond being slower compared to a Co-Allyl bond, though a more detailed analysis cannot be made without knowledge of the exact configuration of the active species, which mass spectrometry is unable to provide. This behavior most likely causes the polymer chain that was initiated first to start growing before the second chain is initiated, resulting in imbalanced chain growth and a slightly increased polydispersity.

Compared to typical living polymerizations, this model system shares the feature of persistent active centers, but the reversibility of the propagation will always result in a distinctly broader mass distribution. Similarly, the slow initiation compared to the propagation further prevents the system from being assigned the status of a controlled polymerization.²¹¹ As the kinetic analysis by ESI-MS only requires the active species to be charged and persistent, the model system being not controlled does not impact said analysis negatively. Instead, it only serves to further prove the potential of ESI-MS for the analysis of slow coordinative polymerizations, as deviations from expected behavior as observed here may not be as immediately obvious as such or may be misinterpreted when investigating the same system using more traditional analytical methods.

Regarding the accuracy of the obtained kinetic parameters, various factors that may influence the results negatively such as mass bias have already been discussed. To ensure that the mass distributions obtained from ESI-MS are accurate, ^1H NMR spectroscopy and MALDI mass spectrometry was performed on isolated samples (experimental data provided by Dr. F. Kreyenschmidt).²¹²

The isolated samples were created by terminating a solution of $\text{CoCl}_2/\text{PhLi}$ and 20 equivalents of isoprene in THF after reacting for 30 min, resulting in an oligomer of the type $\text{H}(\text{DE}^1)_n\text{Ph}$ instead of the charged dimer $\text{Co}(\text{DE}^1)_n\text{Ph}_2^-$. In order to enable a direct comparison between the methods, a theoretical mass of the terminated oligomer was estimated. For this, a single diene was assumed not to be incorporated into the terminated oligomer, resulting in the transformation being $\text{Co}(\text{DE}^1)_n\text{Ph}_2^- \rightarrow 2 \text{H}(\text{DE}^1)_{(n-1)/2}\text{Ph}$ (**Table 6**). From the NMR experiments, the average molar mass was obtained by comparing the phenyl end group signals with terminal alkene protons (2 per monomer unit). For the MALDI experiments, salts containing Ag^+ or Cu^+ were added to facilitate the ionization by forming adducts of the type $[\text{H}(\text{DE}^1)_n\text{Ph}+\text{M}]^+$. The lower limit of the mass range was m/z 500, resulting in species containing less than 5 or 6 units of monomer (for Ag^+ and Cu^+ , respectively) to be cut off. To emulate this limitation, a truncated mass distribution containing $\text{Co}(\text{DE}^1)_n\text{Ph}_2^-$ with $n \geq 13$ was estimated.

Table 6: Molar mass distributions determined by ESI-MS, a simulation based on ESI-MS, MALDI-MS and ^1H NMR spectroscopy for oligomer produced by the reaction of CoCl_2 , PhLi (4 equiv.) and isoprene (DE^1 , 20 equiv.) in THF after a reaction time of 30 min.

	$M_n / (\text{g mol}^{-1})$	$M_w / (\text{g mol}^{-1})$	M_n / M_w
NMR	350 – 420	–	–
ESI-MS ^a	383 ± 16	485 ± 9	1.27
Kinetic modeling	362	474	1.31
MALDI-MS ^b	695 ± 15	751 ± 23	1.08
ESI-MS, truncated ^{a,c}	635 ± 7	661 ± 10	1.04
Kinetic modeling, truncated ^d	650	688	1.06

a) Average of 4 runs. b) Contains species $[\text{H}(\text{DE}^1)_n\text{Ph}+\text{M}]^+$ for $6 \leq n \leq 18$, $\text{M} = \text{Ag}^+, \text{Cu}^+$. c) Contains species $\text{Co}(\text{DE}^1)_n\text{Ph}_2^-$ for $13 \leq n \leq 30$. d) Contains species $\text{Co}(\text{DE}^1)_n\text{Ph}_2^-$ for $13 \leq n \leq 40$.

The average molar mass determined by ^1H NMR spectroscopy varied depending on the exact placement of the integration intervals, though either extreme is still in reasonable agreement with the average molar mass from ESI-MS analysis. The mass distributions

from direct ESI-MS and from kinetic modeling agree in both number-average and weight-average molar mass, despite the former being determined from a reaction solution containing 20 equivalents of isoprene, whereas the latter is based on time profiles determined for a solution containing 30 equivalents. The tentative polydispersity obtained from ESI-MS was large compared to typical values for controlled polymerizations, but low when compared to uncontrolled reactions, as was expected due to the reversibility of the propagation and the delayed initiation.

The truncated ESI-MS average molar mass falls a bit short compared to that derived from MALDI-MS. This is in line with the unequal chain growth of the 2 initiating organyls. For the truncated mass distribution, an equal split of the monomer units was assumed, e.g. $\text{Co}(\text{DE}^{\text{I}})_{11}\text{Ph}_2^- \rightarrow 2 \text{H}(\text{DE}^{\text{I}})_5\text{Ph}$, while the actual split would be a mixture of one short and one long oligomer. The former of those would fall below the lower mass limit of the MALDI-MS experiment, resulting in an overall elevated average molar mass. The ratio of weight-average to number-average molar mass cannot be equated to the polydispersity in this case due to the lower mass cut-off, but still serves to reflect the broadness of the mass distribution. Due to the way they are calculated, the weight-average molar mass is affected more strongly by the imbalanced split of the monomer during termination than the number-average molar mass is. This is reflected by the increased ratio between the averages when compared to the truncated ESI-MS mass distribution.

The difference between the in-situ active species and the terminated product can make it more difficult to draw conclusions about the product of a polymerization by observing the growing oligomer in solution. However, this deficit is more than made up for by enabling a direct investigation of the type and reactivity of the active species, which allows for the establishment of an accurate mechanistic assessment that would not be afforded by traditional methods. Other than that, the quantitative and kinetic investigation of coordination polymerization reactions by ESI-MS was shown to be successful, provided all initiating groups are persistent throughout the reaction. As with the anionic oligomerization, ESI-MS combines the benefits of in-situ measurements with fast experiments, easy sample preparation and stoichiometrically exact results that enable the estimation of the whole mass distribution.

3.4 Thermodynamic Parameter Determination

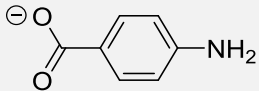
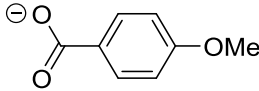
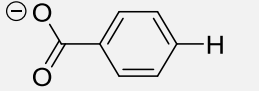
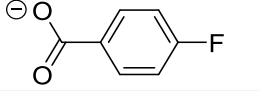
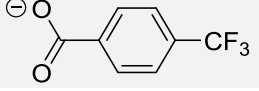
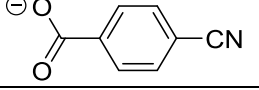
Aside from direct kinetic measurements, ESI-MS can also be used to explore thermodynamic parameters of various synthetically relevant carbanions. During the in-situ measurements of carbanions, a tendency to form aggregates of the type $[M_{n-1}A_n]^-$ was observed for species containing two electron-withdrawing groups. This behavior will be used to determine alkali metal cation affinities for these synthetically important anions. These parameters are as of yet unexplored and should be of great interest, as they may reveal trends that translate to the condensed phase.

Various heteroleptic aggregates containing one carbanion and one reference ion were generated from suitable solutions, then mass-selected and fragmented. From the signal intensities of the different fragment ions, the relative affinity towards the bridging cation will be determined via the kinetic method (eq. 11).^{45,47} Entropic and enthalpic effects were separated by performing the fragmentation with multiple fragmentation energies.

$$\ln I_1/I_2 = \ln k_1/k_2 = \frac{\Delta(\Delta H_{M+}) - T_{\text{eff}}\Delta(\Delta S_{M+})}{RT_{\text{eff}}} = \frac{\Delta H_{M+}(B_i)}{RT_{\text{eff}}} - \frac{\Delta G_{M+}^{\text{app}}}{RT_{\text{eff}}} \quad \text{eq. 11}$$

The largest difficulty to overcome is the lack of known values that can be used to serve as references. For the affinity of anions to cations, absolute methods such as threshold CID or equilibrium methods are not applicable. For this reason, calculated affinity values for a series of reference compounds were used.²¹⁵ The chosen compounds were a series of *para*-substituted benzoate anions pB_R^- (Table 7). They had recently been shown to be amenable to calculation via quantum chemical methods by confirming their relative affinities experimentally.⁶¹ By using calculated affinity values of a total of six reference molecules in a single plot, slight deviations in the relative affinity within the series of reference compounds are mitigated through interpolation. This combination of experimental and calculated data should provide a collection of anions with improved thermodynamic accuracy that can be used as reference compounds themselves in the future. Systematic deviations of the absolute values cannot be precluded entirely, though two separate calculations using different methods deviated by less than 1 kcal/mol.^{61,215} Furthermore, the interpretation of the mass spectrometric data using the kinetic method can easily be updated with more accurate reference values once they are available, either from improved calculations or from novel experimental methods.

Table 7: Alkali metal ion affinities of *para*-substituted benzoate anions, calculated with the method DLPNO-CCSD(T)/cc-pVQZ (M: cc-pwCVQZ)//PBE0 D3BJ/def2-TZVP.²¹⁵

pB_R^-	$\Delta H_{K^+} / (\text{kJ mol}^{-1})$	$\Delta H_{Na^+} / (\text{kJ mol}^{-1})$	$\Delta H_{Li^+} / (\text{kJ mol}^{-1})$
	534	604	711
	529	598	704
	526	595	699
	518	586	689
	504	572	673
	495	562	661

For the metal cations $M^+ = K^+, Na^+$ and Li^+ , sample solutions were prepared by mixing solutions of the investigated carbon acids AH with solutions of the benzoic acid pB_RH and the alkali metal hydroxide MOH in MeCN/ H_2O . Final concentrations were 1.5 mM AH, 0.5 mM pB_RH and 2.0 mM MOH in 90/10 MeCN/ H_2O . The ratio of benzoic acid to carbon acid was chosen due to a generally higher responsiveness of benzoate anions towards ESI-MS. A total of six carbon acids were selected from methylenes featuring a mix of two cyano, keto, ester or amide groups. The combinations were chosen in a way to create overlaps between the groups, enabling the establishment of a relative order of the influence the various functional groups have on the alkali metal ion affinity. Water was already shown not to interfere with the detection of similar carbanions (chapter 3.1.2) and was added to improve the solubility of MOH.

For each metal, every combination of carbon acid and reference benzoic acid was prepared. The heterodimer was mass-selected and then fragmented using six fragmentation voltage amplitudes $V_{exc} = 0.4 \text{ V} - 0.9 \text{ V}$, ranging from moderate to full fragmentation.

3.4.1 Alkali Metal Cation Affinity Determination for Carbanions

When using MOH ($M^+ = K^+, Na^+, Li^+$) to provide the bridging metal cation, the mixed dimer aggregates formed readily and could be detected in high intensity. The fragmentation of the mass-selected heterodimers resulted in the expected free anions in ratios dependent on the combination of substrate and reference (e.g. **Figure 35**).

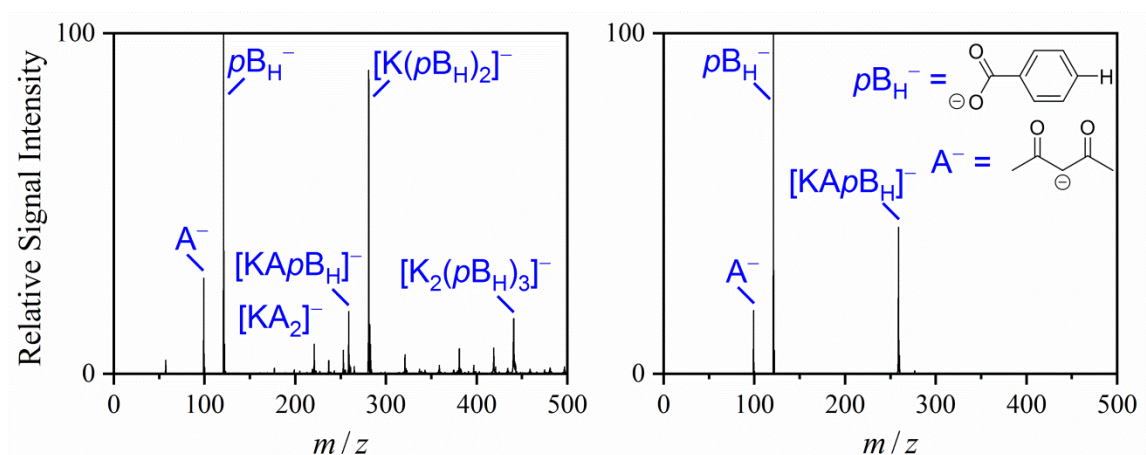


Figure 35: Negative-ion mode ESI mass spectrum of a solution of acetylacetone (AH, 1.5 mM), benzoic acid (pB_H , 0.5 mM) and KOH (2 mM) in MeCN/H₂O (90/10) (left) and fragmentation pattern upon CID of mass-selected $[KA_pB_H]^-$ (m/z 259) with $V_{exc} = 0.4$ V (right).

For $M = K^+$, fragment ions indicating consecutive fragmentation or alternative reaction pathways were present only in few cases and in minor amounts, due to the facile loss of alcohols from ester-bearing carbanions. For $M = Na^+$ or Li^+ , the signal intensities of alternative pathway products were more pronounced. This is a result of a stronger binding towards the smaller alkali metal cations than to K^+ . For the same reason, higher excitation energies were required to achieve the same degree of fragmentation when working with the smaller cations. These alternative pathways are expected to slightly decrease the accuracy of the determined values, though only to a limited degree due to the logarithmic nature of the fragment ion ratios when calculating the affinity.

The signal intensity ratios of A^- and pB_R^- resulting from CID of the various heterodimers were plotted against the calculated potassium ion affinities of the benzoate anions (e.g. **Figure 36**).²¹⁵ Every series of different fragmentation energies was considered separately in order to estimate the entropic contributions.

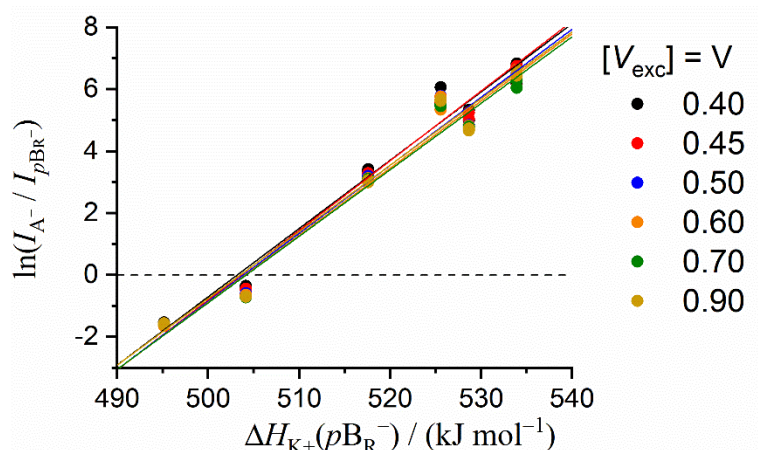
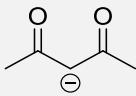
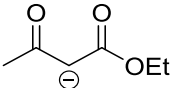
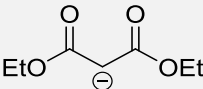
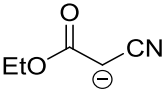
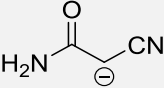
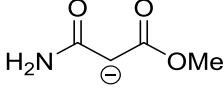


Figure 36: Logarithmic branching ratios for the fragmentation of $[KA_pB_R]^-$ (A^- = acetylacetonate, pB_R^- = *para*-substituted benzoate anions) by CID using different excitation energies V_{exc} against the potassium cation affinities of substituted benzoates.

The correlation of the logarithmic fragment ion ratios to the calculated alkali metal cation affinities of the benzoates was for the most part linear, as was expected. Only for pB_{OMe}^- and pB_H^- , the resulting ratios did not represent the order of the calculated affinities. This was observed for all carbanions and all metal cations. The same erroneous order in alkali metal cation affinities had previously been suggested by calculations conducted by Gal as well.⁶¹ This exemplifies the improvement in certainty of the thermodynamic parameters by combining the calculated reference values with experiments, as individual inaccuracies are mitigated by interpolation.

For K^+ , the standard deviation of the x -intercepts for the different V_{exc} across six carbanions A^- was, on average, 0.5 kJ/mol. For Na^+ and Li^+ , the deviations were larger, but no correlation between V_{exc} and $\Delta G_{M^+}^{app}$ could be made for any of the metals. Therefore, as well as other fragmentations possibly complicating entropic considerations, an analysis according to the authenticated method was deemed to be more suitable. This means the following assumptions were made: $\Delta(\Delta S_{M^+}) \approx 0$ and $\Delta G_{M^+}^{app} = \Delta H_{M^+}(A)$. Every V_{exc} is considered equal, with the final affinity parameters being the average of 12 individual measurements (**Table 8**).

Table 8: Experimental alkali metal cation affinities of carbanions A^- . Given errors correspond to a 95% confidence interval.

A^-	$\Delta H_{K^+} / (\text{kJ mol}^{-1})$	$\Delta H_{Na^+} / (\text{kJ mol}^{-1})$	$\Delta H_{Li^+} / (\text{kJ mol}^{-1})$
	536 ± 1	613 ± 5	– [a]
	528 ± 1	605 ± 1	$734 \pm 9^{[b]}$
	524 ± 1	600 ± 1	$731 \pm 18^{[b]}$
	504 ± 1	566 ± 1	657 ± 5
	$516 \pm 2^{[c]}$	585 ± 2	689 ± 5
	518 ± 1	595 ± 1	$725 \pm 4^{[b]}$

a) ΔH_{Li^+} too far outside the scope of references. b) pB_{CN^-} not included as a reference. c) Reproduced twice, for a total of 18 experiments.

The accuracy of the determined values strongly depends on the difference to the references. For K^+ , the affinity range provided by the substituted benzoates was 495 – 534 kJ/mol, which was a near-perfect fit for the chosen carbanions. Only one species had to be extrapolated. For Na^+ , the difference between references and the most cation affine carbanion was larger, leading to an increased uncertainty. For Li^+ , only two carbanions could be interpolated. For three of the remaining species, the differences to pB_{CN^-} grew too large to accurately display the branching ratios of fragment ions. It has thus been excluded from the analysis. The affinity of the last species could not be determined at all, as it was too far apart from the affinity range provided by the references.

Theoretical alkali metal cation affinities for the 6 carbanions were also determined using the same method as for the calculation of the affinities of the benzoate anions that have been used as reference species (DLPNO-CCSD(T)/cc-pVQZ (M: cc-pwCVQZ)//PBE0 D3BJ/def2-TZVP).²¹⁵ The agreement between experimental and theoretical values was, with few exceptions, very good (**Figure 37**). The mean deviation between theoretical and experimental affinities to K^+ was 3 kJ/mol, while even the mean deviation for Li^+ was only 5 kJ/mol.

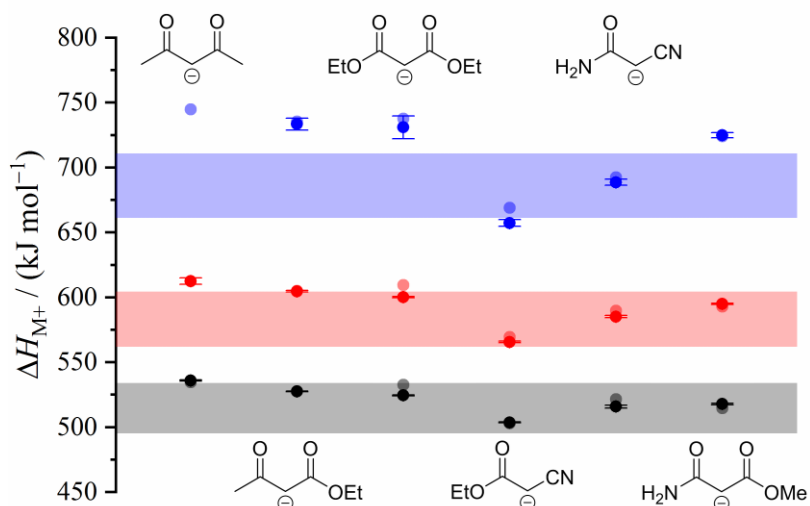


Figure 37: Experimental (opaque) and theoretical (semi-transparent) alkali metal cation affinities of carbanions. Colored areas indicate the affinity range opened up by the substituted benzoate anions that were used as reference substrates.

The kinetic method has thus been shown to be suitable for the affinity determination of carbanions towards simple cations by interconnecting the separate calculations. For the absolute values, however, a systematic deviation cannot be ruled out, due to the experiment being based on calculated reference values. This potential deviation will remain until the cation affinity of these or other anions can be measured using an absolute method. The relative affinity order on the other hand is expected to be accurate.

To check for unexpected interactions between the carbanions and the benzoate anions interfering with the results, heterodimers composed of two different carbanions and a bridging K^+ were generated and fragmented. After measuring every available combination of carbanions and applying a least-square approach, a relative affinity order was obtained. The high degree of agreement between this relative order and the absolute values using calculated references precludes unexpected interferences (**Figure 38**).

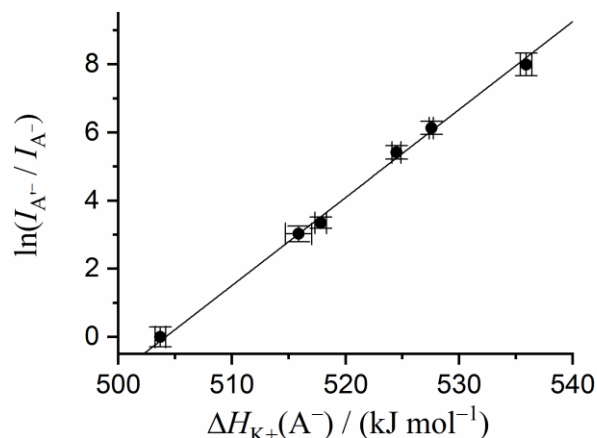
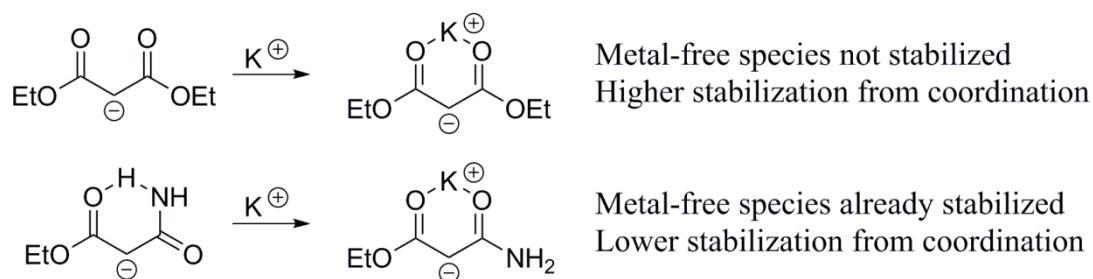


Figure 38: Relative potassium cation affinity order from the fragmentation of $[KAB]^-$, with A, B = carbanions, against the absolute potassium cation affinity from the fragmentation of $[KA_pB_R]^-$. The relative order is anchored to the ethyl cyanoacetate anion (A'^-). $R^2 = 0.994$.

Regarding the effect of the different functional groups on the cation affinity, the trend that is most obvious is a low affinity being associated with the cyano group. From a purely electronic point of view, the cyano group is more electron-withdrawing than carbonyl groups, as seen for example in their Hammett parameters ($\sigma_{m,p}(\text{CN}) = 0.56; 0.66$ vs $\sigma_{m,p}(\text{COOMe}) = 0.37; 0.45$)²¹⁶, which causes the lithium cation basicity of the neutral MeCN to be slightly lower than that of methyl acetate ($\Delta G_{\text{Li}^+} = 151.1$ vs 153.7 kJ/mol)²¹⁷. Access to an additional electron to be distributed mainly across the two groups may invert this order or enlarge the difference a bit, but seems unlikely to be a sufficient explanation for the drastic difference between cyano and carbonyl groups recorded here. An additional contributing factor can be expected to be the low flexibility of the linear cyano group. The carbanions cannot twist in a way to reach the optimal geometric configuration that would allow the chelating properties of having two electron-withdrawing groups to fully take effect.

For the carbonyl groups, the relative affinity order is less clear in comparison. This is exemplified when considering ethyl cyanoacetate and cyanoacetamide. By exchanging the cyano group for an ester group, the potassium cation affinity of the former increases by 20 kJ/mol, while the latter remains almost unchanged. This precludes the use of an incremental system in order to predict the alkali metal cation affinity of similar carbanions. The reason for this behavior was suggested to be a conformational change, forming hydrogen bonds between an amide proton and the second carbonyl's oxygen (**Scheme 12**). The resulting stabilization of the free anion in the gas phase reduces the amount of energy obtained from stabilizing the free anion through coordination to an

alkali metal cation, thus lowering the corresponding affinity. For the diethyl malonate, no oxygen is available to act as a donor for hydrogen-bridges, so this extra stabilization is not available.



Scheme 12: Intramolecular hydrogen bond in metal-free gas-phase carbanions carrying suitable functional groups reduces the alkali metal cation affinity.

This suggestion was later confirmed by calculating the formation enthalpy of the free gas-phase carbanions in various geometries.²¹⁵ A similar effect was also observed for carbanions containing both a keto group and a second carbonyl, though to a lesser degree than for the amide-carbonyl combination as C-H-O bonds are formed instead of N-H-O. An incremental system can still be considered by using values that were calculated for species undergoing no geometric changes after dissociation from the metal complex (eq. 12, values given for K^+). This system is of limited practical use, as it is only applicable when no strong intramolecular interactions can occur. However, considering the previously shown accuracy of calculated relative affinities, insights into the behavior of the various groups may still be gained.

$$\Delta H_{M^+}: \text{CN} < \underset{26}{\text{C(O)OR}} < \underset{16}{\text{C(O)R}} < \underset{7 \text{ kJ/mol}}{\text{C(O)NH}_2} \quad \text{eq. 12}$$

The order of the carbonyl groups regarding their influence on cation affinities does not correspond to the electronegativity order of the substituents, as may have been expected. Possibly a mesomeric effect exerted by the nitrogen's free electrons exceeds the inductive effect, resulting in an overall higher electron density in the coordinating atoms and thus a higher cation affinity.

When comparing these results with the aggregation behavior observed for various carbanions, some parallels can be drawn. The anion of deprotonated acetylacetone tended to form larger clusters than diethyl malonate, which is in accord with the stronger cation affinity induced by keto groups compared to esters. Malononitrile, featuring two cyano groups, preferably forms larger aggregates, which is in line with the inability to act as a

chelating ligand, forcing a μ_2 binding geometry. Finally, the cation affinity of all carbanions increases when exchanging K^+ for Na^+ or Li^+ . Similarly, solutions containing Na^+ or Li^+ were shown to form larger aggregates during ESI-MS, at the expense of the free anion. This trend of increasing affinity to smaller cations was also present for the benzoate anions, though to a lesser degree. This difference in size-affinity-correlation, possibly due to geometric constraints within the carboxylate group when attempting to coordinate smaller ions, led to the larger mismatch between the carbanions and references for Li^+ -bound dimers.

These gas-phase considerations represent an option to determine trends within a series of similar ions that would not be accessible directly from solution. However, not every observation may be transferred to the condensed phase directly. For example, the association constants of acetylacetonate with Li^+ and Na^+ in DMSO are smaller than those for diethyl malonate,⁸² despite their gas-phase affinities determined here suggest otherwise. In order to apply the trends to solutions, solvent effects need to be estimated or calculated.²¹⁸ When doing so, it is important to also consider the conformation of the carbanion, which can easily shift while in solution but is fixed when coordinated to a cation in the gas phase. As an example, acetylacetonate may form the *E,E*, *E,Z* and *Z,Z* conformations, of which only the latter is able to form a chelating complex.²¹⁹ So while the behavior in solution depends on all available conformations and their relative abundance, the gas-phase complex is expected to consist of only the *Z,Z* conformer, as all other conformers do not survive the transfer into the gas phase.

Overall, the kinetic method for the determination of alkali metal cation affinities of carbanions was successful, providing easy access to data that is not accessible by alternative methods. *Para*-substituted benzoate anions for the most part proved themselves to be highly suitable as references due to the similarity in affinity when compared to doubly-substituted carbanions. While not directly relevant to condensed phase chemistry, the values were obtained with high relative accuracy and could be used to draw conclusions regarding both the investigated structures and the method itself. An excellent agreement between experimental and theoretical affinities was achieved. The main aspect in need of improvement is anchoring the absolute affinity scale by using experimentally determined absolute reference values instead of calculated ones. As mentioned above, the produced data may be updated using new reference values once they are available, and do not require further experimentation.

3.5 Comparison with Other Analytical Methods

During the discussions regarding the separate experiments, various alternative analytical methods have already been mentioned or utilized in order to compare them with ESI-MS for the analysis of carbanions and radical anions. What yet remains is a concluding evaluation, summarizing the advantages and limits in regard to different applications.

HPLC. While strictly not an analytical method by itself, as it requires the combination with another method to serve as the detector, high performance liquid chromatography has long since been used for precise quantification of the components of reactive solutions.²²⁰ Due to the flexibility in columns, mobile phase and the detector, HPLC can be used for the investigation of virtually any reaction. However, the detected species are limited to products and reactants, excluding intermediates. Transient species can sometimes be included indirectly, for example by adding another reagent that reacts with the transient species faster than the original reaction of interest.²²¹ Finally, HPLC analysis requires long times due to both the required sample preparation and the chromatographic separation time. Both can be shortened significantly by automatization, optimizing the setup for the expected species, and through the use of modern systems, with separation times of single-digit minutes, sometimes even removing the need to quench reacting samples.²²²

ESI-MS in the context of carbanionic reactions was shown to be advantageous regarding the length of analysis, taking only as long as the reaction itself, though very slow reactions may preferably be investigated by drawing aliquots instead. The detection of intermediates is technically possible for ESI-MS, due to the resulting mass spectrum reflecting species as present in solution, though limitations in the stability of reactive species and their lifetimes may prevent this. Other factors hindering their detection are ion suppression effects, especially in solutions containing high concentrations of charged species, and the enhanced reactivity in microdroplets during the spray process that may force intermediates to react faster, either to the product or the reverse reaction to the reactant. Overall, ESI-MS is a strong option for reaction monitoring and kinetic investigation of ionic reactions, provided the relevant species are of sufficient stability. However for complex reactions containing multiple possible products, especially stereoisomers, the analysis with HPLC provides more options for their characterization and quantification than purely ESI-MS.

SEC. Technically a variant of HPLC analysis, the size-exclusion chromatography is of sufficient significance to deserve a separate discussion. SEC is used predominately for the analysis of polymers, providing a separation based on the logarithm of the hydrodynamic radius. By providing a calibration using known standards, the retention times are translated into approximate molecular weights. By coupling the column to a mass spectrometer, exact masses can be assigned to the individual slices. Common detectors utilize infrared absorption or measure changes in the refractive index, both of which are mostly determined by the total amount of monomer subunits, giving quantitative response when the end groups are negligible due to the length of the total molecule. Other than that, SEC behaves similarly to regular HPLC, sharing both strengths and weaknesses.¹¹²

The use of ESI-MS for polymers on the other hand has often been attempted and usually been deemed inaccurate due to mass bias, often resulting from chain-length dependent ionization efficiency and the formation of multi-charged ions.¹¹⁹ In this work, ESI-MS was used for oligomers carrying one permanent charge instead of ionizing neutral chains, thus preventing a significant amount of the expected mass bias. By limiting the reaction to a low-mass range, results were obtained that are believed to be mostly accurate and that may not be easily accessible from SEC as the end groups are not negligible for the detector response for oligomers.²⁰⁵ This way, ESI-MS may provide complimentary information regarding the kinetics at the initial stages of a polymerization, but in no way will it be able to fully replace SEC for the analysis of actual polymers. Furthermore, large limitations are expected regarding the accessible polymerizations, as the extreme reactivity and sensitivity of the active species both impact the general detectability and cause most reactions to surpass the mass range in a time frame too short to be monitored.

NMR. Nuclear magnetic resonance spectroscopy shares many of the advantages ESI-MS provides for the analysis of in-situ species and reactions. Similarly fast in their preparation, though NMR usually requires deuterated solvents instead, both methods provide information about the species contained within the solution, can track changes over time and can be equipped with means to control the temperature.²²³ The differences are found mainly in their selectivity and sensitivity. NMR spectroscopy characterizes species depending on the chemical environment of a selected isotope, while MS is limited to ions. This means that polymers cannot be distinguished regarding their chain length by NMR spectroscopy, only providing number-average molecular weights. Transient species or reactants of low relative concentration often cannot be observed, as their signals are

overlapping with or covered by unrelated signals. This is exacerbated in more complex reaction systems, as every species can have multiple signals, especially for ^1H - and ^{13}C -NMR spectroscopy. ESI-MS on the other hand fully disregards neutral species, allowing for the detection of ions despite a large excess of neutral reactants, facilitating pseudo-first order reaction conditions. The extreme sensitivity and usually large dynamic range allows for the detection of elusive species which can be crucial to the elucidation of reaction mechanisms. The structural information gained from the m/z ratio and from fragmentation experiments is complementary to those gained from NMR spectroscopy.

IR. Infrared (and other) spectroscopy requires the least sample preparation among the various in-situ analytical techniques and shares most of the advantages of NMR spectroscopy, though overlapping signals is an even larger issue. Kinetic observations are mostly limited to the intensity decrease or increase of one specific wavelength associated with a unique functional group.²²⁴ This enables the determination of the overall reaction rate, but is less useful for detailed mechanistic insights or structural information, for which ESI-MS is the superior technique in the context of ionic reactions. However, the combination of various spectroscopic methods can increase the information gained.²²⁵

EPR. Electron paramagnetic resonance spectroscopy is to unpaired-electron species what mass spectrometry is to ions.¹⁹⁶ In this context, it will be compared to ESI-MS for the in-situ analysis of radical anions exclusively. In this capacity, EPR spectroscopy is more sensitive than ESI-MS, which furthermore suffers from the inability to distinguish in-situ species and those formed during the ionization. As during EPR spectroscopy the sample solution does not experience any significant perturbation, in contrast to the ionization process during ESI-MS, the spectrum represents the in-situ species more accurately. The fast scanning speed allows for the detection of short-lived species.¹⁹⁷ By complimenting experimental results with simulated spectra, the expected signal structure of suggested species can be compared to the experiment. Less structural information is gained without a proposed structure. For most applications regarding radical anions, EPR spectroscopy will be preferable to ESI-MS. The exception to this rule is for reactions of two radical anions to two even-electron anions as seen for the reaction of chlorinated semiquinone with benzoquinone, followed by a second reaction with another semiquinone. In such cases, the simultaneous detection of product anions provided by ESI-MS is advantageous, but experiments should, when possible, be complimented by EPR spectroscopy in order to analyze radical intermediates that are too susceptible or too short-lived for ESI-MS.

4 Conclusion

Modern electrospray-ionization mass spectrometry finds increased use to investigate the mechanism and kinetics of reacting systems by in-situ measurements. Despite that, prior to this research, no systematic attempt had been made to test the scope and limitations for the direct detection of small, reactive, organic, and metal-free anionic species. Carbanions and carbon-based radical anions in particular were investigated by comparing the influences the molecular structure and various experimental conditions have on the measurability and signal intensity during negative-ion mode ESI-MS of these species. Similarly, the formation of alkali metal aggregates, depending on the species and conditions, was evaluated.

For the detection of carbanions, various carbon acids were deprotonated with a strong base and the resulting solution injected into the ESI source directly. A correlation between detectability and the analytes' acidity was found, though the trend could not be narrowed down to either pK_a in solution or the gas-phase proton affinity. With the given instrument, a clean spectrum could be obtained for species with an acidity up to fluorene (pK_a 22.6)⁸³. The most basic species observed was deprotonated acetone (pK_a 26.5),⁶⁵ which was accompanied by a plethora of other signals that may interfere during some applications. For species containing two functional groups that are able to coordinate a metal cation, aggregates of the type $[M_{n-1}A_n]^-$ were formed, with M^+ being the alkali metal cation and A^- being the carbanion. The amount of aggregation was dependent on the solvent. Smaller cations tended to form larger aggregates. The addition of crown ether increased the amount of free anions and in some cases resulted in less accompanying unknown signals, though attempts to detect less acidic species than acetone remained unsuccessful.

The detection of radical anions was investigated in a similar fashion. The successful application was shown to depend strongly on the electron affinity of the neutral species. Performing the radical anions by adding a reducing agent enabled the detection of species of sufficient EA, with the limit for the utilized instrument and settings being approx. 1.3 – 1.4 eV. The limit was suggested to depend on the internal energy of the ions during the ionization process. Without performing the radicals, the lower limit appeared to be ~1.5 eV, with all ions being detected at drastically lower signal intensities.

Two types of exemplary applications derived from the previous results were presented: Kinetic analysis of reactions and thermodynamic parameter estimation. The former made use of the correlation between signal intensity and concentrations during the in-situ monitoring of a reacting solution. For simple reaction systems, this works reasonably well, as demonstrated by the good agreement between ESI-MS and HPLC experimental results for a Michael-addition reaction. For a larger reacting system, the correlation between concentrations and signal intensity of the various species could only be made through some approximations and by mitigating mass bias effects wherever possible. The final rate constants for the oligomerization of doubly-substituted cyclopropane agreed reasonably well with experimental results reported in the literature.²⁰² By enabling a rough molar mass distribution to be determined in-situ, individual rate constants were obtained for the first 10 propagation steps, which would not be accessible using other analytical techniques. Additionally, the sample preparation was easy and the analysis straightforward compared to alternative methods for in-situ measurements of kinetics, as the reaction solution could be fed directly into the instrument.

Regarding the limitations of ESI-MS for kinetic analysis, as mentioned above, not all species can be detected. The upper limit of reaction rates that can be monitored, while dependent on the exact setup, is lower than for some other methods like reactive IR. This likely holds true even when coupling the instrument to a microreactor. Finally, for reaction systems containing multiple charged species of drastically different types or when the relevant species are only partially ionized, ESI-MS can only be used to record qualitative changes, such as the observation of side products.

The limitation in species changes when considering metal-bound ligands. Complexes containing, for example, the very basic Me^- and Ph^- can be detected by ESI-MS, whereas the free anions cannot.⁹⁸ This has been made use of for the in-situ monitoring of a Co(I)-based coordination polymerization of isoprene. The unique advantages of ESI-MS enabled the investigation of the active species and the discovery of a reversible propagation mechanism that might go unnoticed when relying on snapshots of the reaction products instead. Once again, rate constants could be assigned to individual reaction steps during the early phase of the polymerization, reflecting an increase in reactivity as the cobalt's ligands change.

The second application made use of the demonstrated tendency to form aggregates for the determination of thermodynamic parameters. By using the kinetic method, the relative affinity of a series of similar carbanions towards alkali metal cations was investigated. Absolute values were obtained by anchoring the results to calculated affinities and were internally consistent. Affinities between oppositely charged ions are often not accessible by other methods, leaving ESI-MS, and the kinetic method in particular, as the easiest method to provide values, despite the shortcoming of having to use calculated values as an anchor point. By combining calculations and experiments, more accurate results were obtained, which can now be used as new reference values. The nature of the method enables adjusting the experimental results to incorporate new, experimentally determined reference values directly, without requiring further experimentation, once such values become available in the future.

The detection of radical anions by ESI-MS is more limited regarding possible applications than its use for carbanions. Radical anions are usually only formed in small quantities during reactions, acting either as a catalyst or as a redox partner. Whenever a mixture of radical anion and neutral precursor is present in solution, the distinction between preformed radical anions and those generated by in-source reduction is difficult. Furthermore, most reactions relying on electron transfer occur faster than accessible by non-specialized instruments. No formation of electron-bridged aggregates was observed, precluding the kinetic method from being used, though such experiments have been recorded in the literature.⁵⁹ Specialized instruments may be required. Finally, transferring radical anions into the gas phase in order to subject them to analytical methods other than or in addition to mass analysis is possible, but negative-ion mode chemical ionization is preferable in most cases, due to a superior lower limit in EA. For cases where the EA is not a limiting factor, ESI-MS of preformed radical anions may be the easier and more accessible method.

The direct comparison of ESI-MS and other analytical techniques once more emphasized both the advantages and limitations of the method, being a superior or at least complementary option in many situations, due to the accuracy, sensitivity and ease of use, combined with a large potential for integrating further methods and techniques to analyze the gas-phase ions.

5 Outlook

Further improvements regarding the systematic investigation in the detectability of reactive species are likely to be found especially in the comparison between various instruments. This includes different setups for the ion transmission, which may affect aggregate formation and general stability of the more reactive ions, but also different source designs. Use of nano-ESI-MS²²⁶ or specialized source chambers that prevent water and oxygen from entering may drastically influence the resulting mass spectra and change the limitations in species. Another area of improvement that can benefit from changing the experimental setup is the reaction rate limitation. By optimizing scan rates and using a microreactor for faster sample preparation, the scope of accessible reactions may be increased.

In order to improve the accuracy of the mass-spectrometric analysis, direct coupling with other analytical techniques is required, the most obvious of which would be direct IR spectroscopy of the reacting solution. Depending on the application, other techniques may be more suitable, although they might require some sort of automated sample procession. This would enable the correlation between concentration and signal intensity to be established without relying on assumptions and approximations. Additional gas-phase methods in addition to fragmentation, e.g. spectroscopy or ion mobility, would provide more structural information, such as the exact structure of the species $\text{Co}(\text{DE}^{\text{I}})_n\text{Ph}_2^-$.

Both the optimization of short reaction times and the parallel usage of orthogonal methods would benefit from automated sample procession, mostly in the way of precise liquid handling. The most direct examples would be split-flow techniques or dilution and mixing by using a T-piece. A specialized analytical instrument that is optimized for the detection of elusive species and the reduction of mass bias in both hard- and software and that is capable of precisely controlling reaction conditions should be a promising tool to rapidly progress research in the kinetic and mechanistic understanding of ionic reactions.

Aside from improvements regarding the instrument and the general experimental setup, there are other avenues worth exploring that may further broaden the scope of applications that may profit from direct ESI-MS experiments. For very fast reactions or those containing reactants or intermediates that are too reactive for the current method, characteristic products upon the reaction with additives that are introduced downstream

may be monitored instead. A similar effect might be achieved by crossing two separate microdroplet sprays. Either setup would require highly individualized experiments, as the additives and the temporal order would need to be chosen on an individual basis. This would allow for even shorter reaction times and support or disprove hypotheses regarding the structure and reactivity of intermediates.

Similarly, applying conditions where the microdroplets formed during the ESI process are longer-lived, then using their increased reactivity as an experimental platform may yield interesting results by shifting reaction equilibria and altering the solvation effects by performing reactions halfway into the gas phase.

Regarding possible applications of ESI-MS for the direct detection of carbanions as was used here, two fields of use were shown. The determination of thermodynamic parameters through the kinetic method is well-known, though it had rarely been used for alkali metal cation affinities of anions before. Now that initial values were determined that can be used as new references, this field can be explored further to better understand counterion effects in synthetic chemistry and in biological contexts. For the second type of application, the experiments were focused on the quantification of species and the kinetic measurements of reactions whose mechanistic pathways were already known. This in itself provides valuable data, but ESI-MS also has the potential to distinguish intermediates, reveal rearrangements, and predict selectivity; especially in combination with fragmentation experiments. For this, however, more research is required. Limitations in species were obtained for solutions mostly containing one type of analyte anion, but the ratio of intermediates to other charged analytes can also be expected to be relevant to detecting intermediates due to ion suppression effects and should be explored further.

Despite all that, already with the experiments as performed here, a multitude of reactions' kinetics can be investigated and thus be optimized. In combination with a design of experiments strategy, various influences on a reaction can be screened in a fast and easy manner. Furthermore, due to the similarity of the techniques, most of the results obtained for ESI-MS should be directly transferable to acoustic mist ionization mass spectrometry. This technique was developed as a high-throughput method and should enable an even faster screening than purely by ESI-MS. Altogether I hope that ESI-MS and related techniques will see the increase in use they deserve in the context of carbanions, especially for the in-situ monitoring of reactions that are inaccessible to other methods.

6 Experimental Section

6.1 Materials

If not specified otherwise, all chemicals were bought and used as obtained. Dry MeCN was prepared by distillation from NaH (~1 g/L of a 60% dispersion in mineral oil) and stored over freshly heated molecular sieve 3 Å. MeOH was dried by storing it over freshly heated molecular sieve 3 Å for at least 3 days. THF was distilled freshly from Na/benzophenone immediately before use. Cyclopentadiene was obtained from the distillation of dicyclopentadiene.

Cobaltocene (CoCp₂) was synthesized based on the procedure by Wilkinson et al.²²⁷ Traces of moisture in anhydrous CoCl₂ (2.8 g) were removed by heating until the powder turned blue entirely. Cyclopentadiene (3.5 mL) was slowly added to NaH (1.7 g 60% dispersion in mineral oil) in THF. The prepared CoCl₂ was added to the solution and stirred for 2 h at room temperature. The solvent was removed under reduced pressure and the resulting solid purified by resublimation. The product (2.6 g, 64%) was stored inside an argon-filled glovebox.

Ethyl 1-cyanocyclopropane-1-carboxylate was prepared according to the procedure by Penelle et al.¹²⁹ A solution of K₂CO₃ (106 g), ethyl cyanoacetate (27.5 mL) and 1,2-dibromoethane (35.5 mL) in DMSO (210 mL) was stirred vigorously for 24 h. Water (500 mL) was added and the resulting solution extracted using diethyl ether (3 × 400 mL). The organic layer was washed with water (100 mL), dried over Na₂SO₄, concentrated by evaporation and fractionally distilled (152-154 °C, 173 mbar). The product (22.1 g, 66%) was subjected to 3 freeze-pump-thaw-cycles and stored over freshly heated molecular sieve 3 Å.

6.2 Instruments

All mass spectrometric measurements excluding those regarding the coordination polymerization of isoprene were performed using an amaZon speed mass spectrometer (Bruker Daltonik) equipped with an electrospray-ionization (ESI) source, two ion funnels, a multipole ion guide, and a 3D ion trap mass analyzer. Nitrogen was used as nebulizer gas and drying gas. The ion trap was filled with helium (1.8×10^{-6} mbar) for

thermalization and as collision gas during fragmentation experiments. The source was operated at 4.5 kV capillary voltage and 0.5 kV end plate offset. The nebulizer operated at 0.7 bar, the drying gas was set to 5 L/min and 150 °C. Other settings were adjusted using *Smart Parameter Settings*, with compound stability and trap drive level set to 100% and the target mass to m/z 200. Sample solutions were transferred to the ion source using gastight syringes and a syringe pump running at 0.5 mL/h. All mass spectrometric measurements, excluding time courses, were averaged over at least 1 min.

For experiments containing radical anions and the in-situ monitoring of an anionic oligomerization, the drying gas temperature was set to 100 °C instead. During the oligomerization, the target mass was adjusted sequentially, ranging from m/z 109 to 2891. For the analysis of coordination polymerization experiments, a micrOTOF-Q mass spectrometer (Bruker Daltonik) equipped with an ESI ion source, two ion funnels, a multipole ion guide, a collision cell, and a reflectron time-of-flight mass analyzer was used. The instrument settings were adjusted according to previous work performed by Dr. F. Kreyenschmidt.²¹²

For fragmentation experiments, collision-induced dissociation (CID) was utilized. Ions of interest were mass-selected with an isolation width of 3 u centered on the main isotope signal, reduced to a width of 1 u when necessary due to neighboring signals. The isolated ions were excited by subjecting them to a resonance frequency voltage for 40 ms. The amplitude of this voltage, V_{exc} , determines the strength of this excitation and was chosen depending on the structure. This process requires a lower mass cutoff, which was usually set to 27% of the source ion. Only for selected exceptions the cutoff was reduced to 20% when an expected fragment ion was inaccessible otherwise.

Analysis of data acquired using either instrument was performed using the Compass software package (Bruker Daltonik). Mass spectra were analyzed and signal intensities extracted using Compass DataAnalysis. Theoretical isotope ratios were calculated using Compass IsotopePattern.

For most time-resolved experiments, a pressurized sample infusion setup was used.¹⁶⁵ The sample solution was prepared in a Schlenk flask that was connected to an argon flow held at ~30 mbar overpressure. The inlet line connected to the ESI source was inserted into the gas phase inside the flask through a septum. Once the flask reached the correct temperature using a heating bath when necessary, a final component of the reaction was

added to the stirred solution and the mass spectrometric analysis initiated simultaneously. After few seconds of mixing time, the inlet line was inserted into the solution, with the total time between initiating the reaction by adding the last component and the first meaningful scan being ~30 s.

^1H NMR spectra were recorded using an Avance III 400 instrument (Bruker) at room temperature. Spectra were processed using TopSpin 4.0 (Bruker) and analyzed using MestReNova 10.0 (Mestrelab Research).

6.3 Experimental Procedures

Standard Schlenk techniques were used for all experiments. Argon was used as inert gas. Glassware was heated to 200 °C under vacuum for at least 10 min and flushed with argon 3 times before use. All experiments were conducted at least twice. Solutions for mass spectrometric measurements were 2-mM if not stated otherwise.

Solutions for the investigation of the general detectability of carbanions were prepared by dissolving the carbon acid in dry MeCN before using gastight syringes to add KO^tBu (1 equiv.) as a 1-M solution in THF. After shaking the flask briefly, part of the solution was transferred directly to the ESI source. The same procedure was used for related experiments, replacing either the solvent or the base. For the latter, NaH was added to the flask as a solid before adding MeCN, while LDA was used as a 1-M solution in THF/hexanes. For the concentration dependence, a standard solution was prepared and diluted in 1 or 2 steps. For the effect of counterions, diethyl malonate was dissolved in MeCN, to which a solution of MOH (M = Li⁺, Na⁺, K⁺, NBu₄⁺) in MeOH was added.

Radical anion solutions were prepared in a similar fashion. The reducing agent was prepared as a 0.25-M solution (CoCp₂ in toluene, C₂(NMe₂)₄ in MeCN, C₁₀H₈/Na in THF) and added to a solution of the neutral precursor in MeCN. Solutions with reduced concentrations were prepared by diluting the standard solution in a single step.

Heterodimeric species for the determination of alkali metal cation affinities according to the kinetic method were generated from 1:1 mixtures of a carbon acid (3 mM) in MeCN and a benzoic acid (1 mM) and the alkali metal hydroxide (4 mM) in MeCN/H₂O 80/20. For the latter, MOH was dissolved in pure H₂O before the aqueous base was added to the

various solutions of benzoic acids in MeCN. The heterodimer anions in the gas phase were mass-selected and fragmented with $V_{\text{exc}} = 0.4; 0.45; 0.5; 0.6; 0.7; 0.9$ V.

The in-situ monitoring of a Michael-addition was conducted using a PSI setup. A solution of deprotonated dimedone was prepared as usual. Butenone (20 equiv.) was added fast to the stirring solution using a syringe, which was used as the starting time for the mass spectrometric recording. For the comparison of using HPLC for the determination of concentrations, the same reaction solution was prepared, without the PSI setup. Instead, the flask was set in a water bath at 25 °C in order to mitigate temperature changes that occurred when opening the flask to take aliquots using an argon counter flow. The aliquots were diluted 1/100 using a solution of NH₄Cl (10 g/L) in MeCN/H₂O 50/50, which was sufficient to protonate the carbanions quantitatively and stop further reactions from occurring. An injection volume of 10 μL was used for the HPLC measurement. The stationary phase was a Synergi 4 μm MAX-RP 80 Å column (150×2.0 mm). The mobile phase was run at a gradient, changing from 70/30 to 0/100 of H₂O and MeOH respectively, each with 0.05% formic acid, over 15 min before being held at 0/100 for another 7 min. For the quantification, an LTQ Orbitrap XL mass spectrometer (Thermo Fisher Scientific) was used, operating in positive-ion mode.

In a similar fashion to the Michael-addition, the in-situ monitoring of the anionic oligomerization using a PSI setup was initiated by adding specified amounts of ethyl 1-cyanocyclopropane-1-carboxylate to a solution of PhSH, KO^tBu (1.3 equiv.) and 18-crown-6 (1.7 equiv.) in THF that was being stirred at 70 °C bath temperature. Isolated oligomer samples were obtained by increasing the concentrations. To 60 (90) μL PhSH, 72 (108) mg KO^tBu and 170 (265) mg 18C6 in 1 mL THF was given 750 (570) μL M^{cyclic} and the solution stirred for 2 (1) h at 70 °C. 0.5 mL 10% HCl and then an excess of MeOH and H₂O were added, the precipitate filtered and washed with more MeOH and H₂O. The solid was dried under reduced pressure at 60 °C. The solid samples were then dissolved in THF with KO^tBu and 18C6, replicating the regular ESI-MS measurement conditions, dissolved in DMSO-*d*₆ for ¹H NMR spectroscopy or sent to PSS Polymer Standard Service for external SEC experiments. For the latter, a combination of PSS GRAM 10 μm columns was used: Guard (8×50 mm), 100 Å, 30 Å, 3000 Å (each 8×300 mm). The separation was run at 70 °C and 1 mL/min flow rate of DMF + 0.01 M

LiBr, with an injection volume of 50 μ L of 3 g/L sample solutions. The SECcurity² refractive index detector was calibrated using poly(methyl methacrylate) standards.

Coordination polymerization reaction solutions were prepared by adding THF to rigorously dried CoCl₂ (13 mM). Once the salt was fully dissolved, the solution was cooled to -78 °C and PhLi (4 equiv.) was added as a 1.8-M solution in dibutyl ether. After stirring for 10 min, isoprene (20-30 equiv.) was added and stirred for another 5 min. The solution was drawn up into a gastight glass syringe and connected to the inlet line of the ESI source. Inside the syringe, the solution quickly reached approximately room temperature, initiating the polymerization. A PSI setup would not have allowed the temperature to rise fast enough, so it was not used in this case. The isolation of samples and MALDI-MS measurements were carried out by Dr. F. Kreyenschmidt and Dr. H. Frauendorf. For details, see Ref. 212.

7 References

- ¹ J. Li, H. Šimek, D. Ilioaie, N. Jung, S. Bräse, H. Zappe, R. Dittmeyer, B. P. Ladewig, *React. Chem. Eng.* **2021**, *6*, 1497-1507.
- ² J. B. Fenn, *J. Biomol. Tech.* **2002**, *13*, 101-118.
- ³ M. J. Hülsey, G. Sun, P. Sautet, N. Yan, *Angew. Chem. Int. Ed.* **2021**, *60*, 4764-4773.
- ⁴ K. K. Murray, R. K. Boyd, M. N. Eberlin, G. J. Langley, L. Li, Y. Naito, *Pure Appl. Chem.* **2013**, *85*, 1515-1609.
- ⁵ J. H. Gross, "Introduction" in **Mass Spectrometry**, 3rd edition, 2017, Springer International Publishing AG, Cham, CH, DOI 10.1007/978-3-319-54398-7.
- ⁶ T. Portolés, E. Pitarch, F. J. López, F. Hernández, W. M. A. Niessen, *Rapid Commun. Mass Spectrom.* **2011**, *25*, 1589-1599.
- ⁷ P. Palma, G. Famiglini, H. Trufelli, E. Pierini, V. Termopoli, A. Cappiello, *Anal. Bioanal. Chem.* **2011**, *39*, 2683-2693.
- ⁸ K. Tang, J. S. Page, R. D. Smith, *J. Am. Soc. Mass. Spectrom.* **2004**, *15*, 1416-1423.
- ⁹ T. R. Covey, B. A. Thomson, B. B. Schneider, *Mass Spectrom. Rev.* **2009**, *28*, 870-897.
- ¹⁰ M. Anbar, W. H. Aberth, *Anal. Chem.* **1974**, *46*, 59-64.
- ¹¹ L. C. Chen, M. Rahman, K. Hiraoka, *J. Mass Spectrom.* **2012**, *47*, 1083-1089.
- ¹² V. V. Laiko, M. A. Baldwin, A. L. Burlingame, *Anal. Chem.* **2000**, *72*, 652-657.
- ¹³ M. Barber, R. S. Bordoli, G. J. Elliott, R. D. Sedgwick, A. N. Tyler, *Anal. Chem.* **1982**, *54*, 645-657.
- ¹⁴ R. E. Honig, *J. Appl. Phys.* **1958**, *29*, 549-555.
- ¹⁵ H. B. Linden, *Eur. J. Mass Spectrom.* **2004**, *10*, 459-468.
- ¹⁶ J. H. Gross, "Chemical Ionization" in **Mass Spectrometry**, 3rd edition, 2017, Springer International Publishing AG, Cham, CH, ISBN 978-3-319-54398-7.
- ¹⁷ Z. Takáts, J. M. Wiseman, B. Gologan, R. G. Cooks, *Science*, **2004**, *306*, 471-473.

- ¹⁸ I. Sinclair, M. Bachman, D. Addison, M. Rohman, D. C. Murray, G. Davies, E. Mouchet, M. E. Tonge, R. G. Stearns, L. Ghislain, S. S. Datwani, L. Majlof, E. Hall, G. R. Jones, E. Hoyes, J. Olechno, R. N. Ellson, P. E. Barran, S. D. Pringle, M. R. Morris, J. Wingfield, *Anal. Chem.* **2019**, *91*, 3790-3794.
- ¹⁹ A. Raffaelli, A. Saba, *Mass Spectrom. Rev.* **2003**, *22*, 318-331.
- ²⁰ N. B. Cech, C. G. Enke, *Mass Spectrom. Rev.* **2001**, *20*, 362-387.
- ²¹ M. Dole, L. L. Mack, R. L. Hines, R. C. Mobley, L. D. Ferguson, M. B. Alice, *J. Chem. Phys.* **1968**, *49*, 2240-2249.
- ²² L. L. Mack, P. Kralik, A. Rheude, M. Dole, *J. Chem. Phys.* **1970**, *52*, 4977-4986
- ²³ E. Aliyari, L. Konermann, *Anal. Chem.* **2022**, *94*, 7713-7721.
- ²⁴ J. Fernández de la Mora, *J. Colloid Interface Sci.* **1996**, *178*, 209-218.
- ²⁵ M. Wilm, *Mol. Cell. Proteomics* **2011**, *10*, M111.009407.
- ²⁶ J. V. Iribarne, B. A. Thomson, *J. Chem. Phys.* **1976**, *64*, 2287-2294.
- ²⁷ L. Konermann, E. Ahadi, A. D. Rodriguez, S. Vahidi, *Anal. Chem.* **2013**, *85*, 2-9.
- ²⁸ C. G. Enke, *Anal. Chem.* **1997**, *69*, 4885-4893.
- ²⁹ **amaZon Series User Manual**, Revision A, 2016, Bruker Daltonik GmbH, Bremen, DE.
- ³⁰ **micrOTOF-Q User Manual**, Version 1.2, 2008, Bruker Daltonik GmbH, Bremen, DE.
- ³¹ T. W. Burgoyne, G. M. Hieftje, *Mass Spectrom. Rev.* **1996**, *15*, 241-259.
- ³² F. H. Read, *J. Phys. E: Sci. Instrum.* **1969**, *2*, 679-684.
- ³³ R. T. Kelly, A. V. Tolmachev, J. S. Page, K. Tang, R. D. Smith, *Mass Spectrom. Rev.* **2010**, *29*, 294-312.
- ³⁴ H. Wollnik, "Quadrupole lenses" in **Optics of Charged Particles**, 2nd edition, 2021, Academic Press, San Diego, US-CA, ISBN 978-0-12-818652-7.
- ³⁵ A. Galejs, C. E. Kuyatt, *J. Vac. Sci. Technol.* **1978**, *15*, 865-867.
- ³⁶ P. Agarwal, A. Goyal, *Int. J. Pharma. Bio. Sci.* **2017**, *8*, 140-152.

- ³⁷ W. Paul, *Angew. Chem.* **1990**, *102*, 780-789.
- ³⁸ D. T. Synder, W.-P. Peng, R. G. Cooks, *Chem. Phys. Lett.* **2017**, *668*, 69-89.
- ³⁹ B. A. Mamyryn, *Int. J. Mass Spectrom.* **2001**, *206*, 251-266.
- ⁴⁰ Y.-F. Xu, W. Lu, J. D. Rabinowitz, *Anal. Chem.* **2015**, *87*, 2273-2281.
- ⁴¹ H. I. Kenttämä, R. G. Cooks, *Int. J. Mass Spectrom. Ion Processes.* **1985**, *64*, 79-83.
- ⁴² D. J. Dit Fouque, A. Maroto, A. Memboeuf, *J. Mass Spectrom.* **2021**, *56*, e4698.
- ⁴³ L. Sleno, D. A. Volmer, *J. Mass Spectrom.* **2004**, *39*, 1091-1112.
- ⁴⁴ R. A. J. O'Hair, *Chem. Commun.* **2006**, 1469-1481.
- ⁴⁵ R. G. Cooks, T. L. Kruger, *J. Am. Chem. Soc.* **1977**, *99*, 1279-1281.
- ⁴⁶ S. A. McLuckey, D. Cameron, R. G. Cooks, *J. Am. Chem. Soc.* **1981**, *103*, 1313-1317.
- ⁴⁷ R. G. Cooks, J. T. Koskinen, P. D. Thomas, *J. Mass Spectrom.* **1999**, *34*, 85-92.
- ⁴⁸ K. Vékey, *J. Mass Spectrom.* **1996**, *31*, 445-463.
- ⁴⁹ J. M. Jasinski, J. I. Brauman, *J. Am. Chem. Soc.* **1980**, *102*, 2906-2913.
- ⁵⁰ R. G. Cooks, J. S. Patrick, T. Kotiaho, S. A. McLuckey, *Mass Spectrom. Rev.* **1994**, *13*, 287-339.
- ⁵¹ S. R. Logan, *J. Chem. Educ.* **1982**, *59*, 279-281.
- ⁵² X. Cheng, Z. Wu, C. Fenselau, *J. Am. Chem. Soc.* **1993**, *115*, 4844-4848.
- ⁵³ S.A. McLuckey, R. G. Cooks, J. E. Fulford, *Int. J. Mass Spectrom. Ion Processes* **1983**, *52*, 165-174.
- ⁵⁴ L. Drahos, C. Peltz, K. Vékey, *J. Mass Spectrom.* **2004**, *39*, 1016-1024.
- ⁵⁵ L. Zhang, D. J. Hinz, G. S. M. Kiruba, X. Ding, J. K. Lee, *J. Phys. Org. Chem.* **2022**, *35*, e4343.
- ⁵⁶ T. Bieńkowski, P. Świder, K. Błaziak, W. Danikiewicz, *Int. J. Mass Spectrom.* **2014**, *357*, 29-33.

- ⁵⁷ C.-C. Liou, J. S. Brodbelt, *J. Am. Soc. Mass Spectrom.* **1992**, *3*, 543-548.
- ⁵⁸ R. Augusti, D. V. Augusti, H. Chen, R. G. Cooks, *Eur. J. Mass Spectrom.* **2004**, *10*, 847-855.
- ⁵⁹ E. Gruber, S. Kollotzek, S. Bergmeister, F. Zappa, M. Ončák, P. Scheier, O. Echt, *Phys. Chem. Chem. Phys.* **2022**, *24*, 5138-5143.
- ⁶⁰ C. Mayeux, J.-F. Gal, L. Charles, L. Massi, P.-C. Maria, J. Tammiku-Taul, E.-L. Lohu, P. Burk, *J. Mass Spectrom.* **2010**, *45*, 520-527.
- ⁶¹ C. Mayeux, P. Burk, J.-F. Gal, I. Leito, L. Massi, *J. Phys. Chem. A* **2020**, *124*, 4390-4399.
- ⁶² P. Muller, *Pure Appl. Chem.* **1994**, *66*, 1077-1084.
- ⁶³ R. G. Pearson, *J. Am. Chem. Soc.* **1963**, *85*, 3533-3539.
- ⁶⁴ M. Hamell, R. Levine, *J. Org. Chem.* **1950**, *15*, 162-168.
- ⁶⁵ F. G. Bordwell, *Acc. Chem. Res.* **1988**, *21*, 456-463.
- ⁶⁶ A. Kütt, S. Tshepelevitsh, J. Saame, M. Lõkov, I. Kaljurand, S. Selberg, I. Leito, *Eur. J. Org. Chem.* **2021**, *9*, 1407-1419.
- ⁶⁷ J. Ho, *Aust. J. Chem.* **2014**, *67*, 1441-1460.
- ⁶⁸ Q. Yang, Y. Li, J.-D. Yang, Y. Liu, L. Zhang, S. Luo, J.-P. Cheng, *Angew. Chem. Int. Ed.* **2020**, *59*, 19282-19291.
- ⁶⁹ H. Mayr, M. Patz, *Angew. Chem. Int. Ed.* **1994**, *33*, 938-957.
- ⁷⁰ L. R. Domingo, M. J. Aurell, P. Pérez, R. Contreras, *Tetrahedron* **2002**, *58*, 4417-4423.
- ⁷¹ L. R. Domingo, P. Pérez, *Org. Biomol. Chem.* **2011**, *9*, 7168-7175.
- ⁷² J. F. Rusling, S. L. Suib, *Adv. Mater.* **1994**, *6*, 922-930.
- ⁷³ N. G. Tsierkezos, *J. Solution Chem.* **2007**, *36*, 289-302.
- ⁷⁴ H. Yoshida, *Anal. Bioanal. Chem.* **2014**, *406*, 2231-2237.
- ⁷⁵ K. Siegbahn, *Rev Mod. Phys.* **1982**, *54*, 709-728.
- ⁷⁶ E. C. M. Chen, W. E. Wentworth, *Mol. Cryst. Liq. Cryst.* **1989**, *171*, 271-285.

- ⁷⁷ J. A. Dixon, D. H. Fishman, *J. Am Chem. Soc.* **1963**, *85*, 1356-1357.
- ⁷⁸ P. Stanetty, M. D. Mihovilovic, *J. Org. Chem.* **1997**, *62*, 1514-1515.
- ⁷⁹ E. M. Arnett, S. G. Maroldo, S. L. Schilling, J. A. Harrelson, *J. Am. Chem. Soc.* **1984**, *106*, 6759-6767.
- ⁸⁰ F. G. Bordwell, G. E. Drucker, H. E. Fried, *J. Org. Chem.* **1981**, *46*, 632-635.
- ⁸¹ F. G. Bordwell, M. J. Bausch, *J. Am. Chem. Soc.* **1983**, *105*, 6188-6189.
- ⁸² W. N. Olmstead, F. G. Bordwell, *J. Org. Chem.* **1980**, *45*, 3299-3305.
- ⁸³ W. S. Matthews, J. E. Bares, J. E. Bartmess, F. G. Bordwell, F. J. Cornforth, G. E. Drucker, Z. Margolin, R. J. McCallum, G. J. McCollum, N. R. Vanier, *J. Am. Chem. Soc.* **1975**, *97*, 7006-7014.
- ⁸⁴ M. Braun, „Fundamentals and Transition-state Models. Aldol Additions of Group 1 and 2 Enolates” in **Modern Aldol Reactions, Vol. 1**, Ed. R. Mahrwald, 2004, WILEY-VCH Verlag GmbH & Co. KGaA, Weinheim, DE, DOI 10.1002/9783527619566.
- ⁸⁵ H. O. House, M. Gall, H. D. Olmstead, *J. Org. Chem.* **1971**, *36*, 2361-2371.
- ⁸⁶ H. O. House, R. A. Auerbach, M. Gall, N. P. Peet, *J. Org. Chem.* **1973**, *38*, 514-522.
- ⁸⁷ Z. Khademi, M. M. Heravi, *Tetrahedron* **2022**, *103*, 132573.
- ⁸⁸ K. Ando, *J. Org. Chem.* **1999**, *64*, 6815-6821.
- ⁸⁹ P. A. Byrne, D. G. Gilheany, *Chem. Soc. Rev.* **2013**, *42*, 6670-6696.
- ⁹⁰ E. J. Corey, D. Seebach, *Angew. Chem. Int. Ed.* **1965**, *4*, 1075-1077.
- ⁹¹ K. Ziegler, H. Colonius, *Ann.* **1930**, *479*, 135-149.
- ⁹² D. Seyferth, *Organometallics* **2009**, *28*, 1598-1605.
- ⁹³ J. P. Richard, G. Williams, A. C. O'Donoghue, T. L. Amyes, *J. Am. Chem. Soc.* **2002**, *124*, 2957-2968.
- ⁹⁴ J. P. Richard, T. L. Amyes, M. M. Toteva, *Acc. Chem. Res.* **2001**, *34*, 981-988.
- ⁹⁵ H. H. Szmant, *Angew. Chem. Int. Ed.* **1968**, *7*, 120-128.
- ⁹⁶ M. Ghavre, *Asian J. Org. Chem.* **2020**, *9*, 1901-1923.

- ⁹⁷ K. Bergander, R. He, N. Chandrakumar, O. Eppers, H. Günther, *Tetrahedron*, **1994**, *50*, 5861-5868.
- ⁹⁸ S. Lülfi, L. Guo, T. Parchomyk, J. N. Harvey, K. Koszinowski, *Chem. Eur. J.* **2022**, e202202030.
- ⁹⁹ N. L. Holy, J. D. Marcum, *Angew. Chem. Int. Ed.* **1971**, *10*, 115-124.
- ¹⁰⁰ S. H. Hilal, L. A. Carreira, S. W. Karickhoff, C. M. Melton, *Quant. Struct.-Act. Relat.* **1993**, *12*, 389-396.
- ¹⁰¹ N. El-Najjar, H. Gali-Muhtasib, R. A. Ketola, P. Vuorela, A. Urtili, H. Vuorela, *Phytochem. Rev.* **2011**, *10*, 353-370.
- ¹⁰² S. Lerch, L.-N. Unkel, P. Wienefeld, M. Brasholz, *Synlett* **2014**, *25*, 2673-2680.
- ¹⁰³ M. Nakamura, R. Dohno, T. Majima, *J. Org. Chem.* **1998**, *63*, 6258-6265.
- ¹⁰⁴ J. I. Bardagi, I. Ghosh, M. Schmalzbauer, T. Ghosh, B. König, *Eur. J. Org. Chem.* **2018**, *1*, 34-40.
- ¹⁰⁵ M. Neumeier, D. Sampedro, M. Májek, V. A. de la Peña O'Shea, A. J. von Wangelin, R. Pérez-Ruiz, *Chem. Eur. J.* **2018**, *24*, 105-108.
- ¹⁰⁶ N. A. Romero, D. A. Nicewicz, *Chem. Rev.* **2016**, *116*, 10075-10166.
- ¹⁰⁷ K. Matyjaszewski, *J. Phys. Org. Chem.* **1995**, *8*, 197-207.
- ¹⁰⁸ W. A. Braunecker, K. Matyjaszewski, *Prog. Polym. Sci.* **2007**, *32*, 93-146.
- ¹⁰⁹ M. Szwarc, "Living polymers and mechanisms of anionic polymerization" in **Advances in Polymer Science, Vol. 49**. 1983, Springer-Verlag GmbH, Heidelberg, DE, DOI 10.1007/3-540-12047-5_1.
- ¹¹⁰ P. J. Flory, *J. Am. Chem. Soc.* **1940**, *62*, 1561-1565.
- ¹¹¹ P. Hong, S. Koza, E. S. P. Bouvier, *J. Liq. Chromatogr. Relat. Technol.* **2012**, *35*, 2923-2950.
- ¹¹² H. G. Barth, B. E. Boyes, C. Jackson, *Anal. Chem.* **1994**, *66*, 595R-620R.
- ¹¹³ L. K. Kostanski, D. M. Keller, A. E. Hamielec, *J. Biochem. Biophys. Methods* **2004**, *58*, 159-186.
- ¹¹⁴ K. Jovic, T. Nitsche, C. Lang, J. P. Blinco, K. De Bruycker, C. Barner-Kowollik, *Polym. Chem.* **2019**, *10*, 3241-3256.

- ¹¹⁵ E. Frick, C. Schweigert, B. B. Noble, H. A. Ernst, A. Lauer, Y. Liang, D. Voll, M. L. Coote, A.-N. Unterreiner, C. Barner-Kowollik, *Macromolecules* **2016**, *49*, 80-89.
- ¹¹⁶ A. Schaffer, M. Kränzlein, B. Rieger, *Macromolecules* **2020**, *53*, 4345-4354.
- ¹¹⁷ D. E. Fast, A. Lauer, J. P. Menzel, A.-M. Kelterer, G. Gescheidt, C. Barner-Kowollik, *Macromolecules* **2017**, *50*, 1815-1823.
- ¹¹⁸ G. Montaudo, F. Samperi, M. S. Montaudo, *Prog. Polym. Sci.* **2006**, *31*, 277-357.
- ¹¹⁹ T. Gruending, S. Weidner, J. Falkenhagen, C. Barner-Kowollik, *Polym. Chem.* **2010**, *1*, 599-617.
- ¹²⁰ C. M. Guttman, K. M. Flynn, W. E. Wallace, A. J. Kearsley, *Macromolecules* **2009**, *42*, 1695-1702.
- ¹²¹ G. Montaudo, M. S. Montaudo, C. Puglisi, F. Samperi, *Rapid Commun. Mass Spectrom.* **1995**, *9*, 453-460.
- ¹²² J. J. Haven, J. Vandenberg, T. Junkers, *Chem. Commun.* **2015**, *51*, 4611-4614.
- ¹²³ G. Moad, E. Rizzardo, S. H. Thang, *Chem. Asian J.* **2013**, *8*, 1634-1644.
- ¹²⁴ H. Sinn, W. Kaminsky, H.-J. Vollmer, R. Woldt, *Angew. Chem. Int. Ed.* **1980**, *19*, 390-392.
- ¹²⁵ L. S. Santos, J. O. Metzger, *Angew. Chem. Int. Ed.* **2006**, *45*, 977-981.
- ¹²⁶ C. Hinderling, P. Chen, *Angew. Chem. Int. Ed.* **1999**, *38*, 2253-2256.
- ¹²⁷ C. Hinderling, P. Chen, *Int. J. Mass Spectrom.* **2000**, *195/196*, 377-383.
- ¹²⁸ A. Benlahouès, B. Brissault, S. Boileau, J. Penelle, *Macromol. Chem. Phys.* **2018**, *219*, 1700463.
- ¹²⁹ J. Penelle, H. Hérion, T. Xie, P. Gorissen, *Macromol. Chem. Phys.* **1998**, *199*, 1329-1336.
- ¹³⁰ J. Penelle, T. Xie, *Macromolecules* **2001**, *34*, 5083-5089.
- ¹³¹ J. Penelle, T. Xie, *Macromolecules* **2000**, *33*, 4667-4672.
- ¹³² N. Illy, S. Boileau, M. A. Winnik, J. Penelle, V. Barbier, *Polymer* **2012**, *53*, 903-912.

- ¹³³ D. C. Pepper, *Polymer J.* **1980**, *12*, 629-637.
- ¹³⁴ F. Kreyenschmidt, K. Koszinowski, *Chem. Eur. J.* **2018**, *24*, 1168-1177.
- ¹³⁵ S. T. Graul, R. R. Squires, *J. Am. Chem. Soc.* **1990**, *112*, 2506-2516.
- ¹³⁶ A. Fattahi, L. Lis, Z. A. Tehrani, S. S. Marimanikkuppam, S. R. Kass, *J. Org. Chem.* **2012**, *77*, 1904-1914.
- ¹³⁷ S. T. Graul, R. R. Squires, *J. Am. Chem. Soc.* **1988**, *110*, 607-608.
- ¹³⁸ C. Liu, Y. Zhang, A. B. Attygalle, *J. Mass Spectrom.* **2014**, *49*, 692-699.
- ¹³⁹ D. R. Reed, S. R. Kass, K. R. Mondanaro, W. P. Dailey, *J. Am. Chem. Soc.* **2002**, *124*, 2790-2795.
- ¹⁴⁰ E. H. Perez, T. Schleif, J. P. Messinger, A. G. Rullán Buxó, O. C. Moss, K. Greis, M. A. Johnson, *J. Am. Soc. Mass Spectrom.* **2022**, *33*, 1914-1920.
- ¹⁴¹ D. R. Reed, M. Hare, S. R. Kass, *J. Am. Chem. Soc.* **2000**, *122*, 10689-10696.
- ¹⁴² P. G. Wenthold, J. Hu, B. T. Hill, R. R. Squires, *Int. J. Mass Spectrom.* **1998**, *179-180*, 173-183.
- ¹⁴³ R. K. Curran, R. E. Fox, *J. Chem. Phys.* **1961**, *34*, 1590-1594.
- ¹⁴⁴ J. Lee, P. K. Chou, P. Dowd, J. J. Grabowski, *J. Am. Chem. Soc.* **1993**, *115*, 7902 – 7903.
- ¹⁴⁵ C. A. Mayhew, R. Peverall, P. Watts, *Int. J. Mass Spectrom. Ion Proc.* **1993**, *125*, 81 – 93.
- ¹⁴⁶ K. O. Zhurov, L. Fornelli, M. D. Wodrich, Ü. A. Laskay, Y. O. Tsybin, *Chem. Soc. Rev.* **2013**, *42*, 5014-5030.
- ¹⁴⁷ D. A. Horke, J. R. R. Verlet, *Phys. Chem. Chem. Phys.* **2011**, *13*, 19546-19552.
- ¹⁴⁸ A. Dupont, J.-P. Gisselbrecht, E. Leize, L. Wagner, A. Van Dorselaer, *Tetrahedron Lett.* **1994**, *35*, 6083-6086.
- ¹⁴⁹ I. Hassan, J. Pavlov, R. Errabelli, A. B. Attygalle, *J. Am. Soc. Mass. Spectrom.* **2017**, *28*, 270-277.
- ¹⁵⁰ J. R. Lloyd, S. Hess, *J. Am. Soc. Mass Spectrom.* **2009**, *20*, 1988-1996.
- ¹⁵¹ J. Pei, C.-C. Hsu, Y. Wang, K. Yu, *RSC Adv.* **2017**, *7*, 43540-43545.

- ¹⁵² B. L. Thompson, Z. M. Heiden, *Phys. Chem. Chem. Phys.* **2021**, *23*, 9822-9831.
- ¹⁵³ K. L. Vikse, Z. Ahmadi, J. S. McIndoe, *Coord. Chem. Rev.* **2014**, *279*, 96-114.
- ¹⁵⁴ T. Parchomyk, K. Koszinowski, *Chem. Eur. J.* **2016**, *22*, 15609-15613.
- ¹⁵⁵ M. Kolter, K. Koszinowski, *Chem. Eur. J.* **2019**, *25*, 13376-13384.
- ¹⁵⁶ K. Koszinowski, *J. Am. Chem. Soc.* **2010**, *132*, 6032-6040.
- ¹⁵⁷ F. Kreyenschmidt, S. E. Meurer, K. Koszinowski, *Chem. Eur. J.* **2019**, *25*, 5912-5921.
- ¹⁵⁸ O. Bortolini, G. Fantin, V. Ferretti, M. Fogagnolo, P. P. Giovannini, A. Massi, S. Pacifico, D. Ragno, *Adv. Synth. Catal.* **2013**, *355*, 3244-3252.
- ¹⁵⁹ I. Binkowska, *J. Mass Spectrom.* **2016**, *411*, 27-33.
- ¹⁶⁰ I. Binkowska, A. Huczyński, B. Brzezinski, A. Jarczewski, *J. Mol. Struct.* **2008**, *892*, 188-194.
- ¹⁶¹ D. A. Alonso, M. Fuensanta, E. Gómez-Bengoa, C. Nájera, *Eur. J. Org. Chem.* **2008**, *17*, 2915-2922.
- ¹⁶² A. Kumar, S. Mondal, M. Mofidfar, R. N. Zare, S. Banerjee, *J. Am. Chem. Soc.* **2022**, *144*, 7573-7577.
- ¹⁶³ J. E. Bartmess, "Negative Ion Energetics Data" in ***NIST Chemistry WebBook, NIST Standard Reference Database Number 69***, Eds. P. J. Linstrom, W. G. Mallard, National Institute of Standards and Technology, Gaithersburg, MD, DOI 10.18434/T4D303 (accessed October 1, 2020).
- ¹⁶⁴ N. F. Eisele, K. Koszinowski, *J. Org. Chem.* **2021**, *86*, 3750-3757.
- ¹⁶⁵ G. T. Thomas, S. Donnecke, I. C. Chagunda, J. S. McIndoe, *Chem.-Methods* **2022**, *2*, e202100068.
- ¹⁶⁶ W. N. Olmstead, Z. Margolin, F. G. Bordwell, *J. Org. Chem.* **1980**, *45*, 3295-3299.
- ¹⁶⁷ B. K. Freed, J. Biesecker, W. J. Middleton, *J. Fluor. Chem.* **1990**, *48*, 63-75.
- ¹⁶⁸ G. Wang, R. B. Cole, *J. Am. Soc. Mass Spectrom.* **1996**, *7*, 1050-1058.
- ¹⁶⁹ R. M. Bain, C. J. Pulliam, R. G. Cooks, *Chem. Sci.* **2015**, *6*, 397-401.

- ¹⁷⁰ X. Yan, R. M. Bain, R. G. Cooks, *Angew. Chem. Int. Ed.* **2016**, *55*, 12960-12972.
- ¹⁷¹ C.-C. Liou, J. S. Brodbelt, *J. Am. Soc. Mass. Spectrom.* **1992**, *3*, 543-548.
- ¹⁷² F. G. Bordwell, H. E. Fried, *J. Org. Chem.* **1981**, *46*, 4327-4331..
- ¹⁷³ F. G. Bordwell, J. A. Harrelson Jr., *Can. J. Chem.* **1990**, *68*, 1714-1718.
- ¹⁷⁴ F. G. Bordwell, D. Algrim, N. R. Vanier, *J. Org. Chem.* **1977**, *42*, 1817-1819.
- ¹⁷⁵ X. M. Zhang, F. G. Bordwell, M. Van Der Puy, H. E. Fried, *J. Org. Chem.* **1993**, *58*, 3060-3066.
- ¹⁷⁶ R. E. Dinnebier, U. Behrens, F. Olbrich, *Organometallics* **1997**, *16*, 3855-3858.
- ¹⁷⁷ G. Maniara, K. Rajamoorthi, S. Rajan, G. W. Stockton, *Anal. Chem.* **1998**, *70*, 4921-4928.
- ¹⁷⁸ S. Zhou, M. Hamburger, *Rapid Commun. Mass Spectrom.* **1995**, *9*, 1516-1521.
- ¹⁷⁹ R. B. Cole, A. K. Harrata, *J. Am. Soc. Mass Spectrom.* **1993**, *4*, 546-556.
- ¹⁸⁰ J. Saame, T. Rodima, S. Tshepelevitsh, A. Kütt, I. Kaljurand, T. Haljasorg, I. A. Koppel, I. Leito, *J. Org. Chem.* **2016**, *81*, 7349-7361.
- ¹⁸¹ M. Born, S. Ingemann, N. M. M. Nibbering, *Mass Spectrom. Rev.* **1997**, *16*, 181-200.
- ¹⁸² N. G. Connelly, W. E. Geiger, *Chem. Rev.* **1996**, *96*, 877-910.
- ¹⁸³ S. Chowdhury, T. Heinis, E. P. Grimsrud, P. Kebarle, *J. Phys. Chem.* **1986**, *90*, 2747-2752.
- ¹⁸⁴ T. Heinis, S. Chowdhury, S. L. Scott, P. Kebarle, *J. Am. Chem. Soc.* **1988**, *110*, 400-407.
- ¹⁸⁵ P. Kebarle, S. Chowdhury, *Chem. Rev.* **1987**, *87*, 513-534.
- ¹⁸⁶ V. Gabelica, E. De Pauw, *Mass Spectrom. Rev.* **2005**, *24*, 566-587.
- ¹⁸⁷ R. Rahrt, T. Auth, M. Demireva, P. B. Armentrout, K. Koszinowski, *Anal. Chem.* **2019**, *91*, 11703-11711.
- ¹⁸⁸ M. E. Peover, *J. Chem. Soc.* **1962**, 4540-4549.

- ¹⁸⁹ R. Vessecchi, A. E. M. Crotti, T. Guaratini, P. Colepicolo, S. E. Galembeck, N. P. Lopes, *Mini-Rev. Org. Chem.* **2007**, *4*, 75-87.
- ¹⁹⁰ K. M. Ervin, I. Anusiewicz, P. Skurski, J. Simons, W. C. Lineberger, *J. Phys. Chem. A* **2003**, *107*, 8521-8529.
- ¹⁹¹ L. Tang, P. Kebarle, *Anal. Chem.* **1993**, *65*, 3654-3668.
- ¹⁹² <https://www.sigmaaldrich.com/DE/de/product/sigald/34851> accessed 01.11.22.
- ¹⁹³ C. Burkholder, W. R. Dolbier Jr., *J. Org. Chem.* **1998**, *63*, 5385-5394.
- ¹⁹⁴ G. Pampaloni, U. Koelle, *J. Organomet. Chem.* **1994**, *481*, 1-6.
- ¹⁹⁵ R. L. Stoddard, J. Luo, N. van der Wal, N. F. O'Rourke, J. E. Wulff, J. S. McIndoe, *New J. Chem.* **2014**, *38*, 5382-5390.
- ¹⁹⁶ M. M. Roessler, E. Salvadori, *Chem. Soc. Rev.* **2018**, *47*, 2534-2553.
- ¹⁹⁷ H. Matsuoka, M. Retegan, L. Schmitt, S. Höger, F. Neese, O. Schiemann, *J. Am. Chem. Soc.* **2017**, *139*, 12968-12975.
- ¹⁹⁸ Y.-C. Chen, P. L. Urban, *Trends Anal. Chem.* **2013**, *44*, 106-120.
- ¹⁹⁹ J. A. Orvik, *J. Am. Chem. Soc.* **1976**, *98*, 3322-3325.
- ²⁰⁰ T. Tokoroyama, *Eur. J. Org. Chem.* **2010**, *10*, 2009-2016.
- ²⁰¹ N. F. Eisele, K. Koszinowski, *J. Org. Chem.* **2021**, *86*, 3750-3757.
- ²⁰² L. C. Kagumba, J. Penelle, *Macromolecules* **2005**, *38*, 4588-4594.
- ²⁰³ J. Penelle, G. Clarebout, I. Balikdjian, *Polym. Bull.* **1994**, *32*, 395-401.
- ²⁰⁴ T. Henriksen, R. K. Juhler, B. Svensmark, N. B. Cech, *J. Am. Soc. Mass Spectrom.* **2005**, *16*, 446-455.
- ²⁰⁵ M. Itakura, K. Sato, M. A. Lusenkova, S. Matsuyama, K. Shimada, T. Saito, S. Kinugasa, *J. Appl. Polym. Sci.* **2004**, *94*, 1101-1106.
- ²⁰⁶ S. Hoops, S. Sahle, R. Gauges, C. Lee, J. Pahle, N. Simus, M. Singhal, L. Xu, P. Mendes, U. Kummer, *Bioinformatics* **2006**, *22*, 3067-3074.
- ²⁰⁷ R. Lucius, R. Loos, H. Mayr, *Angew. Chem. Int. Ed.* **2002**, *41*, 91-95.
- ²⁰⁸ P. M. Jüstel, C. D. Pignot, A. R. Ofial, *J. Org. Chem.* **2021**, *86*, 5965-5972.

- ²⁰⁹ N. S. Asthana, A. K. Kolah, D. T. Vu, C. T. Lira, D. J. Miller, *Ind. Eng. Chem. Res.* **2006**, *45*, 5251-5257.
- ²¹⁰ P. D. Smith, M. P. McDaniel, *J. Polym. Sci. A Polym. Chem.* **1989**, *27*, 2695-2710.
- ²¹¹ R. P. Quirk, B. Lee, *Polym. Int.* **1992**, *27*, 359-367.
- ²¹² F. Kreyenschmidt, N. F. Eisele, V. Hevelke, R. Rahrt, A.-K. Kreyenschmidt, K. Koszinowski, *Angew. Chem. Int. Ed.* **2022**, *61*, e202210211.
- ²¹³ Z. Chen, M. Brookhart, *Acc. Chem. Res.* **2018**, *51*, 1831-1839.
- ²¹⁴ S. A. Svejda, L. K. Johnson, M. Brookhart, *J. Am. Chem. Soc.* **1999**, *121*, 10634-10635.
- ²¹⁵ R. Rahrt, personal communication.
- ²¹⁶ C. Hansch, A. Leo, R. W. Taft, *Chem. Rev.* **1991**, *9*, 165-195.
- ²¹⁷ C. Laurence, J.-F. Gal, "Gas-Phase Cation Affinity and Basicity Scales" in **Lewis Basicity and Affinity Scales: Data and Measurement**, 2009, John Wiley & Sons, Hoboken, US-NJ, ISBN 978-0-470-74957-9.
- ²¹⁸ J. J. Varghese, S. H. Mushrif, *React. Chem. Eng.* **2019**, *4*, 165-206.
- ²¹⁹ M. Raban, E. A. Noe, G. Yamamoto, *J. Am. Chem. Soc.* **1977**, *99*, 6527-6531.
- ²²⁰ D. K. Rogstad, J. L. Herring, J. A. Theravathu, A. Burdzy, C. C. Perry, J. W. Neidigh, L. C. Sowers, *Chem. Res. Toxicol.* **2009**, *22*, 1194-2004.
- ²²¹ J. T. Watson, Y. Yang, J. Wu, *J. Mol. Graph. Model.* **2001**, *19*, 119-128.
- ²²² T. C. Malig, J. D. B. Koenig, H. Situ, N. K. Chehal, P. G. Hultin, J. E. Hein, *React. Chem. Eng.* **2017**, *2*, 309-314.
- ²²³ M. Abdollahi, M. Sharifpour, *Polym. Commun.* **2007**, *48*, 25-30.
- ²²⁴ N. E. Leadbeater, *Chem. Commun.* **2010**, *36*, 6693-6695.
- ²²⁵ K. Grabow, U. Bentrup, *ACS Catal.* **2014**, *4*, 2153-2164.
- ²²⁶ A. Schmidt, M. Karas, T. Dülcks, *J. Am. Soc. Mass Spectrom.* **2003**, *14*, 492-500.
- ²²⁷ G. Wilkinson, F. A. Cotton, J. M. Birmingham, *J. Inorg. Nucl.* **1956**, *2*, 95-113.